AN ABSTRACT OF THE THESIS OF

Jung-Hwan Song for the degree of Doctor of Philosophy in Physics presented on December 7, 2004.

Title: Impurities in a Homogeneous Electron Gas

Abstract approved: Redacted for Privacy

Immersion energies for an impurity in a homogeneous electron gas with a uniform positive background charge density have been calculated numerically using density functional theory. The numerical aspects of this problem are very demanding and have not been properly discussed in previous work. The numerical problems are related to approximations of infinity and continuity, and they have been corrected using physics based on the Friedel sum rule and Friedel oscillations. The numerical precision is tested extensively. Immersion energies are obtained for non-spin-polarized systems, and are compared with published data. Numerical results, such as phase shifts, density of states, dielectric constants, and compressibilities, are obtained and compared with analytical theories. Immersion energies for excited systems are obtained by varying the number of electrons in the bound states of an impurity. The model is extended to spin-polarized systems and is tested in detail for a carbon impurity. The spin-coupling with an external magnetic field is considered mainly for a hydrogen impurity. These new results show very interesting behavior at low densities.

Impurities in a Homogeneous Electron Gas

by

Jung-Hwan Song

A THESIS

submitted to

Oregon State University

in partial fulfillment of
the requirements for the
degree of

Doctor of Philosophy

Presented December 7, 2004
Commencement June 2005

Doctor of Philosophy thesis of Jung-Hwan Song presented on December 7, 2004

APPROVED:

Redacted for Privacy

Major Professor, representing Physics

Redacted for Privacy

Chair of the Department of Physics

Redacted for Privacy

Dean of the Graduate School

I understand that my thesis will become part of the permanent collection of Oregon State University libraries. My signature below authorizes release of my thesis to any reader upon request.

Redacted for privacy

Jung-Hwan Song, Author

ACKNOWLEDGMENT

I would like to thank the people who helped me come to Corvallis and overcome culture differences.

I cannot fully express my gratitude to my Major Professor, Henri J. F. Jansen, who has been a most important contributor to this thesis, and gave me guidelines and helps not only for physics problems but also for my personal problems. He has been very kind, generous, and has answered all my questions, including the trivial ones. I really appreciate his expertise and experience, and look forward to further collaborations.

I would like to express my appreciation to Professors William W. Warren, Rubin H. Landau, Tom Giebultowicz, and Solomon C. S. Yim for serving on my committee.

I am thankful to my friends and office-mates, especially Jae-Hyuk Lee, Pornrat Wattanakasiwich, and David Matusevitsch, for making my stay a very pleasant one.

And finally, I am deeply grateful to my parents and my wife for their unconditional love and support. This thesis might have taken much more time to be finished without helps from my wife, JungIn.

Financial support was partially provided by ONR.

TABLE OF CONTENTS

TABLE OF CONTENTS (Continued)

LIST OF FIGURES

LIST OF FIGURES (Continued)

LIST OF FIGURES (Continued)

LIST OF FIGURES (Continued)

Figure Page

Figure Page

LIST OF FIGURES (Continued)

Figure Page

LIST OF FIGURES (Continued)

Figure Page

Figure Page

LIST OF FIGURES (Continued)

LIST OF TABLES

IMPURITIES IN A HOMOGENEOUS ELECTRON GAS

1. INTRODUCTION

The electronic structure of many-electron systems such as atoms, molecules, metals, and semiconductors is of great importance for analyzing and developing materials. Hartree-Fock or second quantization calculations for many-electron systems, especially for solids, are, however, almost impossible or computationally very demanding. One of the most successful theoretical and practical approaches to such complex systems is density functional theory, in which systems are described by the electron density rather than wave functions. Density functional theory has now been generalized for molecular dynamics, spin-polarized systems, superconductors, excited systems, time-dependent systems, and so on.

In 1964, Hohenberg and Kohn published density functional theory, in which the ground state properties of a many-electron system can be calculated in terms of the electron density by minimizing energy functionals. [1] The Hohenberg-Kohn theorem, however, has a critical shortcoming in that the energy functionals are impossible to determine or can only be approximated for slowly varying charge distributions, as in the Thomas-Fermi theory. The Kohn-Sham equations form an effective implementation of the Hohenberg-Kohn theorem. They were derived by introducing a non-interacting kinetic energy functional and the exchange-correlation energy functional and utilizing the energy variational principle of the Hohenberg-Kohn theorem. [2] Since the exchange-correlation term includes every interaction other than Coulomb interaction and depends on the entire density distribution, it is, at present, not possible to calculate the exchange-correlation interaction exactly.

Hence approximations are needed, for instance, LDA(Local Density Approximation) and GGA(Generalized Gradient Approximation).[1] Since the Kohn-Sham equations are a self-consistent set of one-particle equations, they have been used widely for computer calculations such as the band structure. [3] [4]

Computer calculations for a model of an impurity atom in a homogeneous electron gas were performed in 1981 by Puska, Nieminen, and Maninen. [5] This model has been developed originally to study metal vacancies and has been applied to chemisorbed atoms on metal surfaces and to molecular bonding. [6] [7] The density of states induced by impurities were calculated, as well as the immersion energies. Recently, numerical calculations have also been performed for non-spherical systems, such as an impurity moving through a uniform electronic gas, and diatomic molecules in an electronic gas, within the Kohn-Sham scheme. [8] [9]

The important properties of this model were already discussed by J. Friedel in 1950s in the context of metallic alloys. [10] [11] [12] For a given perturbation potential due to impurity atoms, a free-electron gas shows two important features, the Friedel sum rule and Friedel oscillations, which are related to the total induced charge in the vicinity of an impurity and to the long-range oscillations of the electronic density at large distances. In Friedel's papers, transition metal impurities in metals such as Al and Cu were discussed. He considered the d shell of a transition metal impurity at the Fermi energy and used the concept of virtual bound states.

---

[1]The exchange-correlation interaction in LDA depends only on the local electron density. In GGA it depends not only on the local density but also on the gradient of the local density.

The density of states at the Fermi energy induced by an impurity is used in the discussion of a variety of physical properties such as Pauli paramagnetism, orbital diamagnetism, electrical resistivity, and thermal properties.

This model can be used to study the behavior of a single impurity, for instance, to analyze the violation of Hund's second rule for a single iron atom in metals. This is important for properties like crystalline magnetic anisotropy and quenching of the orbital moment. It can also be considered as a first approximation to analyze any system, consisting of impurities and an electronic gas, when the impurities hardly interact and lattice vibrations can be neglected. This model can be used to investigate the magnetic behavior of an electron gas due to an impurity. Analysis of the spatial distribution of an electron gas and the concentration of impurities may also shed light on phenomena like diffusion and indirect exchange interactions via conduction electrons.

The calculations in this thesis first follow the scheme used in the Puska, Nieminen, and Maninen paper. LDA is used for the exchange-correlation interaction in this work. Their model is extended for excited systems and spin-polarized systems with or without an external magnetic field. The spin-moment for the model system is also calculated, considering spin-coupling only, with an external magnetic field. A variety of results such as immersion energies, phase shifts, potentials, dielectric functions, partial-wave decompositions of the Friedel sum rule, and electronic densities are obtained.

Density functional theory and the Kohn-Sham equation are briefly explained in Chapter 2. The model used in this work is introduced, and theoretical calculations and general properties of an electronic gas are discussed in Chapter 3. The numerical methods developed in this work are explained in Chapter 4. The results and discussion follow in Chapter 5. Chapter 6 is dedicated to conclusions.

2. DENSITY FUNCTIONAL THEORY

The Hohenberg-Kohn theorem provides the theoretical foundation for functional calculations of the electronic structure for interacting particle systems and suggests a universal functional $F_{\mathrm{HK}}[n]$ which is independent of the nature of the external potential in a system. The Kohn-Sham equations can be obtained using a variation principle by comparing with a Schrödinger equation and they incorporate $F_{\mathrm{HK}}[n]$ via the exchange-correlation energy $E_{xc}[n]$. $E_{xc}[n]$ can be approximated as in LDA or GGA, since $F_{\mathrm{HK}}[n]$ is impossible to find. The Kohn-Sham equations are a set of self-consistent one-particle equations and have a variety of applications, especially in a numerical way. In this chapter we will review the Hohenberg-Kohn theorem and the Kohn-Sham equations briefly. The Kohn-Sham equations will be extended for a spin-polarized system. The exchange-correlation energies and potentials will be discussed and expressed explicitly within the LDA scheme.

2.1. The Hohenberg-Kohn theorem

In 1964, Hohenberg and Kohn pointed out that it is possible to derive the ground state properties of a many-electron system in terms of the electron density. [1] The Hamiltonian for interacting particles under the influence of an external potential $v(\boldsymbol{r})$ is of the form [13]

$$\hat{H} = \hat{T} + \hat{V} + \hat{W} \tag{2.1}$$

where, in the second quantized notation,

$$\hat{T} = \sum_{\sigma} \int \psi_{\sigma}^{\dagger}(\boldsymbol{r}) \left[-\frac{\hbar^2}{2m} \boldsymbol{\nabla}^2(\boldsymbol{r}) \right] \psi_{\sigma}(\boldsymbol{r}) \, \mathrm{d}\boldsymbol{r} \tag{2.2}$$

$$\hat{V} = \sum_{\sigma} \int v^{\sigma}(\boldsymbol{r}) \psi_{\sigma}^{\dagger}(\boldsymbol{r}) \psi_{\sigma}(\boldsymbol{r}) \, \mathrm{d}\boldsymbol{r} \tag{2.3}$$

$$\hat{W} = \frac{1}{2} \sum_{\sigma,\sigma'} \int \psi_{\sigma}^{\dagger}(\boldsymbol{r}) \psi_{\sigma'}^{\dagger}(\boldsymbol{r}') w(\boldsymbol{r}, \boldsymbol{r}') \psi_{\sigma'}(\boldsymbol{r}') \psi_{\sigma}(\boldsymbol{r}) \, \mathrm{d}\boldsymbol{r} \mathrm{d}\boldsymbol{r}' \tag{2.4}$$

where σ is for spin degeneracy and m is the mass of particles. Note that $\hat{W}$ indicates a two-particle interaction such as the Coulomb interaction.

We assume for simplicity that the ground state is non-degenerate. (The theory can be, however, easily extended to the degenerate case [13].) Since a non-degenerate ground state ϕ is determined by solving the Schrödinger equation with an external potential $v(\boldsymbol{r})$

$$\hat{H}|\phi\rangle = (\hat{T} + \hat{V} + \hat{W})|\phi\rangle = E_{gs}|\phi\rangle \quad , \tag{2.5}$$

a map $C : V \mapsto \Phi$ is defined from the set of external potentials V to the set of ground states Φ. Now, for any ground state, the electronic density in the ground state ϕ can be calculated by

$$n(\boldsymbol{r}) = \sum_{\sigma} \langle \phi | \psi_{\sigma}^{\dagger}(\boldsymbol{r}) \psi_{\sigma}(\boldsymbol{r}) | \phi \rangle \quad , \tag{2.6}$$

which leads to a second map $D : \Phi \mapsto N$ from the set of ground states to the set of ground state densities. The map $CD : V \mapsto N$ clearly tells us that $n(\boldsymbol{r})$ is a functional of $v(\boldsymbol{r})$.

2.1.1. Uniqueness of the external potential in terms of the density

The Hohenberg - Kohn theorem states that the map C and D are both invertible uniquely, that is, the external potential is uniquely determined up to an additive constant by the ground state density. One can show this simply by

reducio ad absurdum as in [1]. For the map C, assume that two different external potentials give rise to the *same* ground state. Suppose

$$(\hat{T} + \hat{V}_1 + \hat{W})|\phi\rangle = E_{gs,1}|\phi\rangle \tag{2.7}$$

$$\text{and} \quad (\hat{T} + \hat{V}_2 + \hat{W})|\phi\rangle = E_{gs,2}|\phi\rangle \tag{2.8}$$

where $\hat{V}_1 \neq \hat{V}_2 + c$ by assumption. Note that two potentials with only a constant difference are equivalent. By subtraction, one has, due to non-degeneracy,

$$(\hat{V}_1 - \hat{V}_2)|\phi\rangle = (E_{gs,1} - E_{gs,2})|\phi\rangle \tag{2.9}$$

Since $\hat{V}_1$ and $\hat{V}_2$ are multiplicative operators, one must have $\hat{V}_1 - \hat{V}_2 = E_{gs,1} - E_{gs,2}$ which is in contradiction with the assumption at the beginning. More clearly, the statement can be proved as follows. Assume, for simplicity, that the system has a single particle with a spin σ at position $\boldsymbol{r}$. Then,

$$\begin{aligned}
\langle \boldsymbol{r}\sigma|(\hat{V}_1 - \hat{V}_2)|\phi\rangle &= \langle \boldsymbol{r}\sigma|(E_{gs,1} - E_{gs,2})|\phi\rangle \\
(v_1^\sigma(\boldsymbol{r}) - v_2^\sigma(\boldsymbol{r}))\phi_\sigma(\boldsymbol{r}) &= (E_{gs,1} - E_{gs,2})\phi_\sigma(\boldsymbol{r}) \\
(v_1^\sigma(\boldsymbol{r}) - v_2^\sigma(\boldsymbol{r})) &= (E_{gs,1} - E_{gs,2})
\end{aligned}$$

assuming that $|\phi\rangle$ does not vanish. Finally,

$$\begin{aligned}
\hat{V}_1 - \hat{V}_2 &= \sum_\sigma \int \mathrm{d}\boldsymbol{r}\, (v_1^\sigma(\boldsymbol{r}) - v_2^\sigma(\boldsymbol{r})))\psi_\sigma^\dagger(\boldsymbol{r})\psi_\sigma(\boldsymbol{r}) \\
&= (E_{gs,1} - E_{gs,2}) \sum_\sigma \int \mathrm{d}\boldsymbol{r}\, \psi_\sigma^\dagger(\boldsymbol{r})\psi_\sigma(\boldsymbol{r}) \\
&= E_{gs,1} - E_{gs,2}
\end{aligned}$$

Two different potentials, hence, lead to the *different* ground states and the map C is invertible.

The proof for the map D follows by the same procedure. Assume that two different ground states $|\phi_1\rangle$ and $|\phi_2\rangle$ yield the *same* ground state density, $n_1(\boldsymbol{r}) = n_2(\boldsymbol{r})$. Then one has

$$E_{gs,1} = \langle\phi_1|\hat{H}_1|\phi_1\rangle < \langle\phi_2|\hat{H}_1|\phi_2\rangle = \langle\phi_2|\hat{H}_2 + \hat{V}_1 - \hat{V}_2|\phi_2\rangle$$
$$= E_{gs,2} + \int \mathrm{d}\boldsymbol{r}\, n(\boldsymbol{r})(v_1(\boldsymbol{r}) - v_2(\boldsymbol{r}))$$

Similarly

$$E_{gs,2} = \langle\phi_2|\hat{H}_2|\phi_2\rangle < \langle\phi_1|\hat{H}_2|\phi_1\rangle = E_{gs,1} + \int \mathrm{d}\boldsymbol{r}\, n(\boldsymbol{r})(v_2(\boldsymbol{r}) - v_1(\boldsymbol{r}))$$

Now, adding of both inequalities leads to a contradiction again

$$E_{gs,1} + E_{gs,2} < E_{gs,1} + E_{gs,2} \tag{2.10}$$

and two different ground states $|\phi_1\rangle$ and $|\phi_2\rangle$, hence, yield *different* ground state densities. The map D must be invertible. Due to this invertibility, the ground state expectation value of any observable $\hat{O}$ (e.g. $\hat{H}$, the Hamiltonian) is determined by the ground state density and is thus a unique functional of the ground state density.

$$\langle\phi[n]|\hat{O}|\phi[n]\rangle = O[n] \tag{2.11}$$

The map CD is, therefore, invertible and is thus the ground state density uniquely determines the external potential up to an additive constant.

2.1.2. Variational principle

Now, the energy functional with the external potential $\hat{V}$ is, for any density n,

$$E[n] = \langle\phi[n]|\hat{T} + \hat{V} + \hat{W}|\phi[n]\rangle\ . \tag{2.12}$$

Since there exist a non-degenerate ground state density n_{gs} and ground state energy E_{gs} for this specific external potential via the map CD, we derive from the variational principle

$$E_{gs} = E[n_{gs}] = \langle \phi[n_{gs}] | \hat{T} + \hat{V} + \hat{W} | \phi[n_{gs}] \rangle$$
$$E[n] = \langle \phi[n] | \hat{T} + \hat{V} + \hat{W} | \phi[n] \rangle$$
$$E_{gs} < E[n] \quad \text{if} \quad n \neq n_{gs} \quad .$$

The exact ground state density is, therefore, determined by minimizing the energy functional $E[n]$: $E_{gs} = \min_{n \in N} E[n]$.

Therefore, one can conclude that there exists a unique energy functional for a given external potential from the Hohenberg and Kohn theorem and the exact ground state density is determined by the variational equation $\delta E[n] = 0$.

2.1.3. Universal functional $F_{HK}[n]$

Since the map D is independent of the external potential of the particular system, one can write the energy functional $E[n]$ as

$$\begin{aligned} E[n] &= \langle \phi[n] | \hat{T} + \hat{V} + \hat{W} | \phi[n] \rangle \\ &= F_{\mathrm{HK}}[n] + \int \mathrm{d}\boldsymbol{r}\, v_0(\boldsymbol{r}) n(\boldsymbol{r}) \end{aligned} \tag{2.13}$$

where $F_{\mathrm{HK}}[n] = \langle \phi[n] | \hat{T} + \hat{W} | \phi[n] \rangle$. As one can see $F_{\mathrm{HK}}[n]$ does not depend on the external potential (e.g. the interaction between electrons and nuclei), and it is in principle possible to calculate the universal functional $F_{\mathrm{HK}}[n]$, which is the same for all electronic systems such as atoms, molecules and solids since, for these systems, $\hat{W}$ is the Coulomb repulsion between electrons. Now, the functional $F_{\mathrm{HK}}[n]$ has a very important meaning, since once $F_{\mathrm{HK}}[n]$ is known, one can apply it for any systems (any number of particles and any external potential).

2.2. The Kohn-Sham equations

At first sight, density functional theory seems to lead to a new way for the physics of many-body systems. The universal functional $F_{\mathrm{HK}}[n]$ is, however, in most cases not possible to obtain. One can make some progress to find approximate expressions for $F_{\mathrm{HK}}[n]$ for a gas of slowly varying density or almost constant density. [1] Kohn and Sham, in 1965, suggested an alternative way to solve the problem, using a set of self-consistent equations for *single* particles including the exchange-correlation potentials. [2] This single particle picture, the Kohn-Sham equations, of a many-body system is quite accessible especially in a numerical way and, thus, provides a new computational way using single particle aspects of solid state physics.

The key point in deriving the Kohn-Sham equations is that, if n is the ground state density of an *interacting* particle system, one can assume there exists a unique external potential v_{NI} of a *non-interacting* particle system corresponding to the ground state density n. (Uniqueness of v_{NI} is proven from the Hohenberg-Kohn theorem, but the existence of v_{NI} must be assumed.) It is possible, now, to derive one-particle equations of the interacting system by comparison with the non-interacting system.

2.2.1. Non-interacting particle system in an external potential $v_{NI}(\boldsymbol{r})$

The Schrödinger equation for a non-interacting system in an external potential $v_{NI}(\boldsymbol{r})$ is

$$\left[-\frac{\hbar^2}{2m}\nabla^2 + v_{NI}(\boldsymbol{r})\right]\phi_i(\boldsymbol{r}) = \epsilon_i\phi_i(\boldsymbol{r}) \ . \tag{2.14}$$

The ground state is again assumed to be non-degenerate for simplicity.

The ground state density n_{NI} is

$$n_{NI}(\boldsymbol{r}) = \sum_{i}^{N} |\phi_i(\boldsymbol{r})|^2 \ . \tag{2.15}$$

where $\phi_i(\boldsymbol{r})$ occupies the lowest eigenstates.

If the ground state density n_{NI} is given, the external potential $v_{NI}(\boldsymbol{r})$ is determined up to a trivial constant from the Hohenberg-Kohn theorem. Since the wave functions $\phi_i(\boldsymbol{r})$ of the Schrödinger equation are, thus, unique functionals of the density n_{NI}, $\phi_i(\boldsymbol{r}) = \phi_i([n];\boldsymbol{r})$, the kinetic energy $T_{NI}[n]$ of the non-interacting system is a unique functional and hence so is the total energy. The kinetic energy and total energy functional with the ground state density n_{NI} are

$$T_{NI}[n] = \sum_{i,\sigma} \int \mathrm{d}\boldsymbol{r}\, \phi^*_{i,\sigma}(\boldsymbol{r}) \left[-\frac{\hbar^2}{2m} \boldsymbol{\nabla}^2(\boldsymbol{r}) \right] \phi_{i,\sigma}(\boldsymbol{r}) \tag{2.16}$$

$$\text{and} \quad E_{NI}[n] = T_{NI}[n] + \int \mathrm{d}\boldsymbol{r}\, v_{NI}(\boldsymbol{r}) n(\boldsymbol{r}) \ . \tag{2.17}$$

The ground state density, equivalently, can be obtained from the variational principle $\delta E = 0$ [13] of the Hohenberg-Kohn theorem or the Euler equations:

$$\frac{\delta}{\delta n(\boldsymbol{r})} \left[E_{NI}[n] - \mu_{NI} \int n(\boldsymbol{r})\, \mathrm{d}\boldsymbol{r} \right] = \frac{\delta T_{NI}[n]}{\delta n(\boldsymbol{r})} + v_{NI}(\boldsymbol{r}) - \mu_{NI} = 0 \tag{2.18}$$

where μ_{NI} is a Lagrange multiplier to keep the total number of particles constant, $\int n(\boldsymbol{r})\, \mathrm{d}\boldsymbol{r} = N$.

2.2.2. Interacting particle system in an external potential $v(\boldsymbol{r})$

The energy functional for an interacting particle system is, from the Hohenberg-Kohn theorem,

$$E[n] = F_{\mathrm{HK}}[n] + \int \mathrm{d}\boldsymbol{r}\, v_I(\boldsymbol{r}) n(\boldsymbol{r}) \tag{2.19}$$

If we define $E_{xc}[n]$ as

$$E_{xc}[n] = F_{\mathrm{HK}}[n] - \frac{1}{2}\int \mathrm{d}\boldsymbol{r}\,\mathrm{d}\boldsymbol{r}'\, n(\boldsymbol{r})w(\boldsymbol{r},\boldsymbol{r}')n(\boldsymbol{r}') - T_{NI}[n] \tag{2.20}$$

where $T_{NI}[n]$ is the *non-interacting* kinetic energy, the energy functional follows the form

$$E[n] = T_{NI}[n] + \frac{1}{2}\int \mathrm{d}\boldsymbol{r}\,\mathrm{d}\boldsymbol{r}'\, n(\boldsymbol{r})w(\boldsymbol{r},\boldsymbol{r}')n(\boldsymbol{r}') + E_{xc}[n] + \int \mathrm{d}\boldsymbol{r}\, v_I(\boldsymbol{r})n(\boldsymbol{r}) \tag{2.21}$$

The ground state density $n_I(\boldsymbol{r})$ of the interacting system can be obtained from the Euler equation, [14]

$$\frac{\delta}{\delta n(\boldsymbol{r})}[E_I[n] - \mu_I \int \mathrm{d}\boldsymbol{r}\, n(\boldsymbol{r})] \tag{2.22}$$

$$= \frac{\delta T_{NI}[n]}{\delta n(\boldsymbol{r})} + v_I(\boldsymbol{r}) + \int \mathrm{d}\boldsymbol{r}'\, w(\boldsymbol{r},\boldsymbol{r}')n(\boldsymbol{r}') + v_{xc}([n];\boldsymbol{r}) - \mu_I = 0 \tag{2.23}$$

where

$$v_{xc}([n];\boldsymbol{r}) = \frac{\delta E_{xc}[n]}{\delta n(\boldsymbol{r})}\ .$$

As mentioned before, if there exists the unique external potential $v_{NI}(\boldsymbol{r})$ for a *non-interacting* system corresponding to the ground state density $n_I(\boldsymbol{r})$ of the interacting system, one can find from (2.18) and (2.22) that

$$\begin{aligned} v_{NI}(\boldsymbol{r}) &= v_I(\boldsymbol{r}) + \int \mathrm{d}\boldsymbol{r}'\, w(\boldsymbol{r},\boldsymbol{r}')n(\boldsymbol{r}') + v_{xc}([n];\boldsymbol{r}) - (\mu_I - \mu_{NI}) \\ &= v_I(\boldsymbol{r}) + \int \mathrm{d}\boldsymbol{r}'\, w(\boldsymbol{r},\boldsymbol{r}')n(\boldsymbol{r}') + v_{xc}([n];\boldsymbol{r}) \end{aligned} \tag{2.24}$$

where the arbitrary constant in $v_{NI}(\boldsymbol{r})$ is chosen to cancel out the term $(\mu_I - \mu_{NI})$ and, of course, the potentials on both sides of the equation satisfy the same boundary conditions.

One can finally write down, the Kohn-Sham equations, a set of the self-consistent equations of a *non-interacting* system with $v_{NI}(\boldsymbol{r})$ corresponding to the interacting system.

$$[-\frac{\hbar^2}{2m}\nabla^2 + v_I(\boldsymbol{r}) + \int \mathrm{d}\boldsymbol{r}'\, w(\boldsymbol{r},\boldsymbol{r}')n(\boldsymbol{r}') + v_{xc}([n];\boldsymbol{r})]\phi_i(\boldsymbol{r}) = \epsilon_i\phi_i(\boldsymbol{r}) \tag{2.25}$$

$$n(\boldsymbol{r}) = \sum_i^N |\phi_i(\boldsymbol{r})|^2 \quad \text{for the lowest eigenstates } i = 1, \cdots, N \tag{2.26}$$

These equations are the self-consistent equations in a sense that one can solve (2.25) to obtain the ground state density and the effective single particle potential depends on the density.

2.2.3. Ground state energy of an interacting system

The ground state energy for the Kohn-Sham equations can be easily derived. From (2.25),

$$\epsilon_i = \int \mathrm{d}\boldsymbol{r}\, \phi_i^*(\boldsymbol{r})(-\frac{\hbar^2}{2m}\nabla^2)\phi_i(\boldsymbol{r}) + \int \mathrm{d}\boldsymbol{r}\, |\phi_i(\boldsymbol{r})|^2 v_{NI}(\boldsymbol{r}) \tag{2.27}$$

$$T[n] = \sum_i^N \epsilon_i - \int \mathrm{d}\boldsymbol{r}\, n(\boldsymbol{r}) v_{NI}(\boldsymbol{r}) \tag{2.28}$$

where v_{NI} follows (2.24).

By inserting (2.28) into (2.21), the ground state energy E_g is

$$E_g = \sum_i^N \epsilon_i - \frac{1}{2}\int \mathrm{d}\boldsymbol{r}\, \mathrm{d}\boldsymbol{r}'\, n(\boldsymbol{r})w(\boldsymbol{r},\boldsymbol{r}')n(\boldsymbol{r}') + E_{xc}[n] - \int \mathrm{d}\boldsymbol{r}\, v_{xc}(\boldsymbol{r})n(\boldsymbol{r})\ . \tag{2.29}$$

2.2.4. The chemical potential μ and Fermi surface

The following proof is taken from [13].

With the definition of the energy functional (2.21), equation (2.22) leads to

$$\frac{\delta E_I[n]}{\delta n(\boldsymbol{r})} = \mu_I \tag{2.30}$$

If E_N is the ground state energy and n_N is the ground state density of a N-particle system,

$$\left.\frac{\delta E_I[n]}{\delta n(\boldsymbol{r})}\right|_{n_N} = \mu_I[N] \tag{2.31}$$

Then,

$$\begin{aligned}\frac{\partial E_N}{\partial N} = \lim_{\epsilon\to 0}\frac{E_{N+\epsilon}-E_N}{\epsilon} &= \lim_{\epsilon\to 0}\frac{1}{\epsilon}\int \mathrm{d}\boldsymbol{r}\left.\frac{\delta E_I[n]}{\delta n(\boldsymbol{r})}\right|_{n_N}(n_{N+\epsilon}(\boldsymbol{r})-n_N(\boldsymbol{r}))\\ &= \lim_{\epsilon\to 0}\frac{1}{\epsilon}\int \mathrm{d}\boldsymbol{r}\,\mu_I(N)(n_{N+\epsilon}(\boldsymbol{r})-n_N(\boldsymbol{r}))\\ &= \mu_I(N)\end{aligned}$$

The Lagrangian multiplier, therefore, equals the exact chemical potential of the interacting system.

The eigenvalues of the Kohn-Sham equation are less than or equal to the chemical potential μ. The Kohn-Sham Fermi surface in k space is, thus, defined by $\epsilon_{\text{Fermi}} \equiv \mu$. The Kohn-Sham Fermi surface is, in general, not the same as the physical Fermi surface, which can be found from the Dyson equation, since $v_{eff}(\boldsymbol{r})$ in the Kohn-Sham equation is not the same as the self-energy $\Sigma(\boldsymbol{r},\boldsymbol{r}';\epsilon_i)$ in the Dyson equation. They are, however, identical in the case of a uniform system of interacting particles since the Fermi surface must be spherical no matter what equations are used. Even in the case of a non-uniform system, it turns out that the difference between two Fermi surfaces is small since the electrostatic potential(external and Coulomb potentials) which is the primary term to cause the anisotropy of the Fermi surface is the same for both cases. (See Chapter 2, [14] and section 6.4, [13] for more details.)

2.2.5. Excited states; Eigenvalues in the Kohn-Sham equations

Koopmans' theorem states that the eigenvalue of the eigenstate m in the Hartree-Fock equation is the same as the negative of the energy required to remove the electron in the state m. [15] (This theorem does not apply to small systems. See [15].) It is natural, thus, to think of higher eigenstates in the Kohn-Sham equation as those in the Hartree-Fock equation and obtain excitation energies from the Kohn-Sham equation.

Density functional theory is, however, essentially a ground state and static (frequency-independent) theory, which means that eigenvalues or energy levels of the Kohn-Sham equation do not represent excitation energies which are required to excite electrons. The primary reason is that the effective exchange-correlation potentials must vary in the excited system. (See Section 4, [13].) One can also compare the real eigenvalues of the Kohn-Sham equation with the excitation energies of the Dyson equation. The excitation energies of the Dyson equation are, however, in general complex, which means the finite lifetime, and the real parts are in general different from the eigenvalues of the Kohn-Sham equation as well. [14]

In order to find the excitation energy in the Kohn-Sham scheme, one needs to solve two Kohn-Sham equations and find two self-consistent solutions for the ground state and excited state. In this thesis, the excited states for a hydrogen and a carbon impurity will be examined by varying the number of electrons in the bound states. It is, however, possible to find the approximate excitation energy using Janak's theorem and the Slater transition state [13] and also, for an infinite system, derive a theorem of self-consistent equations similar to Koopmans' theorem (P. 142, [14]).

2.2.6. Spin-polarized systems

If there's an external magnetic field, one generally has to consider the electronic orbital coupling as well as spin coupling. In this thesis, only spin coupling is discussed and the Kohn-Sham equations are derived accordingly.

The external potential term, (2.1), is modified as follows. [13]

$$\hat{V} = \sum_{\sigma_1\sigma_2} \int \mathrm{d}\boldsymbol{r}\, \psi^\dagger_{\sigma_1}(\boldsymbol{r}) \left[v^{\sigma_1}(\boldsymbol{r})\delta_{\sigma_1\sigma_2} + \mu_\mathrm{B}\boldsymbol{B}(\boldsymbol{r}) \cdot \boldsymbol{\sigma}_{\sigma_1\sigma_2}(\boldsymbol{r}) \right] \psi_{\sigma_2}(\boldsymbol{r}) \tag{2.32}$$

where $\mu_\mathrm{B} = e\hbar/2mc$ is the Bohr magneton.

The magnetic moment density operator is defined as

$$\hat{\boldsymbol{m}}(\boldsymbol{r}) = -\mu_\mathrm{B} \sum_{\sigma_1\sigma_2} \psi^\dagger_{\sigma_1}(\boldsymbol{r}) \boldsymbol{\sigma}_{\sigma_1\sigma_2}(\boldsymbol{r}) \psi_{\sigma_2}(\boldsymbol{r}) \tag{2.33}$$

where $\boldsymbol{\sigma}$ denotes the vector of Pauli matrices.

With the density operator

$$\hat{n}(\boldsymbol{r}) = \hat{n}_+(\boldsymbol{r}) + \hat{n}_-(\boldsymbol{r}) = \sum_\sigma \hat{n}_\sigma(\boldsymbol{r}) = \sum_\sigma \psi^\dagger_\sigma(\boldsymbol{r}) \psi_\sigma(\boldsymbol{r}) \ , \tag{2.34}$$

the external potential term can be rewritten as

$$\hat{V} = \int \mathrm{d}\boldsymbol{r}\, \left[v(\boldsymbol{r})\hat{n}(\boldsymbol{r}) - \boldsymbol{B}(\boldsymbol{r}) \cdot \hat{\boldsymbol{m}}(\boldsymbol{r}) \right] \ . \tag{2.35}$$

Now the ground state density $n(\boldsymbol{r})$ and magnetization density $\boldsymbol{m}(\boldsymbol{r})$ is

$$n(\boldsymbol{r}) = \langle \phi | \hat{n}(\boldsymbol{r}) | \phi \rangle \tag{2.36}$$

$$\boldsymbol{m}(\boldsymbol{r}) = \langle \phi | \hat{\boldsymbol{m}}(\boldsymbol{r}) | \phi \rangle \ . \tag{2.37}$$

One can work either with $(n(\boldsymbol{r}), \boldsymbol{m}(\boldsymbol{r}))$ or, equivalently, with the ground spin density matrix $n_{\sigma_1\sigma_2}(\boldsymbol{r}) = \langle \phi | \psi^\dagger_{\sigma_1} \boldsymbol{\sigma}_{\sigma_1\sigma_2}(\boldsymbol{r}) \psi_{\sigma_2}(\boldsymbol{r}) | \phi \rangle$. Note that both cases have four independent real functions.

For simplicity, it is assumed that only a z-component in the external magnetic field $B(\boldsymbol{r})$ and the magnetization $m(\boldsymbol{r})$ have a non-vanishing value. Note that, for a z-component of $m(\boldsymbol{r})$,

$$\boldsymbol{m}(\boldsymbol{r}) = -\mu_{\mathrm{B}}(n_+(\boldsymbol{r}) - n_-(\boldsymbol{r})) \ . \tag{2.38}$$

As in the case of the spin-independent Hohenberg-Kohn theorem, two different non-degenerate ground states lead to two different spin density matrices $n_{ss'}(\boldsymbol{r})$ or, equivalently, to two different sets of $(n(\boldsymbol{r}), \boldsymbol{m}(\boldsymbol{r}))$ or $(n_+(\boldsymbol{r}), n_-(\boldsymbol{r}))$.

Now one can derive the Kohn-Sham equations for a spin-polarized system from the variational principle of the Hohenberg-Kohn theorem as in the spin-independent case, Sec. 2.2.

$$[-\frac{\hbar^2}{2m}\nabla^2 + v_I(\boldsymbol{r}) + \sigma\mu_{\mathrm{B}}B(\boldsymbol{r}) + \int \mathrm{d}\boldsymbol{r}'\, w(\boldsymbol{r},\boldsymbol{r}')n(\boldsymbol{r}') + v_{xc}^{\sigma}([n_+,n_-];\boldsymbol{r})]\phi_i^{\sigma}(\boldsymbol{r}) = \epsilon_i^{\sigma}\phi_i^{\sigma}(\boldsymbol{r}) \tag{2.39}$$

$$n_{\sigma}(\boldsymbol{r}) = \sum_{i}^{N} |\phi_i^{\sigma}(\boldsymbol{r})|^2 \text{ for the lowest eigenstates } i = 1, \cdots, N \tag{2.40}$$

where σ denotes $+$ or $-$ corresponding to the spin projection in the z direction.

The exchange-correlation potential $v_{xc}^{\sigma}([n_+,n_-];\boldsymbol{r})$ is, as in the spin independent case,

$$v_{xc}^{\sigma}([n_+,n_-];\boldsymbol{r}) = \frac{\delta E_{xc}^{\sigma}[n_+,n_-]}{\delta n_{\sigma}(\boldsymbol{r})} \ . \tag{2.41}$$

and the functional $E_{xc}^{\sigma}[n_+,n_-]$ is, as in the spin independent case, given by

$$E_{xc}^{\sigma}[n_+,n_-] = F_{\mathrm{HK}}[n_+,n_-] - \frac{1}{2}\int n(\boldsymbol{r})w(\boldsymbol{r},\boldsymbol{r}')n(\boldsymbol{r}') - T_{NI}[n_+,n_-] \tag{2.42}$$

The ground state energy with an analogy to (2.29) is given by

$$E_g = \sum_{i}^{N}\sum_{\sigma}\epsilon_i^{\sigma} - \frac{1}{2}\int \mathrm{d}\boldsymbol{r}\, n(\boldsymbol{r})w(\boldsymbol{r},\boldsymbol{r}')n(\boldsymbol{r}') + E_{xc}[n_+,n_-] - \sum_{\sigma}\int \mathrm{d}\boldsymbol{r}\, v_{xc}^{\sigma}([n_+,n_-];\boldsymbol{r})n_{\sigma}(\boldsymbol{r}) \ . \tag{2.43}$$

2.2.7. Exchange-correlation; LDA

At this point the only problem in the Kohn-Sham scheme is to find a functional $E_{xc}[n]$ instead of a functional $F_{\mathrm{HK}}[n]$ in the Hohenberg-Kohn theorem.

In this work, the local density approximation(LDA) is used for the exchange-correlation functional $E_{xc}[n]$.

2.2.7.1. A functional

Suppose there is a functional $E[n]$ for a system with a varying electron density. A functional $E[n]$, in general, is nonlocal and, thus, $E[n]$ depends on the whole distribution of the electron density. [16]

If $E[n]$ has the form $E[n] = \int e[n]\,\mathrm{d}\boldsymbol{r}$ where $e[n]$ is a density functional, for a very slowly varying density, $e[n]$ can be expanded in Taylor series in terms of a density gradient.

$$e[n] = e_0(n(\boldsymbol{r})) + e_1(n(\boldsymbol{r}))\nabla n(\boldsymbol{r}) + \cdots \tag{2.44}$$

In LDA, using the first term only, the exchange-correlation functional becomes

$$E_{xc}[n] = \int n(\boldsymbol{r})\epsilon_{xc}(n(\boldsymbol{r}))\,\mathrm{d}\boldsymbol{r} \tag{2.45}$$

where $\epsilon_{xc}(n(\boldsymbol{r}))$ is the exchange-correlation energy per electron for a uniform gas of interacting electrons with density n. [17] The problem is now reduced to finding the exchange-correlation energy in a homogeneous electron gas.

2.2.7.2. Exchange-correlation energy

The energy of the Hartree-Fock model with plane-wave states can be easily obtained using the Slater determinant or using the field operators in the second

quantization notation (Ch. 5, [15]) or the exchange term of the self energy (Ch. 5, [18]) since the Hartree energy is zero. The exchange energy, subtracting the kinetic energy, is given by

$$E_x(k) = -\frac{e^2 k_F}{\pi}\left(1 + \frac{k_F^2 - k^2}{2k_F k}\ln\left|\frac{k_F + k}{k_F - k}\right|\right) \tag{2.46}$$

The average exchange energy contribution per particle to the ground state energy is easily obtained as well (See [15] and [18]). Allowing two electrons (spin-up and spin-down) per state,

$$\epsilon_x = 2\frac{1}{2N}\sum_k n_k E_x(k) = -\frac{3}{4}\frac{e^2 k_F}{\pi} \tag{2.47}$$

The exchange part (called the Kohn-Sham or Gáspár potential [17]) of the chemical potential is, using the Seitz's theorem [18], given by

$$\mu_x = \frac{d}{dn}(n\epsilon_x) = -\frac{e^2}{\pi}k_F = \frac{4}{3}\epsilon_x \tag{2.48}$$

Collecting the kinetic term and the exchange term gives the first two terms for the ground state energy per particle

$$\epsilon_{gs} = \frac{2.2099}{r_s^2} - \frac{0.9163}{r_s} + \cdots \text{ Ryd.} \tag{2.49}$$

where r_s is the Wigner-Seitz radius, defined by $n\frac{4\pi}{3}r_s^3 = 1$.

The exclusion principle in the Hartree-Fock model introduces the strong repulsion between the electrons of parallel spin but the Hartree-Fock model fails to correlate the motion of electrons of antiparallel spin since the electrons of antiparallel spin tends to separate due to the Coulomb repulsion. Now the difference between the exact energy and the Hartree-Fock energy is called the correlation energy and thus one can write

$$\epsilon_{gs} = \frac{2.2099}{r_s^2} - \frac{0.9163}{r_s} + \epsilon_c \text{ Ryd.} \tag{2.50}$$

The high density limit of $r_s \to 0$ for ϵ_c was first given by Gell-Mann and Brueckner (1957) and the same result has been obtained by many other people. Quinn and Ferrell (1958) used the Seitz's theorem to find the correlation energy from the correlation chemical potential μ_c. They found μ_c by calculating the self-energy terms of an electron at the Fermi energy. The exchange-correlation terms in the self-energy can be categorized in the Feynman diagrams by the number of internal Coulomb lines [18]. The exchange energy term has only one Coulomb line. The correlation terms have two or more Coulomb lines. The correlation energy from one of self-energy diagrams was given by Onsager *et al.* (1966), which is 0.0436. The correlation energy in the RPA is

$$\epsilon_c = -0.142 + 0.0622 \ln r_s + \cdots \text{ Ryd.} \tag{2.51}$$

Collecting these terms gives the result, with another term from Carr and Maradudin (1964),

$$\epsilon_c = -0.094 + 0.0622 \ln r_s + 0.018 r_s \ln r_s + \cdots \text{ Ryd.} \tag{2.52}$$

This result gives, however, positive values for low densities ($r_s >\sim 2.5$), which is not correct since the correlation energy must be negative considering the pair distribution function. (The correlation effects lower the energy of an interacting electron system and increases the magnitude of the binding energy.) [18]

Wigner (1934) found that the system with the positive background charge gains energy by localization of electrons. The total energy for a simple system in which there is an electron at the center of a sphere in the unit cell of the lattice (Wigner-Seitz model) and the electric field is zero outside of each sphere due to the uniform positive charge is $\sim -1.8/r_s$. In the low density limit, subtracting the exchange correlation energy $-0.9163/r_s$,

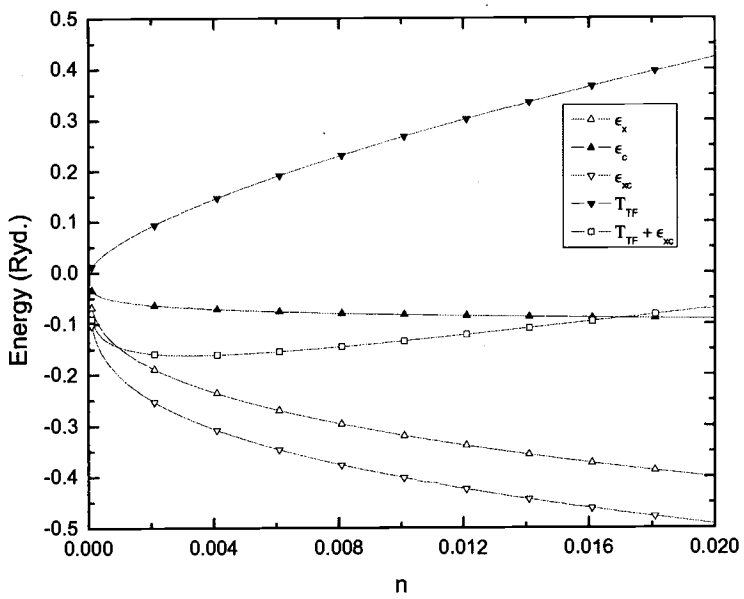

FIGURE 2.1. The exchange ϵ_x , correlation ϵ_c, and Thomas-Fermi kinetic energies $T_{TF} = 2.2099/r_s^2$ per electron from the parametrization of Hedin-Lundqvist.

$$\epsilon_c = -\frac{0.8757}{r_s} \text{ Ryd.} \tag{2.53}$$

Interpolation schemes between these two limits have been made by several people. For instance, Nozières and Pines (1958) recommend, for the range of actual metallic densities, the interpolation result $\epsilon_c \simeq -0.115 + 0.031 \ln r_s$ Ryd.

The correlation energy also can be calculated using dielectric functions for which there are several models such as Thomas-Fermi, RPA, Hubbard, Singwi-Sjölander. The Singwi-Sjölander correlation energy is considered to be the best due to its positive pair distribution function for most densities. [18]

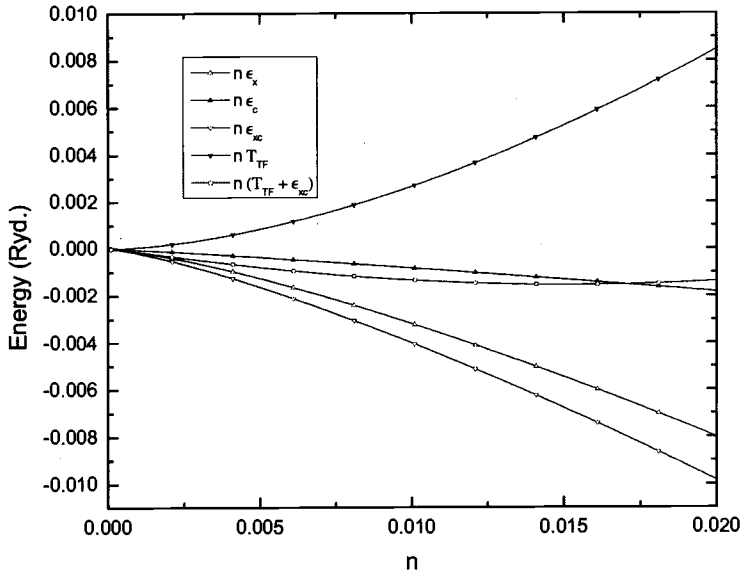

FIGURE 2.2. The exchange ϵ_x , correlation ϵ_c, and Thomas-Fermi kinetic energies $T_{TF} = 2.2099/r_s^2$ multiplied by the electron density n.

2.2.7.3. Interpolation scheme; Spin-independent

In this work, the interpolation scheme by Hedin and Lundqvist (See [17] and [14]) is used. They used a model given by

$$\mu_{xc}(r_s) = \mu_x(r_s) + \mu_c(r_s) = \beta(r_s)\mu_x(r_s) \quad . \tag{2.54}$$

where $\mu_{xc}(r_s)$ is the exchange-correlation contribution to the effective potential v_{eff} and $\beta(r_s)$ is a correlation enhancement factor.

With the expression

$$\beta(r_s) = 1 + Bx \ln\left(1 + \frac{1}{x}\right) \quad , \tag{2.55}$$

one can obtain, using (2.48),

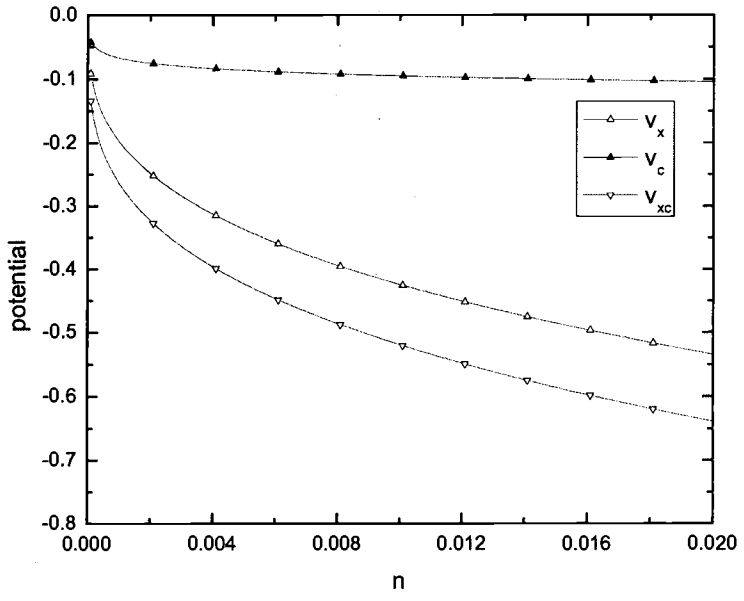

FIGURE 2.3. The exchange v_x and correlation v_c potentials.

$$\mu_c(r_s) = -C \ln\left(1 + \frac{1}{x}\right) \text{ Ryd.} \tag{2.56}$$

$$\epsilon_c(r_s) = -C\left((1+x^3)\ln\left(1+\frac{1}{x}\right) + \frac{x}{2} - x^2 - \frac{1}{3}\right) \text{ Ryd.} \tag{2.57}$$

where $x = r_s/A$ and $C = 2B((9\pi)/4)^{1/3}/\pi A$. The parameters

$$A = 21 \text{ and } C = 0.045 \tag{2.58}$$

are chosen to reproduce the Singwi *et al.* (1970) results for e_{xc}.

Since $\beta(r_s)$ varies from 1.0 to 1.33 for $0 \leq r_s \leq 6$, the exchange effect of ϵ_{xc} dominates the correlation contribution for the range of actual metallic densities. The behavior of the exchange and correlation energies is shown in Fig. 2.1 and Fig. 2.2. The correlation energies are always negative as it should be. A system

of the interacting electrons reaches a lower exchange-correlation energy as the density increases. A simple model, which includes the exchange-correlation and Thomas-Fermi kinetic energy only, as in Fig. 2.2, however, has a minimum energy at $n \simeq 0.015$. One can argue that, if Coulomb effects and the variation of the wave functions are neglected, a system of interacting electrons favors the density $n \simeq 0.015$.

2.2.7.4. Interpolation scheme; Spin-dependent

The LDA can be extended for the spin-polarized case (called the local spin density approximation, LSDA) and, by choosing the z-axis along the local spin direction,

$$E_{xc}[n_+, n_-] = \int \mathrm{d}\boldsymbol{r}\, (n_+(\boldsymbol{r}) + n_-(\boldsymbol{r}))\epsilon_{xc}(n_+(\boldsymbol{r}), n_-(\boldsymbol{r})) \tag{2.59}$$

and the variables are now $n_+(\boldsymbol{r})$ and $n_-(\boldsymbol{r})$ or

$$n(\boldsymbol{r}) = n_+(\boldsymbol{r}) + n_-(\boldsymbol{r})$$
$$\text{and } \zeta(\boldsymbol{r}) = \frac{n_+(\boldsymbol{r}) - n_-(\boldsymbol{r})}{n(\boldsymbol{r})}$$

where ζ describes the degree of local magnetization. For instance, the exchange energy can be, using a simple superposition principle (Ch.5, [13]), written as

$$E_{x,pol}[n, \zeta] = \frac{1}{2}E_x[(1+\zeta)n] + \frac{1}{2}E_x[(1-\zeta)n] \quad ,$$

which can be expanded in a series using a gradient expansion. In lowest order, the exchange energy per particle is

$$\epsilon^0_{x,pol}(\boldsymbol{r}) = \frac{1}{2}[(1+\zeta(\boldsymbol{r}))^{4/3} + (1-\zeta(\boldsymbol{r}))^{4/3}]\epsilon^0_x \tag{2.60}$$

where ϵ^0_x follows the form (2.47).

For the spin-polarized case, there are several parametrizations, such as von Barth and Hedin (1972), Gunnarsson and Lundqvist (1976), and Monte Carlo results of Ceperley and Alder (1980). (See [13] or their papers for more details.) In this work, the parametrization of von Barth and Hedin is used. They used a generalized random phase expression for ϵ_{xc} in terms of the polarization propagator and the two-bubble ring approximation for the irreducible propagator. [19]

The parametrization is based on an interpolation between the paramagnetic(unpolarized, $\zeta = 0$) and the ferromagnetic(fully polarized, $\zeta = \pm 1$) state:

$$\epsilon_{xc}(n(\boldsymbol{r}), \zeta(\boldsymbol{r})) = \epsilon_x(n(\boldsymbol{r}), \zeta(\boldsymbol{r})) + \epsilon_c(n(\boldsymbol{r}), \zeta(\boldsymbol{r})) \tag{2.61}$$

$$\epsilon_i(n(\boldsymbol{r}), \zeta(\boldsymbol{r})) = \epsilon_i(n, \zeta = 0) + (\epsilon_i(n, \zeta = 1) - \epsilon_i(n, \zeta = 0)) f(\zeta(\boldsymbol{r})) \tag{2.62}$$

where i denotes the exchange ($i = x$) or correlation ($i = c$) contribution to the exchange-correlation energy per particle. The interpolation function is:

$$f(\zeta(\boldsymbol{r})) = \frac{(1 + \zeta(\boldsymbol{r}))^{4/3} + (1 - \zeta(\boldsymbol{r}))^{4/3} - 2}{2^{4/3} - 2} \tag{2.63}$$

from which one can obtain again the ζ-dependence of the exchange energy term (2.60). The exchange energy in the paramagnetic limit, $\epsilon_x(n, \zeta = 0)$, is given by (2.47). In the ferromagnetic limit, $\epsilon_x(n, \zeta = \pm 1) = 2^{1/3}\epsilon_x(n, \zeta = 0)$.

The correlation energy follows again the Hedin-Lundqvist form using the parameters

$$\zeta = 0: \quad C^P = 0.0504, \quad A^P = 30$$

$$\zeta = 1: \quad C^F = 0.0254, \quad A^F = 75$$

The exchange-correlation potential can be easily calculated using (2.41) and (2.59).

$$v_{xc}^{\sigma} = \frac{\partial}{\partial n^{\sigma}}((n_+ + n_-)\epsilon_{xc}(n_+, n_-)) \tag{2.64}$$

$$\text{For instance, } v_{xc}^{+} = \epsilon_{xc}(n_+, n_-)) + n\frac{\partial \epsilon_{xc}}{\partial n_+} \tag{2.65}$$

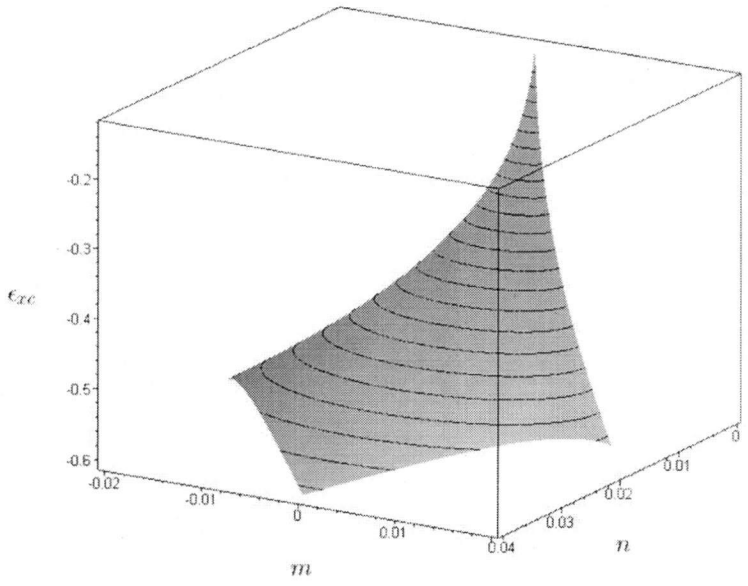

FIGURE 2.4. The exchange-correlation energy per electron ϵ_{xc} from the parametrization of von Barth and Hedin. $m = n\,\zeta$ where n is the total density.

After some algebra,

$$v_{xc}^{+} = (\frac{4}{3}\epsilon_x(n,\zeta=0) + \gamma(\epsilon_c(n,\zeta=\pm 1) - \epsilon_c(n,\zeta=0)))(1+\zeta)^{1/3}$$
$$-C^P \ln\left(1+\frac{A^P}{r_s}\right) - \gamma(\epsilon_c(n,\zeta=\pm 1) - \epsilon_c(n,\zeta=0)) + \tau_c f(\zeta)$$

where $\tau_c = -C^F \ln\left(1+\frac{A^F}{r_s}\right) + C^P \ln\left(1+\frac{A^P}{r_s}\right) - \frac{4}{3}(\epsilon_c(n,\zeta=\pm 1) - \epsilon_c(n,\zeta=0))$ and $\gamma = \frac{4}{3(2^{1/3}-1)}$.

Since the correlation energy for the spin polarized case uses the Hedin-Lundqvist model which is already obtained for the non-spin polarized case (although the coefficients are different) the behavior of e_{xc} and v_{xc} for the spin-polarized case is not much different from those for the non-spin polarized case. (See Fig. 2.4 along $m = 0$.) Note that e_{xc} is the exchange-correlation energy per electron.

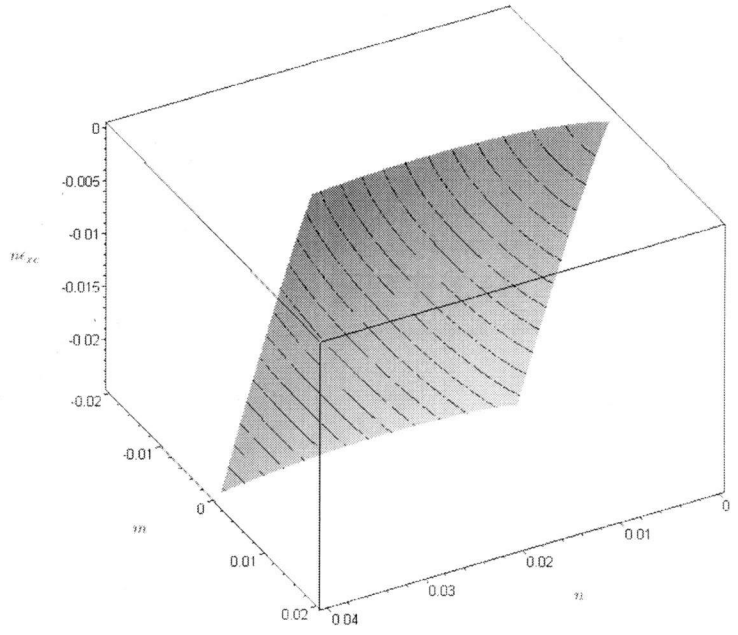

FIGURE 2.5. The exchange-correlation energy $n\epsilon_{xc}$.

The behavior of the correlation effect in a polarized case ($m \neq 0$) is, however, different due to the degree of local magnetization. Notice that the exchange-correlation potential for spin-down has the mirror image of that of spin-up and satisfies the symmetry relation $v_{xc}^{+}(\zeta) = v_{xc}^{-}(-\zeta)$. Along the line $m = n$ (fully polarized limit) in Fig. 2.8 and Fig. 2.9, the exchange potential vanishes and the correlation potential opposes this effect. [13] As a result, the correlation effect reduces the polarization dependence of v_x, which is consistent with the behavior of the pair distribution function. [18]

A system with a uniform density can reach a lower exchange-correlation energy as the magnitude of m increases as shown in Fig. 2.5. The kinetic energy $n \cdot T_{TF}$, however, makes the situation opposite and dominates the exchange-correlation energy especially for high densities. The system reaches a higher energy

due to the term $n \cdot T_{TF}$ as $|m|$ increases in most of the density range.(See Fig. 2.6) One can notice, however, in Fig. 2.7, that for extremely low densities ($n \leq 0.001$) the exchange-correlation energy dominates the kinetic energy $n \cdot T_{TF}$ as $|m|$ increases and thus $n \cdot T_{TF}$ does not keep the system away from a polarized state. The density n at which there's no dominant term between $n \cdot T_{TF}$ and $n \cdot e_{xc}$ and the system is in equilibrium is ~ 0.00153.

One can conclude that the exchange energy favors a spin-polarized solution and the kinetic energy opposes the exchange-correlation effects.

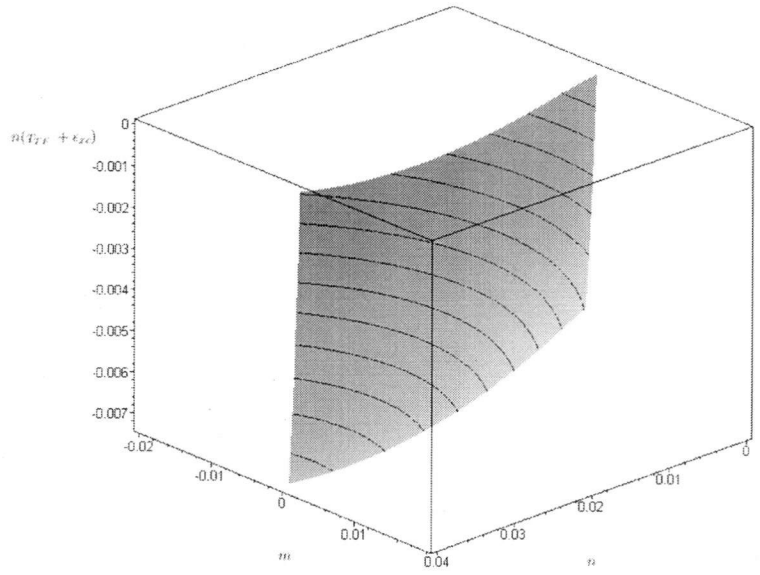

FIGURE 2.6. The exchange-correlation ϵ_{xc} and Thomas-Fermi kinetic energies $T_{TF} = 2.2099/r_s^2$ multiplied by the electron density n.

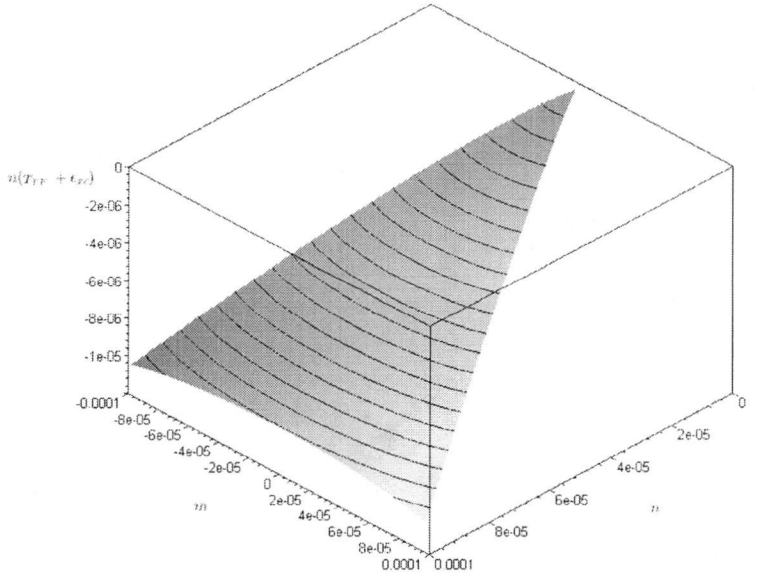

FIGURE 2.7. The exchange-correlation and Thomas-Fermi kinetic energies for extremely low densities.

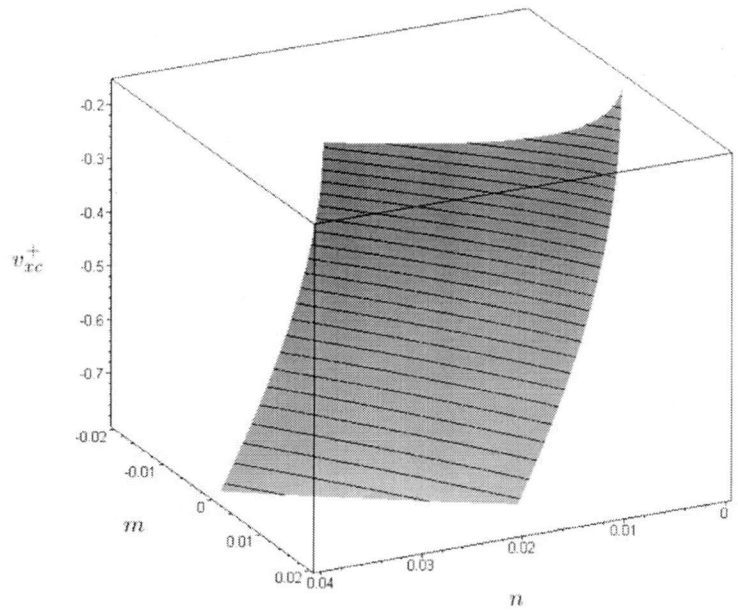

FIGURE 2.8. The exchange-correlation potential v_{xc} for the spin-up density.

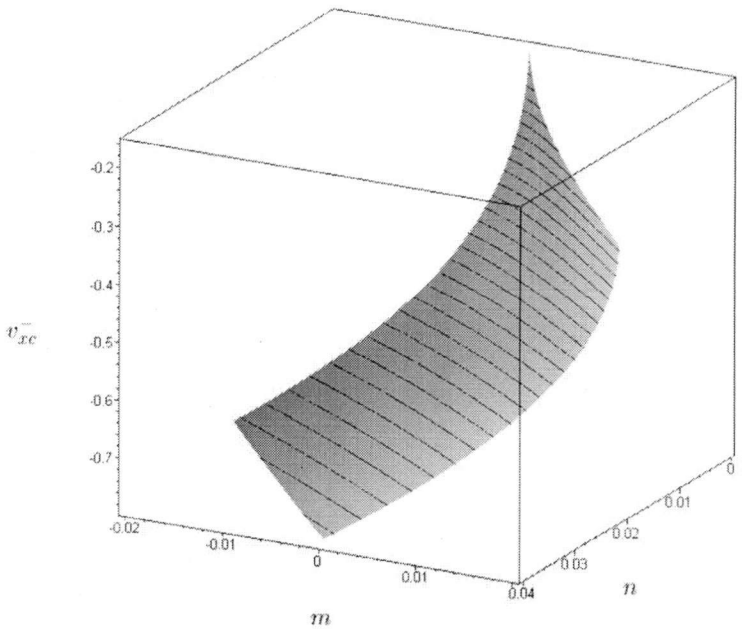

FIGURE 2.9. The exchange-correlation potential v_{xc} for the spin-down density.

3. A MODEL AND ITS PROPERTIES: AN IMPURITY IN A HOMOGENEOUS ELECTRON GAS

Immersion energy calculations for an impurity in a homogeneous electron gas can be simplified using the symmetry of the potentials. Physical quantities, like density of states and phase shifts, are very important in the discussion of theoretical aspects, such as immersion energy calculations and the behavior of an impurity, as well as in the discussion of numerical aspects, such as normalization conditions for scattered wave functions and criteria for the maximum number of angular momentum l for each momentum k. Various aspects of an impurity system can be examined in terms of Friedel oscillations, dielectric functions, virtual bound state resonances, and scattering lengths.

3.1. An impurity in a homogeneous electron gas

The model system used in this work consists of an impurity atom immersed in a homogeneous electron gas with a uniform positive background charge density. (See Fig. 3.1.) This impurity system is neutral and also infinite. The immersion energy is now calculated by subtracting the energies of two isolated systems, an impurity atom and the background, from the impurity system.

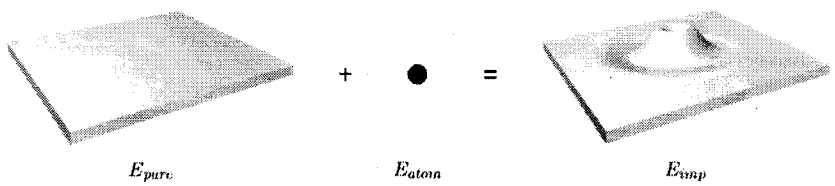

FIGURE 3.1. An impurity system consists of an impurity atom and a homogeneous electron gas. The electron density fluctuates due to the impurity atom.

Atoms	V. B. H.	Experiment[1]	KS-KC[1]	KS-X[1]	HF[1]
Li	−14.710	−14.956	−14.656	−14.349	−14.865
Ne	−256.747	−257.880	−256.349	−254.986	−257.094
K	−1195.943	−1199.97	−1196.215	−1193.387	−1198.329

TABLE 3.1. Energies of free atoms (in Rydbergs).

Atoms	V. B. H.	Experiment[1]	KS-KC[1]	KS-X[1]	HF[1]
Li	0.417	0.396	0.396	0.331	0.393
Ne	1.641	1.585	1.657	1.551	1.461
K	0.347	0.319	0.330	0.271	0.295

TABLE 3.2. Ionization energies of one electron from a neutral atom (in Rydbergs).

$$E_{imm} = E_{imp} - E_{pure} - E_{atom} \tag{3.1}$$

The energy of a free atom E_{atom} is easily calculated by solving the Kohn-Sham equations for bound states. Some examples from this work (V. B. H.), in which spin-polarized and spherically symmetric systems are used, are shown in Table 3.1 and 3.2 and are compared with the results of Tong and Sham [20]. KS-KC denotes the exchange-correlation energy in which the correlation energy is simply interpolated between Gell-Mann and Brueckner and Wigner schemes. KS-K and HF

---

[1]Ref. [20]

denote the exchange energy only ($-\frac{3}{4}\frac{e^2 k_F}{\pi}$) and Hartree-Fock calculations respectively. (See [20] for more details.) Ionization energies can be found by evaluating $E[N] - E[N-1]$, as mentioned in Sec. 2.2.5.

Differences between numerical calculations and experimental values for free atom energies are larger than those for ionization energies. LDA gives relatively large numerical errors for core states such as 1s and 2s states due to the rapid variations in the density. Numerical errors are, however, reduced in ionization energy calculations since core states in $E[N]$ and $E[N-1]$ do not vary much and thus errors are canceled out. The same reasoning applies to immersion energies, which is explained in detail in Sec. 4.4.5.

3.2. Energy calculation

Since this work focuses on spherically symmetric potentials, the Kohn-Sham equations and density and energy calculations can be greatly simplified and the computational work can be reduced using this spherical symmetry. It is, however, important to extend this work to non-spherical systems, since most systems such as molecules and solids have non-spherical potentials and even in the case of a single impurity atom, the electronic structure and immersion energies depend on the non-spherical densities if the angular momentum shell of an impurity atom is not fully occupied and thus the spherical symmetry is broken. Phase shifts are very important quantities used to calculate density of states and energy and also provide boundary conditions for scattered states. In this section, the Kohn-Sham equations for non-spherical potentials are briefly introduced and phase shifts and energy calculations will be reviewed.

3.2.1. Symmetry in potentials and phase shifts

Since angular momentum shells in general have cylindrical symmetry (ϕ symmetry), non-spherical potentials have the same symmetry. (Note that v_{xc} depends on only local density and is ϕ-symmetric. The readers may refer to [21], [9], and [8] for this section.) The Kohn-Sham equations can be simplified accordingly. Therefore, if the input density used to calculate the potentials of the KS equations is ϕ-symmetric, the output density from the KS equations is also ϕ-symmetric since $[H,\ L_z] = 0$ and the iterative procedure of the KS equations does not break the symmetry. The Kohn-Sham equations are, in Rydberg atomic units (APPENDIX B),

$$\left\{-\nabla^2 + V_{eff}(\boldsymbol{r})\right\}\psi_i(\boldsymbol{r}) = \epsilon_i\psi_i(\boldsymbol{r}) \quad . \tag{3.2}$$

The angular dependence of the Kohn-Sham states $\psi_i(\boldsymbol{r})$ can be expanded in terms of spherical harmonics.

$$\psi_i(\boldsymbol{r}) = \sum_{lm} \frac{u_{ilm}(r)}{r} Y_{lm}(\Omega_r) \quad . \tag{3.3}$$

One can express the electronic density $n(\boldsymbol{r})$ as a sum over bound states and scattered states with a reference of zero-energy.

$$\lim_{r\to\infty} V_{eff}(\boldsymbol{r}) = 0 \quad . \tag{3.4}$$

The total density is, as in (2.15),

$$n(\boldsymbol{r}) = n^{\text{bound}}(\boldsymbol{r}) + n^{\text{cond}}(\boldsymbol{r}) = \sum_{i}^{N} |\psi_i^{\text{bound}}(\boldsymbol{r})|^2 + \sum_{j}^{M} |\psi_j^{\text{cond}}(\boldsymbol{r})|^2 \tag{3.5}$$

where i and j are ordering indices for the lowest occupied states, and i in $|\psi_i^{\text{bound}}(\boldsymbol{r})|$ and j in $|\psi_i^{\text{cond}}(\boldsymbol{r})|$ denote the KS states in which $\epsilon_i < 0$ and $\epsilon_j > 0$, respectively.

Note that m is a good quantum number since $[H,\ L_z] = 0$ and the Kohn-Sham equations can be written down for each ϵ_i and m value.

Using (3.3), one obtains coupled equations, similar to radial equations for a spherically symmetric potential,

$$\left\{-\nabla^2 + V_{eff}(\boldsymbol{r})\right\} \sum_{lm} \frac{u_{ilm}(r)}{r} Y_{lm}(\Omega_r) = \epsilon_i \sum_{lm} \frac{u_{ilm}(r)}{r} Y_{lm}(\Omega_r) \quad .$$

by projection onto $Y_{l'm}(\Omega_r)$,

$$\left[\frac{d^2}{dr^2} + \epsilon_i - \frac{l(l+1)}{r^2}\right] u_{ilm}(r) = \sum_{l'} V_{ll'}^m(r) u_{il'm}(r) \quad , \tag{3.6}$$

where

$$V_{ll'}^m(r) = \int \mathrm{d}\boldsymbol{\Omega}\, Y_{lm}^*(\Omega_r) V_{eff}(r,\theta) Y_{l'm}(\Omega_r) \quad . \tag{3.7}$$

Notice that since $V_{eff}(r,\theta)$ does not depend on ϕ, $V_{ll'}^m(r)$ and the solutions in 3.6 are real.

The linearly independent solutions u_{lm}^j (j is a simple ordering index[2] varying from 0 to l_{max}) can be found from coupled equations (3.6) and their behavior at small r is

$$\lim_{r\to 0} u_{lm}^j(r) \sim r^{j+|l-j|+1} \sum_{i=1}^{\infty} b_i^l r^{i-1} \quad , \tag{3.8}$$

which provides the boundary conditions of independent solutions at small r. (See APPENDIX C.)

One can now expand u_{ilm} in terms of linearly independent solutions.

$$u_{ilm}(r) = \sum_j \alpha_j^m u_{ilm}^j(r) \quad , \tag{3.9}$$

---

[2]one has to use the cut-off maximum l_{max} in a computer program.

where the coefficients α_j^m can be determined by the asymptotic behavior of the solutions and do not depend on l but on ϵ_i and m. One can determine α_j^m by boundary conditions, which uniquely determines the radial wave functions $u_{ilm}(r)$ and Kohn-Sham eigenstates $\psi_i(\boldsymbol{r})$. For instance, one has, for bound states, two sets of linearly independent of solutions which are $u_{ilm}^j(r)$ from the outward integration started from the origin and $v_{ilm}^j(r)$ from the inward integration started from the infinity. The asymptotic behavior of $v_{ilm}^j(r)$ is

$$\lim_{r\to\infty} v_{lm}^j(r) \sim \delta_{jl} \exp^{-\sqrt{-\epsilon}r} \quad . \tag{3.10}$$

The condition for the existence of bound states is that the two sets of linearly independent solutions must match at an intermediate r.

$$\sum_j \alpha_j^m u_{ilm}^j(r) = \sum_j \beta_j^m v_{ilm}^j(r) \tag{3.11}$$

$$\sum_j \alpha_j^m \frac{d}{dr} u_{ilm}^j(r) = \sum_j \beta_j^m \frac{d}{dr} v_{ilm}^j(r) \quad . \tag{3.12}$$

Since a nontrivial solution exist only if the determinant of (3.11) is zero, one needs to search for the zeroes of the determinant to find bound states. Notice the Eq. (3.11) becomes the standard Wronskian condition for the spherically symmetric potentials. Once the bound state energy has been determined, one can use the singular value decomposition method (APPENDIX D) to find the eigenfunction $\psi_i(r)$. For scattered states, one can use the asymptotic behavior of the scattered wave function for large r to determine the coefficients α_j^m. Notice that the wave number vector k in $u_{klm}(r)$ also depends on the direction of the incident plane wave, which thus leads to considerably more computational work compared to spherical systems. (The readers refer to [9] and [8] for more details.)

In addition, it is known, in a case of a free atom calculation, that the energy difference between the non-spherical potential and the spherical potential is much smaller than that between the non-spin polarized and spin polarized systems. [22]

A spherical potential can, therefore, be considered the best for a first try and a spin-polarized system with a spherical potential still has many interesting properties. If the potential is spherically symmetric, the angular momentum l is a constant of a motion and also a good quantum number since $[H,\ L^2] = 0$. The eigenenergies do not depend on l and m and eigenstates are degenerate. The coupled equations (3.6) can be simplified to the radial equations.

$$\left[\frac{d^2}{dr^2} + \epsilon_{i,l} - \frac{l(l+1)}{r^2}\right] u_{i,l}(r) = V(r) u_{i,l}(r) \quad . \tag{3.13}$$

For scattered states,

$$\left[\frac{d^2}{dr^2} + k^2 - \frac{l(l+1)}{r^2}\right] u_{k,l}(r) = V(r) u_{k,l}(r) \quad . \tag{3.14}$$

If the potential vanishes for the exterior region $r > R_b$, the solutions for the scattered states in (3.14) follow a form of free particle waves.

$$R_{k,l}(r) = \frac{u_{k,l}(r)}{r} = A_l j_l(kr) + B_l n_l(kr) \qquad r > R_b \tag{3.15}$$

Using the asymptotic approximations [3],

$$\frac{u_{k,l}(r)}{r} = A_l \frac{\sin(kr - l\frac{\pi}{2})}{kr} - B_l \frac{\cos(kr - l\frac{\pi}{2})}{kr} \qquad \text{for } kr \gg l \quad . \tag{3.16}$$

If the potential vanishes at the origin ($r = 0$), B_l must be zero as n_l diverges at the origin. The intensity of scattering by the potential, hence, can be compared with the ratio B_l/A_l. The phase shift δ_l is now defined by

$$\frac{B_l}{A_l} = -\tan\delta_l \quad . \tag{3.17}$$

For large kr, (3.16) can be written as

$$\frac{u_{k,l}(r)}{r} \simeq \frac{\sin(kr - l\frac{\pi}{2} + \delta_l)}{kr} \qquad \text{for } kr \gg l \ , \tag{3.18}$$

from which one can deduce that the quantity δ_l represents the phase difference of the radial wave function between the scattering ($V \neq 0$ and $\delta_l \neq 0$) and the non-scattering ($V = 0$ and $\delta_l = 0$) cases.

The radial-wave solution of a free particle in the scattering case can be rewritten, using (3.17), as

$$R_{k,l}(r) = \frac{u_{k,l}(r)}{r} = e^{i\delta_l}[\cos\delta_{k,l} j_l(kr) - \sin\delta_{k,l} n_l(kr)] \qquad r > R_b \ , \tag{3.19}$$

where the normalization constant is chosen so that $R_{k,l}(r)$ is $j_l(kr)$ for $V = 0$.

Note that the wave function for $r > R_b$ is [23]

$$\psi_{\boldsymbol{k}}(r) = \frac{1}{(2\pi)^{3/2}} \sum_{l=0}^{\infty} (2l+1) R_{k,l}(r) P_l(\cos\theta) \qquad r > R_b \tag{3.20}$$

and thus the electronic density is

$$n(r) = \frac{2}{(2\pi)^3} \int_0^{k_F} \mathrm{d}\boldsymbol{k}\, (|\psi_{\boldsymbol{k}}(\boldsymbol{r})|^2 \tag{3.21}$$

$$= \frac{8\pi}{(2\pi)^3} \sum_l (2l+1) \int_0^{k_F} \mathrm{d}k\, k^2 (R_{k,l}(r))^2 \ . \tag{3.22}$$

The boundary condition for the interior radial wave function ($r < R_b$) is the logarithmic derivative at the boundary.

$$\left(\frac{1}{R^{\text{int}}_{k,l}} \frac{dR^{\text{int}}_{k,l}}{dr} \right)_{r=R_b} = \left(\frac{1}{R^{\text{ext}}_{k,l}} \frac{dR^{\text{ext}}_{k,l}}{dr} \right)_{r=R_b} \tag{3.23}$$

where $R^{\text{int}}_{k,l}$ is a interior radial wave function and $R^{\text{ext}}_{k,l}$ a exterior radial wave function which is given by (3.15).

One can easily obtain, using the phase shift definition (3.17),

$$\tan\delta_l = \frac{kR_b j_l'(kR_b) u_{k,l}(R_b) + j_l(kR_b) u_{k,l}(R_b) - R_b j_l(kR_b) u'_{k,l}(R_b)}{kR_b n_l'(kR_b) u_{k,l}(R_b) + n_l(kR_b) u_{k,l}(R_b) - R_b n_l(kR_b) u'_{k,l}(R_b)} \tag{3.24}$$

where $u_{k,l}(r)$ is a interior solution (for $r < R_b$).

Once the radial equations (3.14) for $r < R_b$ are solved, the phase shift can be obtained by (3.24) and normalization of the radial wave function can be performed by (3.19). For very small kr, one can use the asymptotic approximations[3] again and obtain the expression

$$\tan \delta_l \rightarrow a_l k^{2l+1} \qquad \text{as } k \rightarrow 0 \ . \tag{3.25}$$

For s-waves, this equation becomes

$$\tan \delta_0 \simeq \delta_0 \rightarrow a_0 k \qquad \text{as } k \rightarrow 0 \ . \tag{3.26}$$

One sees that the scattering length[4] a_0 is a slope of $\delta_0(k)$ for small k values, which can be used to determine whether the potential is attractive or repulsive and also to determine the required interval of a k-mesh [5] for small k values. If there's a virtual bound state (scattering resonance) around the bottom of conduction band, the scattering length will be very large due to the large density of induced states for small k values. In this case, one needs to use a corresponding very small interval in a k-mesh around $k = 0$.

---

[3] $r \rightarrow 0$, $krj_l(kr) \simeq (kr)^{l+1}/(\Pi_{i=0}^{l} 2i+1)$ and $-krn_l(kr) \simeq (\Pi_{i=0}^{l-1} 2i+1)/(kr)^l$,
$r \rightarrow \infty$, $krj_l(kr) \simeq \sin(kr - l\pi/2)$ and $-krn_l(kr) \simeq \cos(kr - l\pi/2)$.

[4] a_1 is called the scattering volume.

[5] In the computer program, one has to use discrete values of k for the continuum states $k = 0 \cdots k_F$ and the interval between k values affects the numerical precision of integration in k-space. The larger the magnitude of a_0 is , the smaller the interval between small k values is.

3.2.2. Density of induced states in terms of phase shifts

The density of induced states can easily derived from the phase shifts as follows. [18] If one can assume all charges are contained in a very large sphere of radius R_0 ($V(R_0) \rightarrow \infty$), the radial wave functions for scattered states must vanish at $r = R_0$. The asymptotic approximations[3] can be used again due to the large R_0 and one can obtain, using (3.16), boundary conditions for free particle states and for scattered states. For free particle states,

$$kR_0 - \frac{l\pi}{2} = n_f\pi$$

and for scattered states,

$$kR_0 - \frac{l\pi}{2} + \delta_{l,m}(k) = n_s\pi \quad .$$

One can assume that k is continuous due to a very large radius R_0 ($kR_0 \gg l$) and obtain the number of induced states per k, $\triangle D(k)$,

$$\triangle D(k)dk = \frac{d(n_s - n_f)}{dk}dk = \frac{1}{\pi}\sum_{l,m,\sigma}\frac{d\delta^{\sigma}_{l,m}(k)}{dk}dk \quad , \tag{3.27}$$

where $\frac{d\delta_{l,m}(k)}{dk}$ is summed over l, m, and σ to include the degenerate states.

3.2.3. Immersion energies

If E_{atom} is given in the immersion equation (3.1), the only term which one needs to find is $E_{imp} - E_{pure}$. This is composed of the induced kinetic energy, the electrostatic energy, and the exchange-correlation energy.

$$E_{imp} - E_{pure} = \triangle T + \triangle C + \triangle E_{xc} \tag{3.28}$$

1. The kinetic energy $\triangle T$

The kinetic energy which is similar to (2.28) can be written as

$$\begin{aligned}\triangle T &= \sum_i^N \epsilon_i - \int \mathrm{d}\boldsymbol{r}\, n(\boldsymbol{r}) v_{eff}(\boldsymbol{r}) \\ &= \triangle T^{\text{bound}} + \triangle T^{\text{cond}} \\ &= \sum_i^N \epsilon_i - \left(\int \mathrm{d}\boldsymbol{r}\, n^{\text{bound}}(\boldsymbol{r}) v_{eff}(\boldsymbol{r}) + \int \mathrm{d}\boldsymbol{r}\, n^{\text{cond}}(\boldsymbol{r}) v_{eff}(\boldsymbol{r}) \right) ,\end{aligned}$$

where i includes the spin s and *bound* and *cond* denote bound states and scattered states respectively.

For bound states,

$$\triangle T^{\text{bound}} = \sum_i^N \epsilon_i - \int \mathrm{d}\boldsymbol{r}\, n^{\text{bound}}(\boldsymbol{r}) v_{eff}(\boldsymbol{r}) , \tag{3.29}$$

where i is only for the occupied bound states.

Similarly, for scattered states, since k is continuous,

$$\triangle T^{\text{cond}} = \int_0^{k_F} k^2 \triangle D(k)\, dk - \int \mathrm{d}\boldsymbol{r}\, n^{\text{cond}}(\boldsymbol{r}) v_{eff}(\boldsymbol{r}) , \tag{3.30}$$

where $\triangle D(k)$ is the number of states per k induced by the potential v_{eff}. The first term can be rewritten, using (3.27) and $E = k^2$, as

$$\int_0^{k_F} k^2 \triangle D(k)\, dk = \frac{1}{\pi} \int_0^{k_F} k^2 \sum_{l,m,\sigma} \frac{d\delta^\sigma_{l,m}(k)}{dk} \mathrm{d}k \tag{3.31}$$

$$= \frac{1}{\pi} \sum_{l,m,\sigma} \int_0^{E_F} E \frac{d\delta^\sigma_{l,m}(E)}{dE} \mathrm{d}E \tag{3.32}$$

$$= \frac{1}{\pi} \sum_{l,m,\sigma} E_F \delta^\sigma_{l,m}(E_F) - \frac{1}{\pi} \sum_{l,m,\sigma} \int_0^{E_F} \delta^\sigma_{l,m}(E)\, \mathrm{d}E \tag{3.33}$$

where E_F is the Fermi energy which is k_F^2. Adding the kinetic energies for the bound and scattered states together,

$$\Delta T = \sum_i^N \epsilon_i - \int \mathrm{d}\boldsymbol{r}\, n(\boldsymbol{r}) v_{eff}(\boldsymbol{r}) + \frac{1}{\pi}\sum_{l,m,\sigma} E_F \delta^{\sigma}_{l,m}(E_F) - \frac{1}{\pi}\sum_{l,m,\sigma}\int_0^{E_F} \delta^{\sigma}_{l,m}(E)\,\mathrm{d}E \tag{3.34}$$

Note that the first term in (3.33) is the energy, $E_F Z$, required to add the extra Z electrons to the system, which is easily verified by the Friedel sum rule (See (3.45).) and the second term is the kinetic energy caused by the interaction between an impurity and an electron gas in a metal.

2. The electrostatic energy ΔC

Since the Hartree energy of the background system which has a uniform density n_0 is zero, one can write the Coulomb energy as

$$\Delta C = \frac{1}{2}e^2 \int \mathrm{d}\boldsymbol{r}\,\mathrm{d}\boldsymbol{r}' \frac{\Delta n(\boldsymbol{r})\Delta n(\boldsymbol{r}')}{|\boldsymbol{r}'-\boldsymbol{r}|} - e\int \mathrm{d}\boldsymbol{r}\,\Delta n(\boldsymbol{r}) V_{\text{ext}}(\boldsymbol{r}) \tag{3.35}$$

$$= e^2 \int \mathrm{d}\boldsymbol{r}\left(\frac{1}{2}\int \mathrm{d}\boldsymbol{r}' \frac{\Delta n(\boldsymbol{r}')}{|\boldsymbol{r}'-\boldsymbol{r}|} - \frac{Z}{r}\right)\Delta n(\boldsymbol{r}) \quad , \tag{3.36}$$

where $\Delta n(\boldsymbol{r}) = n(\boldsymbol{r}) - n_0(\boldsymbol{r})$ and the second term $(\frac{eZ}{r})$ is the external potential due to the nucleus of an impurity atom. However, this can be further simplified using [24]

$$\int \mathrm{d}\boldsymbol{r}' \frac{1}{|\boldsymbol{r}-\boldsymbol{r}'|} = \sum_{l=0}^{\infty} \frac{r_<^l}{r_>^{l+1}} \int P_l(\cos\theta) r'^2\,\mathrm{d}r' \sin\theta \mathrm{d}\theta \mathrm{d}\phi \tag{3.37}$$

$$= 2\pi \int_{r_0}^{R_b} \mathrm{d}r'\, r'^2 \sum_{l=0}^{\infty} \frac{r_<^l}{r_>^{l+1}} \int_{-1}^{1} P_l(x)\mathrm{d}x \tag{3.38}$$

where θ is the angle between $\boldsymbol{r}$ and $\boldsymbol{r}'$ and $P_l(x)$ are the Legendre polynomials. Using the fact that $P_0(x) = 1$ and $\int_{-1}^{1} \mathrm{d}x\, P_l(x) P_0(x) = 2 \cdot \delta_{l,0}$,

$$\int \mathrm{d}\boldsymbol{r}' \frac{1}{|\boldsymbol{r}-\boldsymbol{r}'|} = 4\pi \left[\frac{1}{r}\int_{r_0}^{r} r'^2\,\mathrm{d}r' + \int_r^{R_b} r'\,\mathrm{d}r'\right] \quad . \tag{3.39}$$

Finally,

$$\Delta C = 4\pi \int_{r_0}^{R_b} r\Delta n(r) \times e^2 \left[2\pi \int_{r_0}^{r} \Delta n(r') r'^2 \, \mathrm{d}r' + 2\pi r \int_{r}^{R_b} \Delta n(r') r' \, \mathrm{d}r' - Z \right] \mathrm{d}r \quad . \quad (3.40)$$

3. The exchange-correlation energy ΔE_{xc}

   The exchange-correlation energy for non-spin-polarized systems is simply $E_{xc}[n] - E_{xc}[n_0]$, in which n_0 is the background electron density and $E_{xc}[n] = \int \mathrm{d}\boldsymbol{r}\, n(\boldsymbol{r}) \epsilon_{xc}(n(\boldsymbol{r}))$.

   The exchange-correlation energy for spin-polarized systems can be written as

$$\Delta E_{xc} = E_{xc}[n^+, n^-] - E_{xc}[n_0^+, n_0^-] \quad \text{for spin-up} \quad (3.41)$$

$$+ E_{xc}[n^-, n^+] - E_{xc}[n_0^-, n_0^+] \quad \text{for spin-down,} \quad (3.42)$$

   where n^+ is the spin-up density and n^- is the spin-down density.

Now, the immersion energy is

$$\begin{aligned} E_{imm} = & \sum_i^N \epsilon_i - \int \mathrm{d}\boldsymbol{r}\, n(\boldsymbol{r}) v_{eff}(\boldsymbol{r}) \\ & + \frac{1}{\pi} \sum_{l,m,\sigma} E_F \delta_{l,m}^{\sigma}(E_F) - \frac{1}{\pi} \sum_{l,m,\sigma} \int_0^{E_F} \delta_{l,m}^{\sigma}(E) \, \mathrm{d}E \\ & + 4\pi e^2 \int_{r_0}^{R_b} r\Delta n(r) \left[2\pi \int_{r_0}^{r} \Delta n(r') r'^2 \, \mathrm{d}r' + 2\pi r \int_{r}^{R_b} \Delta n(r') r' \, \mathrm{d}r' - Z \right] \mathrm{d}r \\ & + E_{xc}[n^+, n^-] - E_{xc}[n_0^+, n_0^-] \\ & + E_{xc}[n^-, n^+] - E_{xc}[n_0^-, n_0^+] - E_{atom} \end{aligned} \quad (3.43)$$

Note that the effective potential energy is, by (2.24) and (3.39),

$$\begin{aligned} eV_{eff}(r) = & 4\pi e^2 \left[\frac{1}{r} \int_{r_0}^{r} \Delta n(r') r'^2 \, \mathrm{d}r' + \int_{r}^{R_b} \Delta n(r') r' \, \mathrm{d}r' \right] \\ & - \frac{e^2 Z}{r} + v_{xc}(n(r)) - v_{xc}(n_0) \end{aligned} \quad (3.44)$$

3.3. Friedel sum rule and Friedel oscillations

Two important phenomena in many-body problems are the screening of an impurity atom in an electron gas and the oscillatory behavior of the electron density in the vicinity of an impurity atom. [10] [11] [12]

The number of induced electrons due to an impurity atom can be easily obtained using (3.27).

$$\Delta N = Z = \int_0^{k_F} \mathrm{d}k \, \Delta D(k) = \int_0^{k_F} \mathrm{d}k \, \frac{1}{\pi} \sum_{l,m,\sigma} \frac{\delta_{l,m}^{\sigma}(k)}{dk} = \frac{2}{\pi} \sum_{l} (2l+1)\delta_l(k_F) \quad , \quad (3.45)$$

where Z is the positive valence on an impurity, the factor of 2 is the spin degeneracy σ, and $(2l+1)$ is the orbital degeneracy related to m. This relation is called the Friedel sum rule and states that the displaced electronic charge $\Delta N \cdot e$ exactly cancels the charge $Z \cdot |e|$ of the impurity and that the Coulomb potential of $1/r$ becomes a screened potential with the density of the screening electrons determined in a self-consistent way. It should be noted that if an impurity atom has one electron in bound states and thus has an excess valency $Z-1$, one has to remove the contribution δ/π of the single bound state on the right-hand side of (3.45). The value of the phase shift δ for a bound state should be π to be consistent. [15] This is actually another statement of Levinson's theorem.

In order to see how the density varies at large distances (Friedel oscillations), one needs to take the asymptotic limit. (See Sec. 3.2.1, [15], and [18].) Since the radial wave function of free particles depends on only $j_l(kr)$) as mentioned in Sec. 3.2.1,

$$n(r) - n_0 = \Delta n(r) = \frac{2}{(2\pi)^3}\int_0^{k_F} \mathrm{d}\boldsymbol{k}\,(|\psi_{\boldsymbol{k}}(\boldsymbol{r})|^2 - |\phi_{\boldsymbol{k}}(\boldsymbol{r})|^2) \tag{3.46}$$

$$= \frac{8\pi}{(2\pi)^3}\sum_l (2l+1)\int_0^{k_F} \mathrm{d}k\, k^2(\frac{(u_{\boldsymbol{k},l}(r))^2}{r^2} - (j_l(kr))^2) \tag{3.47}$$

$$\lim_{r\to\infty}\Delta n(r) = \frac{1}{\pi^2 r^2}\sum_l (2l+1)\int_0^{k_F} \mathrm{d}k\,(\sin^2(kr+\delta_l(k)-l\pi/2) - (\sin^2(kr-l\pi/2) \tag{3.48}$$

$$= \frac{1}{\pi^2 r^2}\sum_l (2l+1)\int_0^{k_F} \mathrm{d}k\,\frac{1}{2}(\cos(2kr-l\pi) - (\cos(2kr+2\delta_l(k)-l\pi)\ , \tag{3.49}$$

where the normalization constant for radial solutions $\frac{u_{\boldsymbol{k},l}(r)}{r}$ is chosen as in (3.19).

Notice that one can use (3.47) to find the density difference for scattered states numerically.

Approximately using $\delta_l(k) = \delta_l(k_F) + (k-k_F)(d\delta/dk)$, [18]

$$\lim_{r\to\infty}\Delta n(r) \simeq \frac{(-1)^l}{2\pi^2 r^2}\sum_l (2l+1)$$

$$\times \int_0^{k_F} \mathrm{d}k\,\left[\cos(2kr) - \cos(2kr+2\delta_l(k_F) + 2(k-k_F)\frac{d\delta}{dk})\right] \tag{3.50}$$

$$\simeq \frac{(-1)^l}{4\pi^2 r^3}\sum_l (2l+1)\,[\sin(2k_F r) - (\sin(2k_F r + 2\delta_l(k_F)))] \tag{3.51}$$

$$\simeq -\frac{(-1)^l}{4\pi^2 r^3}\sum_l 2(2l+1)\sin(\delta_l(k_F))\cos(2k_F r + \delta_l(k_F)) + O(\frac{1}{r^4}) \tag{3.52}$$

The electronic density difference at large distances oscillates with the wave number $2k_F$ and decreases as r^{-3}. The Friedel's theorem is independent of the nature of the impurity atom and the impurity determines only the values of phase shifts. [18] The wave length $\lambda \sim \pi/k_F$ is thus frequently used to verify the numerical results as in Ch. 4 and 5.

3.4. Dielectric functions

The screening of the Coulomb potential of an impurity and the behavior of the induced electronic density can be derived using dielectric functions as well. [15]

[18] It is convenient to define the dielectric functions using potentials since one has to use potentials in the Kohn-Sham equations and the Fourier components of the potential are easily calculated numerically. The dielectric function can be found in the usual definition,

$$E_{\boldsymbol{q}} + 4\pi P_{\boldsymbol{q}} = D_{\boldsymbol{q}} = \epsilon(w, \boldsymbol{q}) E_{\boldsymbol{q}} \quad , \tag{3.53}$$

where $E_{\boldsymbol{q}}$ is the longitudinal electric field. If one writes the effective potential V^{eff} as the external potential V^{ext} plus the induced potential V^{ind}, $V^{eff} = V^{ext} + V^{ind}$, using $eE_q = -iqV_q$, one can obtain from (3.53)

$$V^{eff}_{\boldsymbol{q}} - V^{ind}_{\boldsymbol{q}} = V^{ext}_{\boldsymbol{q}} = \epsilon(w, \boldsymbol{q}) V^{eff}_{\boldsymbol{q}} \tag{3.54}$$

$$\epsilon(w, \boldsymbol{q}) = \frac{V^{ext}_{\boldsymbol{q}}}{V^{eff}_{\boldsymbol{q}}} \quad . \tag{3.55}$$

Note that $P_q = -E^{ind}_q / 4\pi$. Since the dielectric function is calculated as the ratio of the external potential to the effective potential, one can estimate the response of an electron gas due to an impurity atom, which is very important in a sense that one needs to determine the stability of the self-consistent procedure for a particular impurity atom. (See Sec. 4.2.)

If the charge of the impurity is Z, the external potential becomes

$$\frac{Z}{r} = \frac{1}{(2\pi)^3} \int \mathrm{d}\boldsymbol{q}\, e^{i\boldsymbol{q}\cdot\boldsymbol{r}} \frac{Z 4\pi}{q^2} \quad . \tag{3.56}$$

The effective potential in the linear response region is

$$V^{eff}(\boldsymbol{r}, w) = \frac{1}{(2\pi)^3} \int \mathrm{d}\boldsymbol{q}\, e^{i\boldsymbol{q}\cdot\boldsymbol{r}} V^{eff}(w, \boldsymbol{q}) \tag{3.57}$$

$$= \frac{1}{(2\pi)^3} \int \mathrm{d}\boldsymbol{q}\, e^{i\boldsymbol{q}\cdot\boldsymbol{r}} \frac{V^{ext}(w, \boldsymbol{q})}{\epsilon(w, \boldsymbol{q})} \tag{3.58}$$

$$= \frac{1}{(2\pi)^3} \int \mathrm{d}\boldsymbol{q}\, e^{i\boldsymbol{q}\cdot\boldsymbol{r}} \frac{Z 4\pi}{q^2 \epsilon(w, \boldsymbol{q})} \quad . \tag{3.59}$$

Density functional theory is essentially a static theory and further more if the impurity is stationary, one can use $w = 0$. The Poisson equation is

$$\nabla^2 V^{eff}(\boldsymbol{r}) = -4\pi[\Delta n(\boldsymbol{r}) + Z\delta(\boldsymbol{r})] \ , \tag{3.60}$$

where $\Delta n(\boldsymbol{r})$ is the charge induced by $Z\delta(\boldsymbol{r})$. The screening electronic density is now

$$\Delta n(\boldsymbol{r}) = \frac{Z}{(2\pi)^3} \int \mathrm{d}\boldsymbol{q}\, e^{i\boldsymbol{q}\cdot\boldsymbol{r}} \left(\frac{1}{\epsilon(0,\boldsymbol{q})} - 1 \right) \ . \tag{3.61}$$

One notices that if there is a singularity in the dielectric constant, the screening electronic density will be oscillating as the Friedel oscillations.

The total induced charge is

$$\Delta N = \int \mathrm{d}\boldsymbol{r}\, \Delta n(\boldsymbol{r}) = \frac{Z}{(2\pi)^3} \int \mathrm{d}\boldsymbol{q}\, \mathrm{d}\boldsymbol{r}\, e^{i\boldsymbol{q}\cdot\boldsymbol{r}} \left(\frac{1}{\epsilon(0,\boldsymbol{q})} - 1 \right) \tag{3.62}$$

$$= Z \int \mathrm{d}\boldsymbol{q}\, \delta(\boldsymbol{q}) \left(\frac{1}{\epsilon(0,\boldsymbol{q})} - 1 \right) \tag{3.63}$$

$$= Z \left(\frac{1}{\epsilon(0,0)} - 1 \right) \tag{3.64}$$

If one use the Thomas-Fermi dielectric constant for $\epsilon(0,\boldsymbol{q})$ ([15], [18], and [25]),

$$\epsilon_{TF}(0,\boldsymbol{q}) = \frac{q^2 + k_s^2}{q^2} \tag{3.65}$$

$$\Delta N = Z \left(\frac{1}{\epsilon_{TF}(0,0)} - 1 \right) = -Z \ , \tag{3.66}$$

where $k_s^2 = \frac{4e^2 m k_F}{\hbar^2 \pi} = 4.6/r_s$ and r_s is the Wigner-Seitz radius. The Thomas-Fermi dielectric constant shows the correct Friedel sum rule result but does not include the Friedel oscillations. The effective potential screened by the electron gas is

$$V^{eff}(\boldsymbol{r}, w) = \frac{1}{(2\pi)^3} \int \mathrm{d}\boldsymbol{q}\, e^{i\boldsymbol{q}\cdot\boldsymbol{r}} \frac{Z4\pi}{q^2} \frac{q^2}{q^2 + k_s^2} \tag{3.67}$$

$$= \frac{Z}{r} e^{-k_s r} \ . \tag{3.68}$$

Note that this potential is also exactly the same as the Yukawa potential. The screening length is defined by (3.67) as $l_s = 1/k_s \sim r_s^{1/2}$.

The Lindhard dielectric constant (at $T = 0$) can be derived by the self-consistent field [15] or RPA approximations [18] or straightforward calculations [25]. The dielectric constant in the Lindhard theory is

$$\epsilon_{Lin}(\boldsymbol{q}) = 1 + \frac{4\pi}{q^2}\frac{e^2 m k_F}{2\hbar^2\pi^2}\left[1 + \frac{4k_F^2 - q^2}{4qk_F}\ln\left|\frac{q+2k_F}{q-2k_F}\right|\right] \tag{3.69}$$

Note that the Lindhard dielectric constant is not analytic at $q = 2k_F$, which results in that the induced density and the screened effective potential of an impurity charge oscillate as $\frac{1}{r^3}\cos 2k_F r$. The Friedel's theorem has been verified again with dielectric constants. The limit of the Lindhard dielectric constant as $q \to 0$ is just the Thomas-Fermi dielectric constant. As one can notice, the dielectric constant is in general getting close to 1 as q increases, which means the effective potential at high q's will be almost same as the external potential and thus the induced density at high q's does not contribute much. However, if there is a virtual bound state at high q values, one can see a small peak in the dielectric function at corresponding q values since there's a contribution of the induced density at the q values to the dielectric constant. (see Ch. 5.)

3.5. Virtual bound state resonance

If an impurity atom has bound states, the electrons in bound states will be localized in the vicinity of the impurity ion. If the attractive effective potential of the impurity is reduced or not sufficiently strong enough to have a bound state, the bound state will be merged into the conduction band in a metal. In this case, the electrons with positive energy relative to the bottom of the conduction band still tend to localize around the impurity ion and induce a narrow peak in the density

of states of the conduction band, which is called a virtual bound state resonance. A virtual bound state can be seen very well in the non-interacting Anderson model by calculations of density of states using Green's functions. [26] The Hamiltonian takes the form, in the non-interacting Anderson model,

$$H = \sum_{\sigma} \epsilon_d c^{\dagger}_{d,\sigma} c_{d,\sigma} + \sum_{\boldsymbol{k},\sigma} \epsilon_{\boldsymbol{k}} c^{\dagger}_{\boldsymbol{k},\sigma} c_{\boldsymbol{k},\sigma} + \sum_{\boldsymbol{k},\sigma} (V_{\boldsymbol{k}} c^{\dagger}_{d,\sigma} c_{\boldsymbol{k},\sigma} + V^{*}_{\boldsymbol{k}} c^{\dagger}_{\boldsymbol{k},\sigma} c_{d,\sigma}) \ , \tag{3.70}$$

where $V_{\boldsymbol{k}}$ is an overlap matrix element between the atomic d level of the impurity ion and the conduction electrons and ϵ_d is the energy of the d level of the impurity. By taking appropriate matrix elements of $(\epsilon \pm is - H)G^{\pm}(\epsilon) = I$, one can find the coupled equations of Green's functions, which lead to the T matrix element by comparing with the expression $G^{+} = G^{+}_{0} + G^{+}_{0} T(\epsilon^{+}) G^{+}_{0}$. Note that $\epsilon^{\pm} = \epsilon \pm is$.

$$\langle \boldsymbol{k}|T(\epsilon)|\boldsymbol{k}'\rangle = V^{*}_{\boldsymbol{k}} G^{+}_{d,d}(\epsilon) V_{\boldsymbol{k}'} \ , \tag{3.71}$$

where

$$G^{+}_{d,d}(\epsilon) = \frac{1}{\epsilon + is - \epsilon_d - \sum_{\boldsymbol{k}} \frac{|V_{\boldsymbol{k}}|^2}{\epsilon + is - \epsilon_{\boldsymbol{k}}}} \ . \tag{3.72}$$

One can find the phase shift from T matrix element using the prescription $\lim_{s \to +0} \frac{1}{x - is} = \mathrm{P}\frac{1}{x} + i\pi\delta(x)$.

$$\delta(\epsilon) = \ \arg \det T(\epsilon^{+}) \tag{3.73}$$

$$= \frac{\pi}{2} - \tan^{-1}\left(\frac{-\epsilon + \epsilon_d + \Lambda(\epsilon)}{\Delta(\epsilon)}\right) \tag{3.74}$$

where

$$\Lambda(\epsilon) = \mathrm{P}\sum_{\boldsymbol{k}} \frac{|V_{\boldsymbol{k}}|^2}{\epsilon - \epsilon_{\boldsymbol{k}}}, \qquad \Delta(\epsilon) = \pi \sum_{\boldsymbol{k}} |V_{\boldsymbol{k}}|^2 \delta(\epsilon - \epsilon_{\boldsymbol{k}}) \ . \tag{3.75}$$

One can derive the density of states $\rho(\epsilon)$ from the expression of the Green's function $\rho(\epsilon) = \mp\frac{1}{\pi}\mathrm{Im}\mathrm{Tr}G^{\pm}(\epsilon)$ [26] or from the Friedel sum rule (3.45). The density of state induced by the impurity is given by

$$\Delta\rho(\epsilon) = \frac{1}{\pi}\frac{d\delta(\epsilon)}{d\epsilon} \quad , \tag{3.76}$$

where $\delta(\epsilon) = 2\sum_l (2l+1)\delta_l(\epsilon)$ for spherically symmetric potentials. If one tries to find $\Lambda(\epsilon)$ and $\Delta(\epsilon)$ with a simple density of states,

$$\rho_0(\epsilon) = \rho_0 \qquad \text{for} \quad -D < \epsilon < D \quad , \tag{3.77}$$

by neglecting the $\boldsymbol{k}$ dependence of $V_{\boldsymbol{k}}$, one can obtain

$$\Delta(\epsilon) = \pi\rho_0|V|^2 = C \qquad \text{for} \quad -D < \epsilon < D \quad , \tag{3.78}$$

$$= 0 \qquad\qquad\qquad \text{for} \quad \epsilon \leq -D \text{ or } \epsilon \geq D \tag{3.79}$$

$$\Lambda(\epsilon) = \rho_0|V|^2 \ln\left|\frac{D+\epsilon}{D-\epsilon}\right| \quad . \tag{3.80}$$

Note that $\Lambda(\epsilon)$ can be easily calculated by the Kramers-Kronig relation.

$$\Lambda(\epsilon) = \frac{1}{\pi}\int_{-D}^{D} d\epsilon' \frac{\Delta(\epsilon')}{\epsilon - \epsilon'} \tag{3.81}$$

It can be shown that the density of induced states approximately follows a Lorentzian form and thus there's a virtual bound state at ϵ_d'.

$$\delta(\epsilon) = \frac{\pi}{2} - \tan^{-1}\frac{-\epsilon + \epsilon_d'}{C} \tag{3.82}$$

$$\Delta\rho(\epsilon) = \frac{1}{\pi}\frac{d\delta(\epsilon)}{d\epsilon} = \frac{1}{\pi}\frac{C}{(\epsilon - \epsilon_d')^2 + C^2} \quad , \tag{3.83}$$

where $\epsilon_d' - \epsilon_d - \Lambda(\epsilon_d') = 0$. Fig. 3.3 shows the density of states induced by the impurity with the density of states (Fig. 3.2) in the conduction band. Since the potential ($V = -0.13$) is weak and $\epsilon_d = -0.3$ is well within the conduction band, there is a resonance around the energy of -0.3. This virtual bound state becomes a real bound state below the bottom of the conduction band for $V < -0.6$. (Fig. 3.4) Since there is one electron in a bound state for $V < -0.6$, the number of electrons in the conduction band is zero as shown in Fig. 3.4. Note that in this

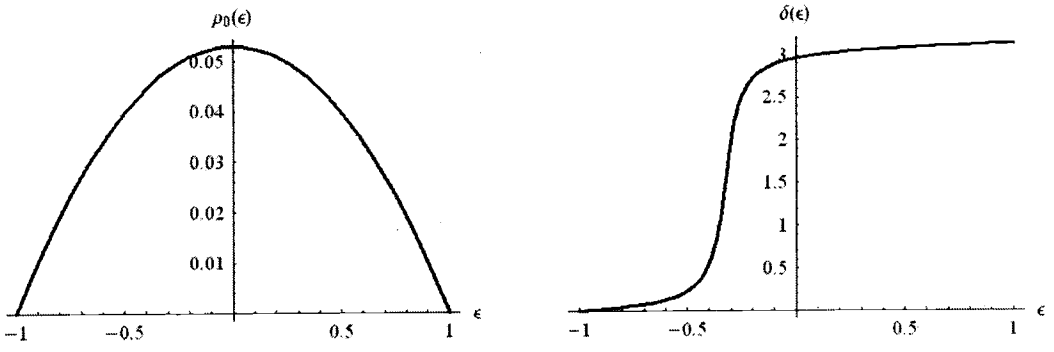

FIGURE 3.2. The density of states $\rho_0(\epsilon)$ in the conduction band and the corresponding phase shift. $\epsilon_d = -0.3$ and $\Delta(\epsilon) = (-0.13)^2\pi\rho_0(\epsilon)$ are used.

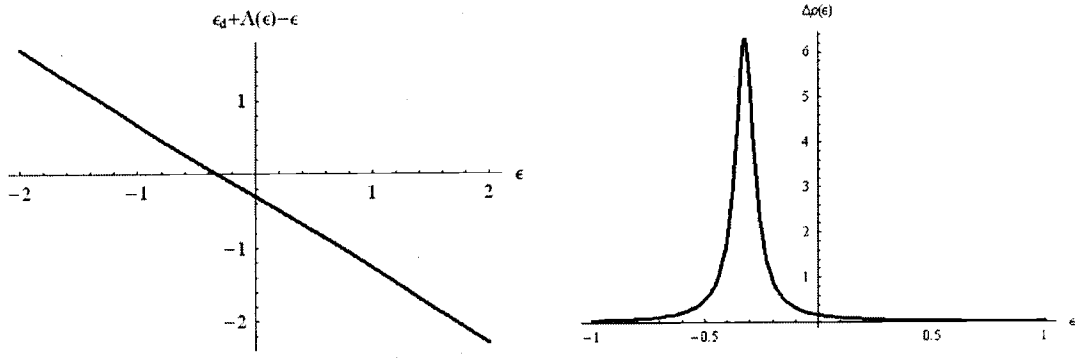

FIGURE 3.3. There is a virtual bound state resonance at the solution of $\epsilon - \epsilon_d - \Lambda(\epsilon) = 0$. The density of states $\Delta\rho(\epsilon)$ induced by the impurity. Calculated from Fig. 3.2 in Mathematica.

case the system has always one extra electron due to the impurity, regardless of the number of virtual bound states. Actually, the transition between bound and unbound states is smooth and the properties such as the total energy are smooth functions of the strength of the potential as well. [27]

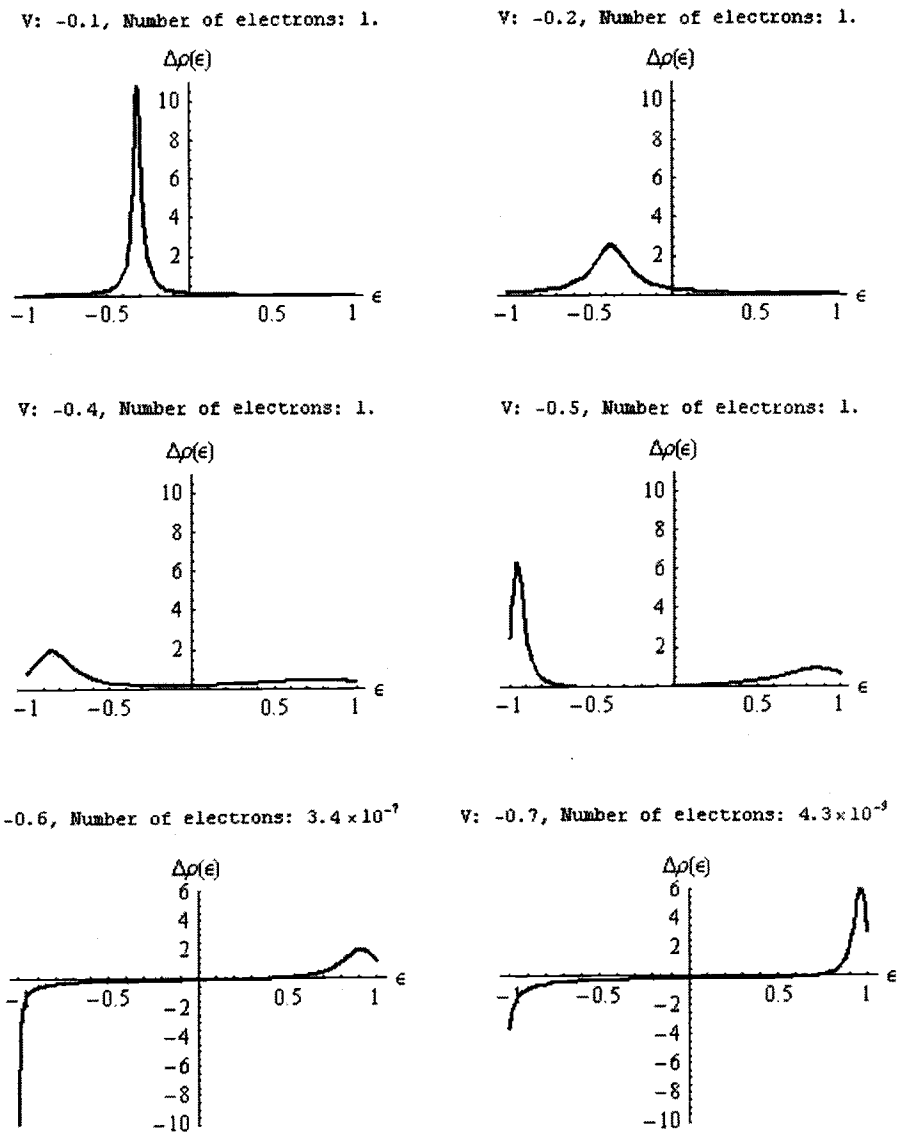

FIGURE 3.4. Shows how the density of states $\Delta\rho(\epsilon)$ varies in the conduction band for the different strength of the potential. Calculated from Fig. 3.2 in Mathematica. The number of electrons in the conduction band is obtained numerically.

3.6. Scattering length and bound state energy

The purpose of this section is to give emphasis to the relationship between the scattering length and the bound state energy, which easily can be derived for

scattering by a spherically symmetric square-well potential at low energies (such as a deuteron system). [28] [29] Notice that it is sufficient to consider only the S-wave for low energies. Suppose the potential has the form,

$$V(r) = -V_0 \qquad \text{for } r < r_0$$
$$= 0 \qquad \text{for } r > r_0 \ . \tag{3.84}$$

One can immediately write the corresponding radial equations and solutions for bound states of the energy E_B,

$$\frac{d^2u(r)}{dr^2} + k^2u(r) = 0 \text{ and } u(r) = A\sin(kr) \qquad \text{for } r < r_0 \tag{3.85}$$
$$\frac{d^2u(r)}{dr^2} - k_B^2u(r) = 0 \text{ and } u(r) = B\exp(-k_Br) \qquad \text{for } r > r_0 \ , \tag{3.86}$$

with $k^2 = V_0 - |E_B|$ and $k_B^2 = |E_B|$. The boundary condition at $r = r_0$ gives rise to

$$k\cot(ka) = -k_B \ . \tag{3.87}$$

Since the deuteron system has a small binding energy $|E|$, using $k_0 \simeq k(k_0 = V_0^{1/2})$,

$$k_0\tan(\frac{\pi}{2} - k_0r_0) = -k_B \ . \tag{3.88}$$

If $k_0r_0 \simeq \pi/2$, one obtains

$$k_0r_0 = \frac{\pi}{2} + \frac{k_B}{k_0} \ . \tag{3.89}$$

For low-energy scattering, similarly,

$$u(r) = A\sin(kr) \qquad \text{for } r < r_0 \tag{3.90}$$
$$u(r) = B\sin(k'r + \delta) \qquad \text{for } r > r_0 \ , \tag{3.91}$$

with $k^2 = V_0 + E$ and $k'^2 = E$. Using the boundary condition at $r = r_0$,

$$k \cot kr_0 = k' \cot(k'r_0 + \delta) \tag{3.92}$$

$$\tan\delta = \frac{\frac{k'}{k}\tan kr_0 - \tan k'r_0}{1 + \frac{k'}{k}\tan kr_0 \tan k'r_0} \quad . \tag{3.93}$$

For $k' \to 0$, one can use $k \to k_0$, which leads to

$$\delta \simeq \tan\delta \simeq k'r_0 \left(\frac{\tan k_0 r_0}{k_0 r_0} - 1\right) \quad . \tag{3.94}$$

Note that the total cross section is given by

$$\lim_{k'\to 0} = \frac{4\pi}{k'^2}\sin^2\delta_0 \simeq 4\pi(\frac{\delta_0}{k'})^2 \tag{3.95}$$

$$= 4\pi\left[r_0\left(\frac{\tan k_0 r_0}{k_0 r_0} - 1\right)\right]^2 \tag{3.96}$$

$$= 4\pi a^2 \quad , \tag{3.97}$$

where the scattering length a is defined by

$$\delta_0 \to -ak' \quad \text{as} \quad k' \to 0 \tag{3.98}$$

$$\text{and } k_0 \cot k_0 r_0 = \frac{1}{r_0 - a} \quad . \tag{3.99}$$

The quantity $4\pi a^2$ only depends on the potential.

One can also rewrite (3.93) to obtain

$$k' \cot\delta = \frac{k \cot kr_0 + k' \tan k'r_0}{1 - \frac{k}{k'}\cot kr_0 \tan k'r_0} \tag{3.100}$$

One finally can expand (3.100) in terms of k' keeping terms up to k'^2, with (3.99), $k = \sqrt{k'^2 + k_0^2} \simeq k_0 + \frac{k'^2}{2k_0}$, and $\tan k'r_0 \simeq k'r_0 + \frac{1}{3}(k'r_0)^3$,

$$k' \cot\delta \simeq -\frac{1}{a} + \frac{1}{2}k'^2 r_{eff} + \cdots \quad , \tag{3.101}$$

where $r_{eff} = r_0\left[1 - \frac{1}{(k_0 r_0)^2}\frac{r_0}{a} - \frac{1}{3}(\frac{r_0}{a})^2\right]$. This result is known as the effective range expansion for $k' \cot\delta$ for low-energy scattering.

Now, in order to relate the bound state energy to the scattering length, one needs to write from (3.89), since $k_B/k_0 \ll 1$,

$$\tan k_0 r_0 = \tan(\pi/2 + k_B/k_0) = -k_0/k_B \quad . \tag{3.102}$$

One can now rewrite (3.100) with $\tan k' r_0 \simeq k' r_0$ as

$$k' \cot \delta \simeq -\frac{k_B}{1 + r_0 k_B} + \frac{r_0}{1 + r_0 k_B} k'^2 \quad . \tag{3.103}$$

By comparing this equation with the effective range expansion (3.101), one can obtain

$$a = r_0 + \frac{1}{k_B} \quad . \tag{3.104}$$

This result provides a way to see whether the self-consistent solutions from the numerical calculations are correct or not by comparing the scattering length a and the binding energy. The potential range r_0 also can be estimated from the equation above.

4. IMPLEMENTATION

In general, the procedure to implement a theory and translate it into computer codes is not easy due to the limitations of a computer. Two numerical problems which directly affect the numerical precision originate from approximations to infinity and continuity, which frequently become the largest problems and can be expressed only approximately in numerical calculations. In most cases, one needs to use a large cut-off value for infinity and very small interval for continuity in numerical calculations to obtain a reasonable answer. It is important to find out how those parameters can be determined. In this chapter, the iterative scheme to accomplish the self-consistent solutions and the numerical methods to find the eigenstates will be introduced. The technique to solve the numerical problems, in which physical understanding is indispensable, will be discussed. It needs to be emphasized that spherically symmetric potentials are used throughout this work.

4.1. Perspective scheme for self-consistent solutions

4.1.1. Non-spin polarized system

Fig. 4.1 shows one possible flow chart to find a self-consistent solution for the KS equations. One can also start with the initial electronic density, but in this case the effective potential is more convenient to deal with since the relative numerical response of the effective potential in r-space is much larger than that of the density. With an input effective potential, one can solve the KS equations to find the density, from which one can construct the output effective potential. A self-consistent solution means that the input effective potential must be the same as the output effective potential. In practice, one can stop the calculations if the

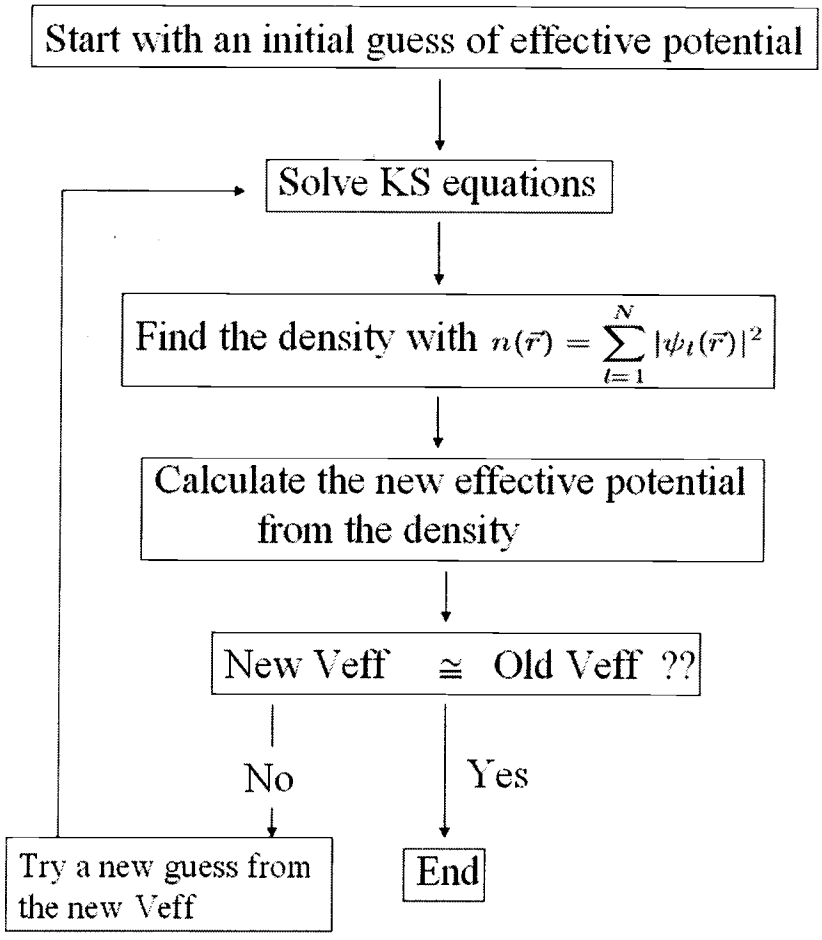

FIGURE 4.1. Flow chart for non-polarized systems.

input potential is very close to the output potential, when numerical precision required for the immersion energy can be achieved and thus further calculations do not affect the final answers. In order to compare the input potential with the output potential, one can use

$$(\Delta V)^2 = \frac{1}{\Omega} \int d\boldsymbol{r} \, [V_{eff}^{input}(\boldsymbol{r}) - V_{eff}^{output}(\boldsymbol{r})]^2 \quad , \tag{4.1}$$

where Ω is the total volume of the system. The potential difference ΔV can be used to find the physical quantities such as immersion energy, bound state energy,

and magnetization since the self-consistent solution means that $\Delta V = 0$. One can attempt to determine the physical quantities corresponding to the zero value of ΔV by using an appropriate fitting method for the data points.

In order to make progress, one needs a numerical method to determine the input potential from the output potential for the next iteration, which will be explained in Sec. 4.2.

4.1.2. Spin polarized system

One big difference between spin polarized systems and non-spin polarized systems is the need to solve two different sets of KS equations, for $n_+(\boldsymbol{r})$ and $n_-(\boldsymbol{r})$, which doubles the calculation time. Only the exchange-correlation energies and potentials are, however, explicitly dependent upon the spin density $(n_+(\boldsymbol{r}) - n_-(\boldsymbol{r}))$ as in (2.41), (2.42), and Sec. 2.2.7.4. The Coulomb potentials and energies do not depend on the spin density, but only on the total density $(n_+(\boldsymbol{r}) + n_-(\boldsymbol{r}))$.

4.2. Mixing scheme

Since the KS equations are solved self-consistently in this work and the time to find self-consistent solutions is directly proportional to the number of iterations of the self-consistent loop in Fig. 4.1, it is important to find an efficient method to construct the next input potential from the output potential. The simplest mixing scheme is $V_{eff}^{initial,i+1}(r) = V_{eff}^{final,i}(r)$. This simple scheme, however, does not work since the response in the output potential is usually enormous compared to the change in the input potential, even for the high densities of an electron

gas.[1] The main purpose of a mixing scheme is to make the convergence faster, that is, to reduce the program-running time to reach self-consistency while the solutions maintain the stability such that they don't diverge. Another straight mixing scheme is

$$V_{eff}^{in,i+1}(r) = V_{eff}^{in,i}(r) + a\ (V_{eff}^{out,i}(r) - V_{eff}^{in,i}(r)) \tag{4.2}$$

where i is the number of the iteration. The mixing ratio a ensures the stability of the convergence during the self-consistent calculations. One can keep reducing a until stability is acquired. One way to speed up the convergence is Broyden's method which is

$$\begin{aligned} V_{eff}^{in,i+1}(r) &= V_{eff}^{in,i}(r) + a(r)\ F^i(r) \\ a(r) &= \frac{V_{eff}^{in,i}(r) - V_{eff}^{in,i-1}(r)}{F^i(r) - F^{i-1}(r)} \end{aligned} ,$$

where $F^i(r) = V_{eff}^{out,i}(r) - V_{eff}^{in,i}(r)$. One can obtain Broyden's method by trying to find the point on the line of $V_{eff}^{in}(r) = V_{eff}^{out}(r)$ between the two points, $(V_{eff}^{in,i-1}(r), V_{eff}^{out,i-1}(r))$ and $(V_{eff}^{in,i}(r), V_{eff}^{out,i}(r))$. Since the mixing ratio in Broyden's method depends on the input and output potentials of last two iterations, discontinuities in the potential of r-space may show up during the calculations and the integration for wave functions based on the potential may go wrong as well. Another problem in this case is the long range tail of Friedel oscillation, which is usually strongly coupled to the electronic density in the vicinity of an impurity due to the Coulomb potential. The idea to avoid this problem and speed up the

---

[1]Results for dielectric constants suggest the response of electron gases of high densities is small compared to those of low densities. See chapter 5.

convergence at the same time is to use the straight mixing scheme and the mixing ratio of an exponential-like function.

$$a(r) = a \exp(-\alpha\, r^2) \quad . \tag{4.3}$$

The mixing scheme is now

$$V_{eff}^{in,i+1}(r) = V_{eff}^{in,i}(r) + a \exp(-\alpha\, r^2)\ (V_{eff}^{out,i}(r) - V_{eff}^{in,i}(r)) \quad . \tag{4.4}$$

There are two parameters a and α in this mixing scheme. a can be determined by considering the response of a region in the vicinity of an impurity and α is a parameter to suppress the strong response of the tail of Friedel oscillations. Now one can allow as large a change as possible in the vicinity of an impurity by increasing the a value while one suppresses the response of the tail by using large value of α. In most cases, 0.02 for a and 0.002 for α have been found appropriate. Another idea to make convergence even faster is to utilize the last two input potentials and add the response of those to the mixing scheme.

$$\begin{aligned} V_{eff}^{in,i+1}(r) &= V_{eff}^{in,i}(r) + a(r)\ (V_{eff}^{out,i}(r) - V_{eff}^{in,i}(r) + V_{eff}^{in,i}(r) - V_{eff}^{in,i-1}(r)) \\ &= V_{eff}^{in,i}(r) + a(r)\ (V_{eff}^{out,i}(r) - V_{eff}^{in,i-1}(r)) \quad . \end{aligned} \tag{4.5}$$

One can make two vectors $V_{eff}^{in,i}(r) \rightarrow V_{eff}^{out,i}(r)$ and $V_{eff}^{in,i-1}(r) \rightarrow V_{eff}^{in,i}(r)$ for each r. If those vectors have the same directions, the mixing scheme (4.5) will accelerate the convergence (large mixing ratio) compared to the previous mixing scheme (4.4) and if they have opposite directions, (4.5) will decelerate the convergence (small mixing ratio) to avoid the possible oscillations of potentials between two iterations.[2]

---

[2]The divergence can be noticed usually by fluctuations of potentials between iterations during the numerical calculations.

Once satisfactory self-consistency is obtained in the vicinity of an impurity, one can reduce a to avoid the possible large variation of the density around the impurity and reduce α to allow now larger variation of the tail of potentials to make convergence faster. One can implement this in the program by calculating the potential difference ΔV of (4.1) and have the program automatically vary the parameters a and α. If ΔV is small enough, especially in the vicinity of an impurity, and the convergence is too slow, a and α can be reduced by a small amount during calculations. One idea is to calculate the relative ratio of ΔV between two iterations.

$$\text{Ratio} = \frac{(\Delta V_i)^2 - (\Delta V_{i-1})^2}{((\Delta V_i)^2 + (\Delta V_{i-1})^2)/2.0} \quad . \tag{4.6}$$

If the ratio is too small, one can try to reduce a and α values. However one needs to find the appropriate iterations at which the parameters can be reduced and the values of parameters by trial and error. It has been found in this work that if the ΔV^2 is smaller than $10^{-8} \sim 10^{-9}$ and the ratio is smaller than $0.002 \sim 0.005$, a and α can be reduced by $10\% \sim 20\%$. A minimum number of iterations between the iterations at which the parameters are reduced, however, often needs to be set to ensure the convergence of the calculations.

4.3. Search for eigenstates and eigenvalues of the infinite system

4.3.1. Bound states

The method for the search for bound states is well established and calculations are quite simple for spherically symmetric potentials. [30] Since only the principle quantum number n and the angular momentum number l for spherically symmetric potentials are necessary to distinguish eigenstates, each eigenstate can

be categorized by n and l or the number of nodes n_{nodes} and l.[3] One can then search for bound states from the minimum energy to the maximum energy using n_{nodes} and l. Note that the possible lowest energy for the bound states can be set to $-\frac{Z^2}{n^2}$ Ryd., which is bound state energy for a pure Coulomb potential, since once the pure Coulomb potential is screened, the energy eigenvalues are always higher than those for the pure Coulomb potential. An upper limit for bound states is zero with a reference of zero energy $\lim_{r\to\infty} V_{eff}(\boldsymbol{r}) = 0$.

The method used in this work is known as the bisectional algorithm. [30] There is a better and faster method than the bisectional algorithm, which has never been tried in this work since the time required to search for bound states is relatively quite small compared to that for scattered states and is usually less than a few seconds for today's computers. For the bisectional algorithm, one takes half the minimum energy as the initial energy for the energy eigenvalue one tries to achieve and integrates the KS equation with this energy. If the current energy is higher or smaller than the eigenenergy, one can use the current energy as an upper limit or a lower limit for the next iteration and integrate the KS equation with the new middle energy between the upper and lower limits. One can try to repeat the process until the bound state energy is obtained within the required tolerance for the numerical error.

In order to decide whether the current energy is higher or smaller than the eigenenergy, one uses two conditions, which both must be satisfied for correct wave functions. The first one is that the number of nodes in the wave functions must be the same as required in $n_{nodes} = n - l - 1$. The second one is that the first

---

[3]Spin-orbit coupling is neglected in this work, and hence $n = n_{nodes} + l + 1$.

derivative of one wave function integrated from the origin outwards must match at a matching point with the first derivative of the other wave function integrated from the maximum radius inwards. The numerical best point for a matching point is an innermost classical turning point, since one can expect that the oscillatory behavior of a solution becomes a decreasing exponential-like behavior at this turning point. Note that Friedel oscillations in the tail of potentials may give rise to a number of turning points. First, one can narrow the range of the energy using the number of nodes. If the number of nodes in a wave function is larger or smaller than that required, the current energy is higher or lower than the eigenenergy. If the number of nodes is correct, one can check if first derivatives of wave functions match at the matching point.[4] If the magnitude of a first derivative of an outward solution is larger or smaller than that of an inward solution, the current energy is higher or lower than the eigenenergy. If the energy is needed to be higher than the initial maximum energy (zero as in (3.4)), one can stop the search since there is no bound state.

The KS equations can be integrated only with appropriate boundary conditions. For bound states,

$$\text{as} \quad r \to 0$$

$$u_{n,l}(r) \to r^{l+1} \quad \text{and} \quad u'_{n,l}(r) \to (l+1)r^{l} \ , \tag{4.7}$$

$$\text{as} \quad r \to \infty$$

$$u_{n,l}(r) \to \exp(-\sqrt{-E}r) \quad \text{and} \quad u'_{n,l}(r) \to -\sqrt{-E}\exp(-\sqrt{-E}r) \ . \tag{4.8}$$

---

[4]Since the numerical solutions are not normalized, one has to ensure they both have the same numerical scale to compare first derivatives, for instance, by using logarithmic derivatives.

The normalization condition for bound states is

$$\int d\boldsymbol{r}\, |u(r)|^2 = 1 \quad . \tag{4.9}$$

The density difference for spherically symmetric potentials due to the bound states of an impurity is given by

$$n(r) - n_0 = \sum_{n,l} 2 \frac{(2l+1)}{4\pi} \frac{u_{n,l}^2(r)}{r^2} \quad , \tag{4.10}$$

where the factor 2 is for spin degeneracy[5]

4.3.2. Scattered states

The Fermi wave vector k_F of a homogeneous electron gas can be calculated as follows.

$$2 \frac{\Omega}{(2\pi)^3} \frac{4\pi}{3} k_F^3 = N$$

where the left hand side is the number of states available in a system of the volume Ω, the factor 2 in the left hand side is for spin degeneracy, and N is the total number of electrons in a system. In the thermodynamic limit, the above equation leads to

$$k_F = (3\pi^2 n_0)^{1/3} \quad , \tag{4.11}$$

where n_0 is the electronic density of the system. Since the system used in this work is extended to infinity, and thus there are no boundary conditions, there are

---

[5]The factor $(2l+1)/4\pi$ is obtained by using the addition theorem:

$$\sum_{m=-l}^{l} |Y_{l,m}(\theta, \phi)|^2 = \frac{2l+1}{4\pi} \quad .$$

no quantized k values and all k values up to k_F are available. In addition, the chemical potential is assumed to be a constant and the same as the Fermi energy of a homogeneous electron gas at $T = 0$ since the dimension of the system is much larger than that of an impurity. Now one needs to integrate the KS equations in the k-mesh for the continuum states $k = 0 \cdots k_F$. The wave functions can be normalized by (3.24) and the density difference for scattered states is given by (3.47).

The main numerical problem is that the maximum number of angular momentum values should be determined for each k. Theoretically kR is a good value for the maximum l where R is the radius of the potential. [23] On the other hand, only 10 l values were used in the work of Puska, Nieminen, and Maninen.(1981) None of these are, however, good criteria for the maximum l value. The kR tends to neglect the low-energy scattering due to very small k values. Ten for the maximum l value is more than enough for small k values and is too small for large k values. It is found that using too small a number for the maximum l value gives an error in the energy and an instability in terms of convergence. A better way is using the values of the phase shift to see how close the scattered state at the current l value is to the free particle state. In other words, if the phase shift is sufficiently small and thus l values larger than the current l value are not important, the calculation for the current k value can be terminated and one begins the calculation for the next k value in the k-mesh. A good value for the smallest phase shift is 10^{-8}, which turns out to give a good convergence.

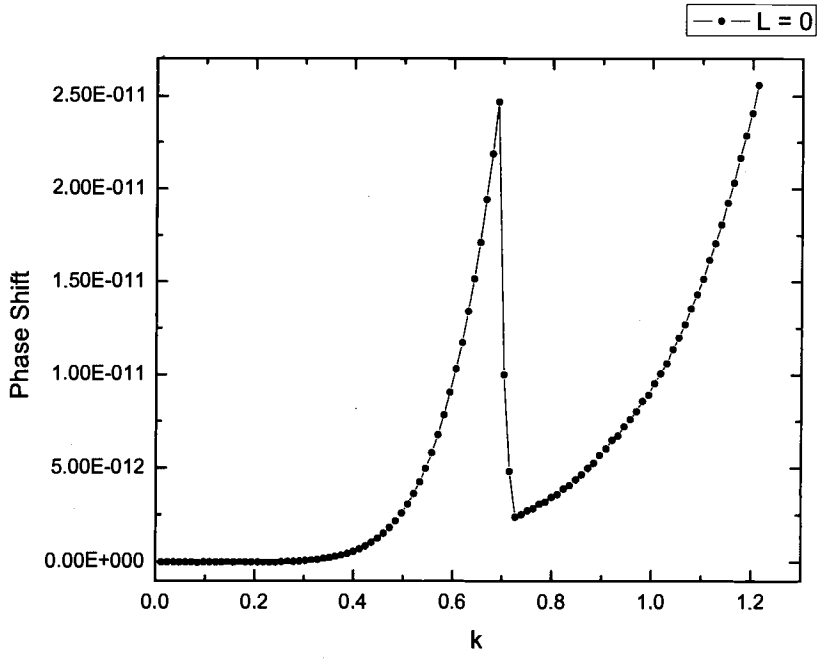

FIGURE 4.2. Phase shift values of $l = 0$ for a zero potential.

4.4. Numerical problems

4.4.1. Convergence of phase shifts

The accuracy of the phase shifts needs to be tested to see if 10^{-8} suggested for the smallest phase shift in the previous section is well within the precision of the numerical error. One idea taken from [21] is to test the phase shift values for zero potential since the phase shift is zero for the zero potential. One can see the peak in Fig. 4.2 around $k = 0.6$ and that the phase shift deviates more strongly from zero after this value. The test has been performed for the electronic density

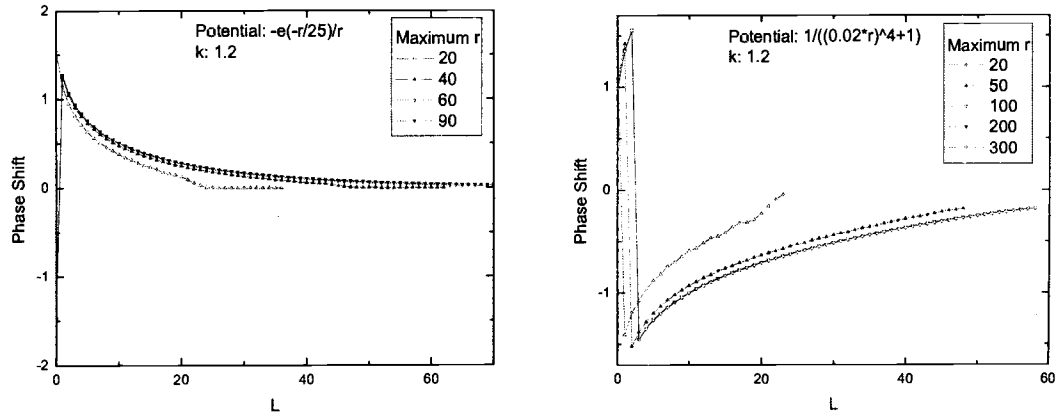

FIGURE 4.3. Phase shift values for an attractive potential of Yukawa type and a repulsive potential.

of $n_0 = 0.6$.[6] One can conclude that the numerical error in the phase shifts is less than $3 \cdot 10^{-11}$ for the range of actual metallic densities. It is found that the numerical error of higher l values is smaller than that of $l = 0$. This numerical behavior may be, however, dependent on the numerical libraries one uses. Fig. 4.3 shows the relationship between the maximum radius R_m used in the numerical calculation and the phase shift values. As seen in Fig. 4.3, if R_m is too small and thus the potential does not go to zero fast enough, the phase shift calculations fail. If the potential has such a long range, phase shift values at very low l show a

---

[6]Parameters for the test are $R_0 = 8.1250520 \cdot 10^{-6}$, $R_{log} = 8.0$, $R_m = 31.02$, $N_{log} = 465$, and $N_{lin} = 230$, where N_{log} is the number of points used in the logarithmic r-space between R_0 and R_{log} and N_{lin} is the number of points used in the linear r-space between R_{log} and R_m.

zig-zag behavior, which is similar to that of hard sphere scattering for high energy approximations. [23] They are, however, eventually approaching zero as l increases. Then one can stop the calculation for each k if phase shift values are small enough, for instance, less than 10^{-8} as argued in the previous section.

4.4.2. Correction for potentials

The main problem in solving the KS equations numerically is that the effective potentials in the KS equations have physically and numerically essential defects, especially at the beginning of calculations. These defects may not only slow down the convergence but also lead the calculations to incorrect self-consistent solutions. The first problem is that, during the numerical calculations, since the effective potential has not reached self-consistency yet, especially at the beginning, there may be a surplus or deficiency of charge to screen the impurity and the system does not satisfy the Friedel sum rule. The effective potentials in this case are oscillating around some constant value due to the extra charge. This extra charge appears as a constant (intersecting point with $r = 0$) in the rV plot of Fig. 4.4. The second problem is that, since the system is extended to infinity, the upper limit of the integral in the Coulomb potential must be infinity as well. No matter how large a radius is used for the numerical calculations, the integral from the maximum radius to infinity in the Coulomb potential is always missing, which appears as a slope in the rV plot in Fig. 4.4. If one uses naively this incorrect output potential to mix with the input potential for the next iteration, the phase shift calculations cannot be performed since the phase shift calculations and thus the normalization for scattered wave functions are based on the fact that the potentials are zero or

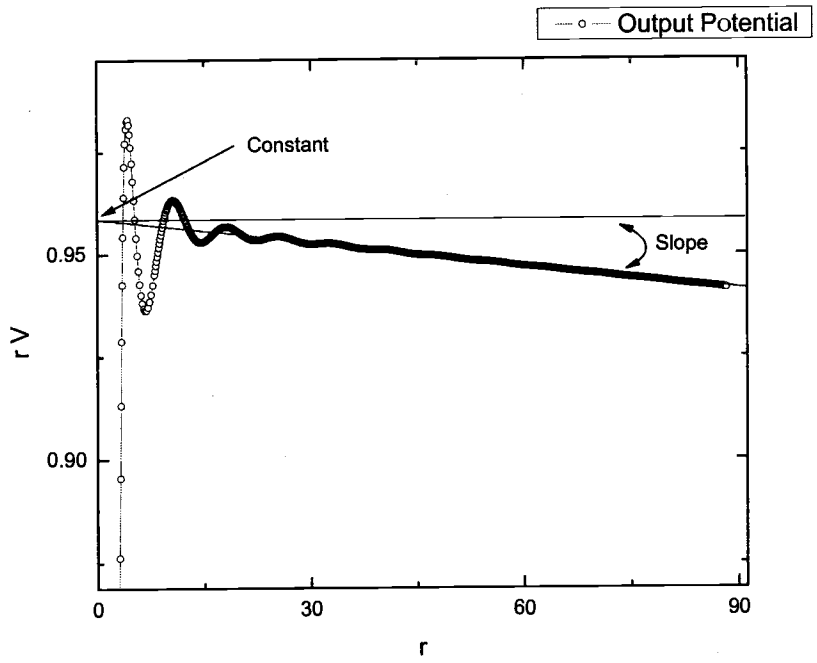

FIGURE 4.4. Typical example showing defects in the output potential during the numerical calculations.

almost zero at the end of the maximum radius.[7] In addition, special phase shifts have to be used for Coulomb potentials.[8]

---

[7]At the maximum radius, it is assumed that an impurity is completely screened and the system satisfies the Friedel sum rule.

[8]This may be much more difficult than zero Coulomb potentials. Besides, allowing non-zero Coulomb potential at the maximum radius may be a wrong guide for a self-consistent solution of the system used in this work.

One can simply make the potential zero at the maximum radius and run the program for many iterations until the extra charge (Constant in Fig. 4.4) disappears. This is, however, not only time consuming, but also the potential is not likely to go to the zero at the maximum radius due to the Friedel oscillations. One can also try to remove the extra slope in the rV plot using an analytic or a numerical model for the missing integral, but this turns out to be not good enough.[9] The best way is simply to determine the extra constant and slope in the rV plot and subtract them from rV. One can not, however, simply subtract the constant from rV because the potential in the vicinity of an impurity is affected by the interaction between the impurity and an electron gas as well as by the Friedel oscillations and thus one has to allow for a variation of the electronic charge around an impurity. Since at the same time the potential must be oscillating around zero at the maximum radius, the formula to correct the potential can be written as

$$r \times V = r \times V - r \times (\text{Slope} + \text{Constant}/R_m) \ , \tag{4.12}$$

where R_m is the maximum radius r in the r-mesh for the numerical calculations. One can try other functions instead of a linear r in $r \times Constant/R_m$. However other functions may suppress the variation around an impurity too much or too little, either of which makes the convergence slower. The slope and constant can be easily calculated by four points of maximum and minimum peaks near the end of the potential. Then one can set up two line equations, from which one can find the average slope and constant at $r = 0$. Fig. 4.5 shows the typical examples of the effective potentials before and after the correction and the right figure in Fig. 4.5 shows that the potential is oscillating around zero at large r values after the

---

[9]It has been found that there is still a noticeable slope after correcting the potential.

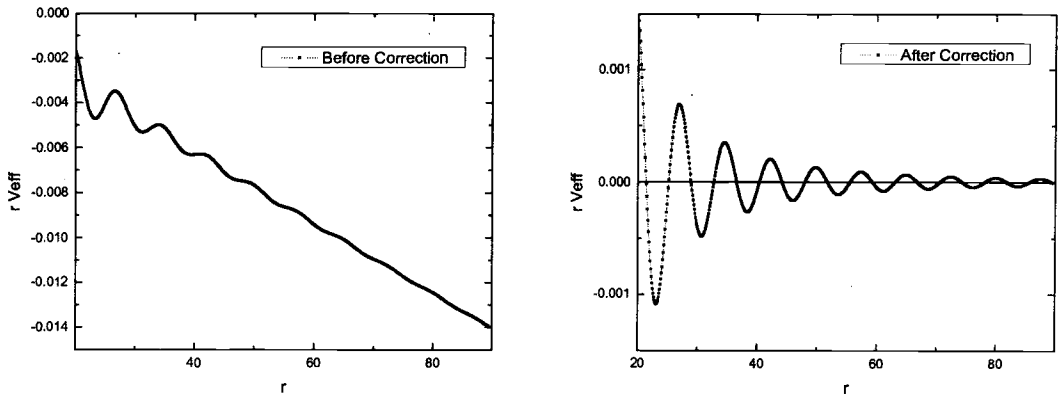

FIGURE 4.5. Typical examples to show how the effective potentials behave before and after the correction. These potentials are calculated for a hydrogen impurity and $n_0 = 0.0025$.

correction, which means an impurity is completely screened and Friedel sum rule is satisfied as it should be.

4.4.3. Calculations for induced electrons and energies

One detail previous papers [5] have overlooked is that after including all of the screening charge around impurity the electronic density is simply oscillating due to the Friedel oscillations and thus the integrated values of the electronic density, needed to find the number of electrons induced due to an impurity, are also oscillating, which is shown in Fig. 4.6. In addition, the number of induced electrons in the system should not depend on the maximum value of r since the system goes to infinity and thus this number can not be found by simply integrating from zero to the maximum of r. In order to find the charge induced in the system, integrated values of the charge density as a function of r should be examined as in

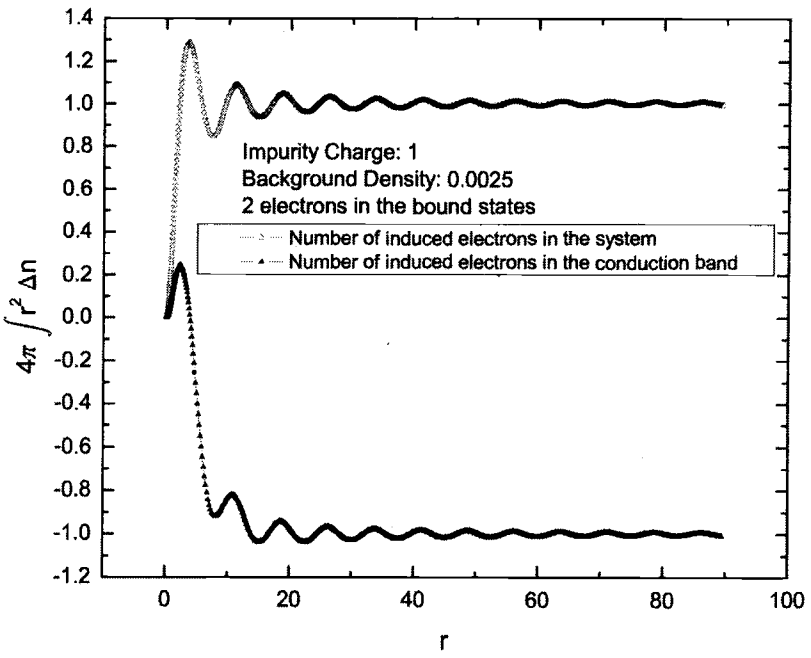

FIGURE 4.6. Calculated for a hydrogen impurity and $n_0 = 0.0025$. This example shows the oscillations of integral values of the induced electronic density as a function of r.

Fig. 4.6 and the average charge from the oscillation should be calculated to find the total number of electrons induced due to an impurity. It is important to note that the r dependence of energies such as the exchange-correlation and the Coulomb energy can be removed in the same way.

4.4.4. Mesh for r-space and k-space

In order to integrate functions numerically, one needs to use small interval to approximate the continuous space over which the functions are to be integrated.

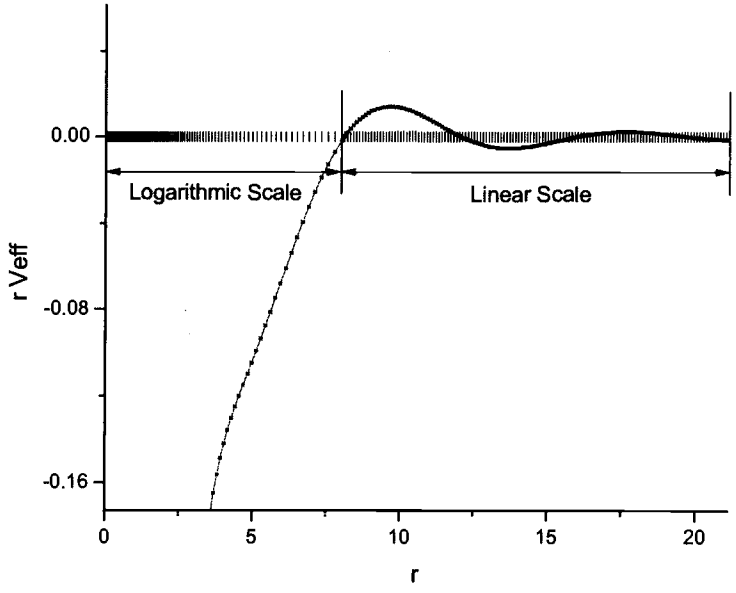

FIGURE 4.7. Typical example for the effective potential. The logarithmic mesh is used for the rapid variation of the potential in the vicinity of the origin.

The term, mesh, is defined in this work as how intervals vary between two adjacent points in a continuous space. If the interval does not vary and is simply a constant, the integral space is called a linear mesh. Since the numerical precision directly depends on the mesh used for the integral in r or k-space, the behavior of functions which are to be integrated needs to be examined to choose the appropriate mesh for each space. The r-space can be categorized into two regions, based on the density variation. The first region covers the core states in which the electronic density usually varies rapidly. In the second region, the net electronic charge induced by a electron gas is almost zero and the Friedel oscillations dominate the density variation. Therefore a logarithmic r-mesh is appropriate for the first region which includes the core states in the vicinity of an impurity and after that, a simple linear

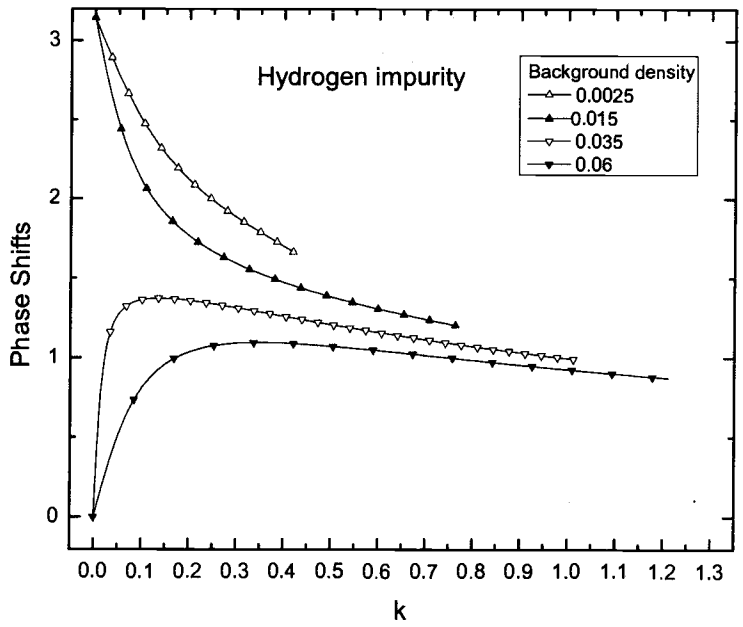

FIGURE 4.8. Example for phase shifts. The phase shift varies rapidly at the bottom of the conduction band if the energy of a bound state is close to the bottom of the conduction band.

r-mesh can be used for the second region as shown in Fig. 4.7. In this work, the *logarithmic* r-mesh always corresponds to the first region and the *linear* r-mesh corresponds to the second region.

Phase shifts at $l = 0$ need to be examined in order to see how the wave functions behave in k-space. Based on this information, one can choose the mesh in k-space. The appropriate mesh in k-space is, however, quite difficult to determine before calculations since at least the energies of bound states, or the scattering lengths are necessary to estimate how large the slopes of phase shifts at $l = 0$ are in the vicinity of the bottom of the conduction band. Note that the scattering length is inversely proportional to the energy of bound states . (See Sec. 3.6.) One

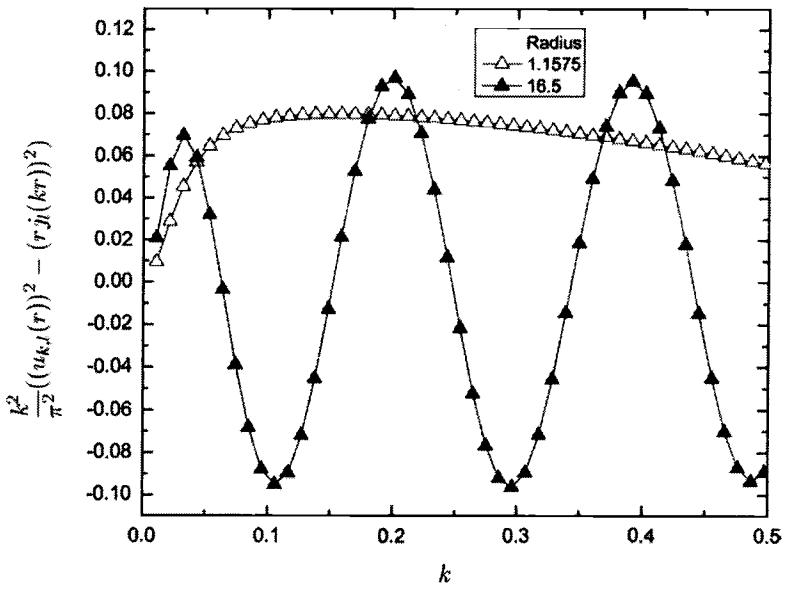

FIGURE 4.9. Integrand in (3.22). Calculated for a Hydrogen impurity at 0.04 background density.

may try very low or high background densities of an electron gas first and try to determine the range of the background densities where the energies of bound states are close to the bottom of the conduction band. (See Fig. 4.8.) If the calculations need to be performed for this range of the background density, the phase shifts in k-space also need to be examined in order to determine the range of k-space where the phase shifts vary fast. In that case, a different k-mesh is necessary due to the different variation of the phase shifts. One can try the logarithmic mesh for the fast variation of phase shifts at the bottom of the conduction band as in r-space. However, it turns out that a logarithmic mesh causes more numerical errors than the simple linear mesh. Fig. 4.9 shows how the wave functions in k-space vary at different r values. A logarithmic mesh may work well at low r values but causes

more numerical errors for the ordinary oscillating wave functions in k-space. A better way is simply to use two different linear k-meshes with different intervals to deal with the rapid variation at the bottom of the conduction band. The very small interval should be used for the range of k in which the phase shifts vary fast. Because of the smooth behavior of the phase shifts, a large interval can be used for large k values in order to reduce the time to integrate in k-space.

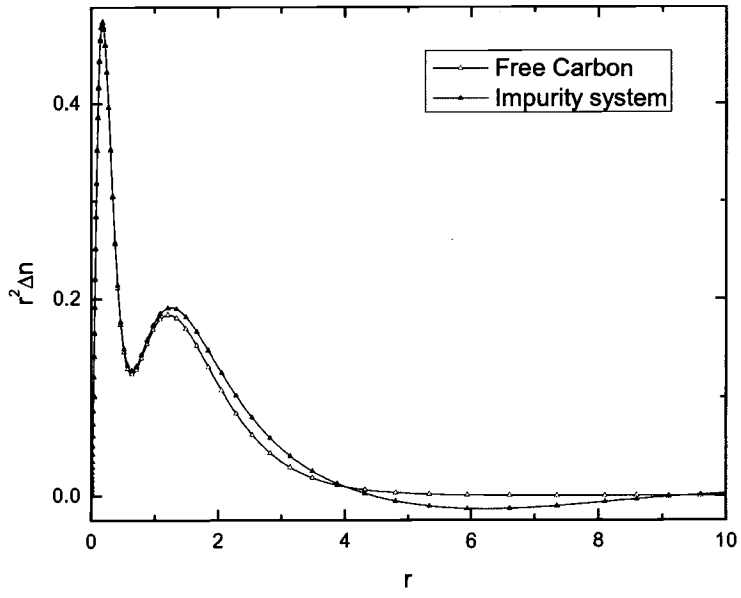

FIGURE 4.10. The density of a free carbon atom and the density induced by a carbon impurity in a homogeneous electron gas. The $1s$ and $2s$ core states remain almost the same. These calculations are performed for a spin polarized system.

4.4.5. Cancelation of numerical errors in immersion energies: Number of r points

In this section, the calculations are based on the logarithmic r-mesh which is used for the range from 0 to 8 a.u. and on the linear r-mesh which is used after 8 a.u. Due to the approximations in LDA, the rapid variation of the density of the core states in the vicinity of an impurity may cause significant numerical errors. However, since the core states hardly interact with the environment, numerical errors of the core states of an impurity system can be reduced by those of a free atom in the immersion energy calculations. That is,

$$O_{impuritysystem} - O_{freeatom} \simeq 0 \quad , \tag{4.13}$$

where O denotes the numerical errors in the core states. Fig. 4.10 shows that the core states of an impurity actually do not interact with a homogeneous electron gas and hence do not contribute to the immersion energy significantly. Table 4.1 and Fig. 4.11 illustrate how the r-mesh in the vicinity of an impurity affects the energies and how numerical errors in the immersion energies can be reduced within a few milli-Rydbergs by calculating the free atom energy with the same r-mesh as for the impurity system. These results may depend on the range of the logarithmic r-mesh which covers the core states. The hydrogen impurity for a non-spin polarized system in Table 4.2 shows the same numerical behavior. Therefore it is important to use the same r-mesh in calculating the free atom energy and the energy of an impurity system to avoid large numerical errors due to the core states.

In order to minimize the remainder of the numerical errors due to the interval in the r-mesh and find the correct immersion energy, one can attempt to use the linear relationship between the immersion energies and the number of r-points as

r-mesh	ΔE	E_{atom}	$E_{imm} = \Delta E - E_{atom}$
525	-73.43094	-73.29770	-0.13324
550	-73.51473	-73.38030	-0.13443
600	-73.64172	-73.50606	-0.13566
650	-73.75003	-73.61365	-0.13638

TABLE 4.1. Energies of a carbon impurity system ΔE and energies of a free carbon atom E_{atom} (in Rydbergs). A carbon impurity in a spin polarized system and a background density of 0.002 are used for calculations. The r-mesh in the table represents the number of r- points used in the range from 0 to 8 a.u., which corresponds to the logarithmic r-mesh and includes most core states. (See Sec. 4.4.4.)

r-mesh	ΔE	E_{atom}	$E_{imm} = \Delta E - E_{atom}$
450	-1.06535	-0.87278	-0.19257
550	-1.07140	-0.87725	-0.19415
650	-1.07576	-0.88037	-0.19539
750	-1.07884	-0.88285	-0.19599
850	-1.08129	-0.88458	-0.19671
1050	-1.08471	-0.88707	-0.19764

TABLE 4.2. Example for a hydrogen impurity. (Non-spin polarized system.) A background density of 0.0025 is used for these calculations.

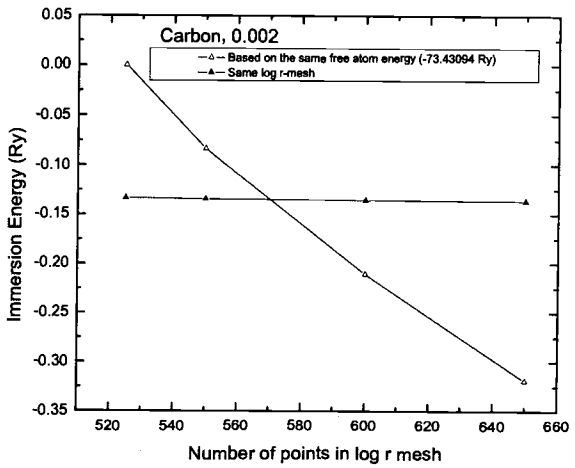

FIGURE 4.11. Comparison between immersion energies calculated with a constant free atom energy and the free atom energy calculated with the same r-mesh as the impurity system. The immersion energies calculated with the same free atom energy show relatively large variation with the different number of r-points due to the numerical errors of core states.

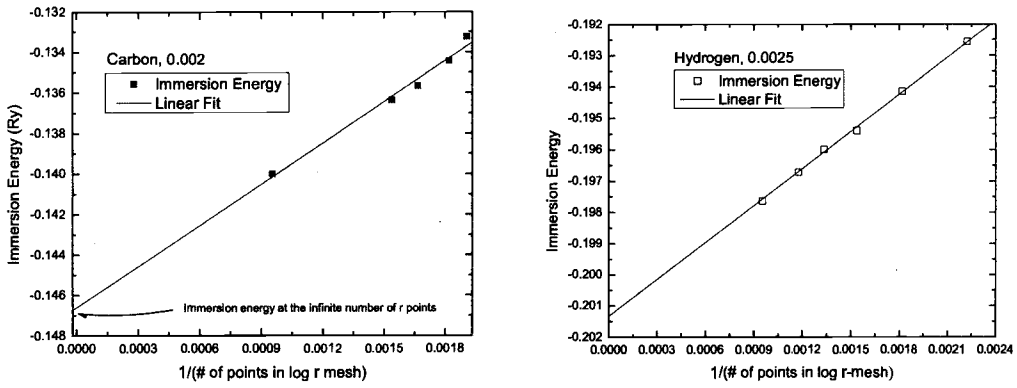

FIGURE 4.12. Fitting by inverse power law to find the correct immersion energy. Data from Table 4.1 and Table 4.2 .

in Fig. 4.12. Now since the number of r-points is in the denominator, the number of r-points can be easily extrapolated to infinity to make the interval of r-mesh zero. Using this method, the immersion energy can be determined up to 1 milli-rydberg.

4.4.6. Further numerical precision tests

The results of numerical calculations may depend on other numerical parameters such as the maximum radius R_{max} and the number of points in k and r-space. The effect of the logarithmic r-mesh in the vicinity of an impurity is already tested in Sec. 4.4.5 and it is shown that the immersion energy can be obtained within 1 milli-rydberg. Other important parameters are the maximum radius R_{max} and the number of points in k and r-space. The tests in this section have been performed for a Hydrogen impurity in a non-spin polarized system of a homogeneous electron gas. The electronic density is 0.0025. The logarithmic r-mesh is used for the range from 0 to 8 a.u. and the linear r-mesh is used after 8 a.u. The maximum radius

R_{max}	Immersion energy(Ry.)
40	Not converged
50	-0.19392
60	-0.19449
70	-0.19395
80	-0.19402
90	-0.19415
120	-0.19411

TABLE 4.3. Immersion energies for a hydrogen impurity. 70 k points, 550 r points for the logarithmic r-mesh, and 0.1 for the interval of the linear r-mesh are used for these calculations.

is a very important parameter for convergence and stability of the calculations. Since the phase shift calculations are based on a zero potential at the maximum radius R_{max}, the Coulomb potential due to the extra charge must vanish at least at R_{max}. Therefore it is important to include enough Friedel oscillations and also not to loose any significant charge of the bound states. For instance, the convergence required to obtain an immersion energy within a error bar of 1 milli-Rydberg ($(\Delta V)^2 \lesssim 10^{-11}$, See Sec. 4.1.1.) can not be accomplished for $R_{max} = 40$ in Table 4.3. Since the bound state has a very short range at this background density, the main reason is the long tail of Friedel oscillations which prevent the self-consistent calculations from converging. (See Fig. 4.13.) One good barometer for the Friedel oscillations is to include at least 10 λ's where $\lambda = \pi/k_F$. As the background density increases, the bound state plays a more important role and the extended bound state should be considered to determine the maximum radius R_{max}.

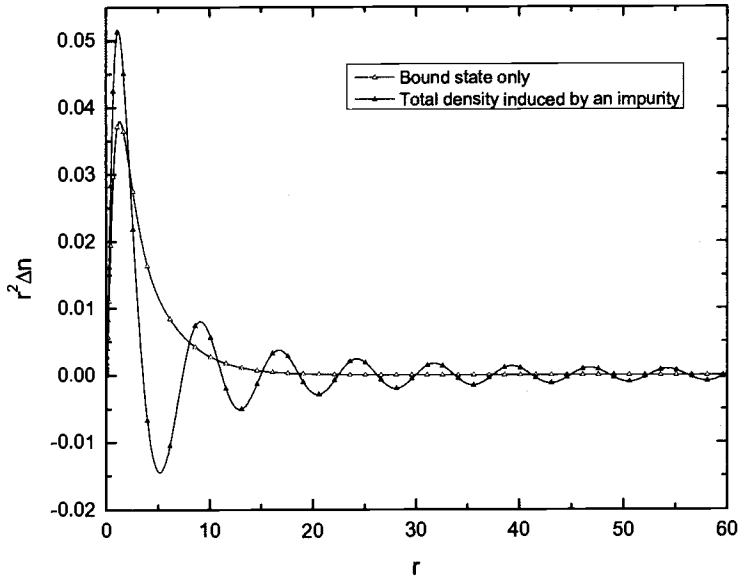

FIGURE 4.13. Extra densities induced by an impurity.

The immersion energies in Table 4.3 show small fluctuation, less than 1 milli-Rydberg, especially for R_{max} larger than 70. Note that the convergence process is smooth for R_{max} larger than 70. The results for the number of r points in the linear r-mesh show a very regular pattern in Table 4.4, similar to that for the number of r points in the logarithmic r-mesh. Fig. 4.14 shows that the immersion energy decreases as the number of r points for the linear r-mesh increases. The difference is, however, not larger than 1 milli-Rydberg. One can use simply 0.1 for the interval of the linear r-mesh to obtain the immersion energy within an error bar of 1 milli-Rydberg. Another important parameter is the number of k points in k-mesh. Since the k-mesh is a simple linear mesh, one can expect simply that a larger number of k points give rise to the better results. However, for smooth

Number of r points	Immersion energy(Ry.)
320	-0.19353
520	-0.19387
720	-0.19402
920	-0.19411
1120	-0.19417

TABLE 4.4. Immersion energies for a hydrogen impurity. 70 k points, 80 for R_{max}, and 550 r points for the logarithmic r-mesh are used for calculations.

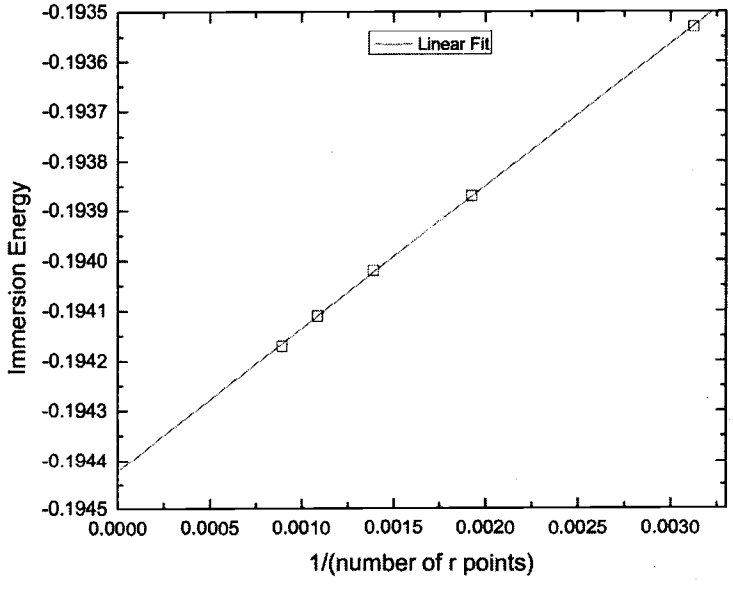

FIGURE 4.14. Immersion energy versus the inverse of the number of r points in the linear r-mesh. Data from Table 4.4.

Number of k points	Immersion energy(Ry.)
60	-0.19403
70	-0.19402
80	-0.19402
90	-0.19402
100	-0.19402

TABLE 4.5. Immersion energies for a hydrogen impurity. There is no difference within 10^{-5} Rydbergs for k points more than 70. 80 for R_{max} and 550 r points for the logarithmic r-mesh are used for these calculations.

behavior of phase shifts, increasing the number of k points does not improve the results significantly. The results for different number of k points are given in Table 4.5, which show there is no noticeable improvements within 10^{-5} Ry. in the immersion energies for more than 70 k points. It should be noted that this result may be quite different for systems which have a large scattering length as mentioned in Sec. 4.4.4. Increasing the number of k points for those systems can adjust the significant charge amount correctly and yield better immersion energies.

4.5. Self-consistent solutions

The self-consistent solutions may depend on the methods to solve numerical problems as well as the boundary conditions. Incorrect numerical parameters or methods may lead to incorrect self-consistent solutions. That is, self-consistency is not a sufficient condition for a correct solution. The only way to obtain the correct self-consistent solutions is to compare the solutions with the results of

other theories or experiments. There are several ways to see if the iterative process converges correctly. The extra charge induced by an impurity can be calculated by the Friedel sum rule, integrating the electronic density in r-space, or integrating the density of states in energy space.

$$Z = 4\pi \int dr\ r^2 \Delta n(r) = \int_{-\infty}^{\epsilon_F} d\epsilon\, \Delta\rho(\epsilon) = Z_b + \frac{2}{\pi}\sum_l (2l+1)\delta_l(k_F) \quad ,$$

where Z_b is the number of electrons in the bound states and the density of states $\Delta\rho(\epsilon)$ can be calculated from the phase shift values as in (3.27):

$$\Delta\rho(\epsilon) = \frac{2}{\pi}\sum_l (2l+1)\frac{d\delta_l(\epsilon)}{d\epsilon} \quad . \tag{4.14}$$

All three results for the extra charge must be very close to each other after the required convergence is achieved. The electronic density far away from an impurity should follow the form of the Friedel oscillations as mentioned in Ch. 3.

$$\sim C_F \frac{\cos(2k_F r + \delta)}{r^3} \qquad \text{at large } r \ \Rightarrow\ \lambda \sim\ 2\pi/2k_F$$

Therefore the wave length of oscillations of the electronic density, λ, should be about $2\pi/2k_F$ at large distances. There could be a virtual bound state if the number of bound state electrons is smaller than that of the positive charge of the impurity. At low background densities, since only low energies are allowed for the conduction band, only s-waves can contribute to the virtual bound state resonance in the density of states. The scattering length can be very important as in the case of a hydrogen impurity when the virtual bound state resonance is located near the conduction band minimum and the non-zero angular momentum states can be neglected. In that case, the sign of the scattering length can also be used to verify the behavior of the conduction band during the iterative loops of the numerical calculations.

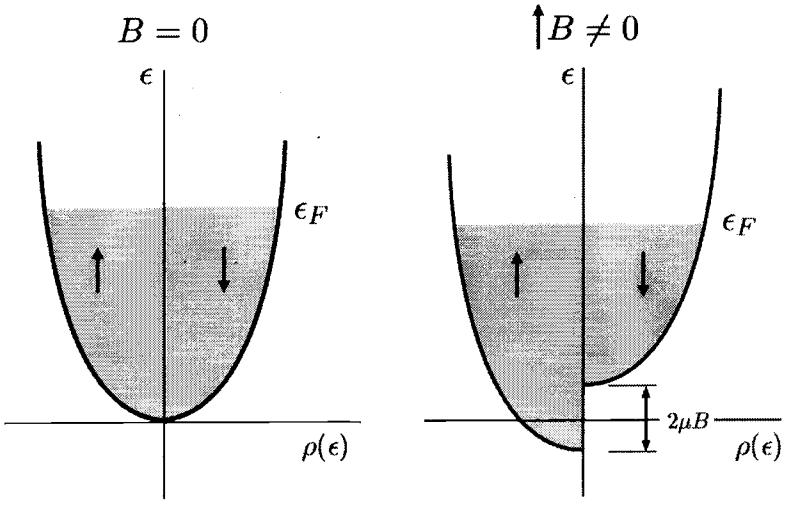

FIGURE 4.15. The density of states at absolute zero temperature. With an external magnetic field, the energy of the spins (magnetic-moment-up) parallel to the field is lowered by μB, while the energy of the spins (magnetic-moment-down) antiparallel to the field is raised by μB. The chemical potential of the spin-up band is equal to that of the spin-down band.

4.6. Spin paramagnetism

A system with an external magnetic field is discussed in Sec. 2.2.6. In this section, details of the numerical implementation will be discussed. Note that the spin-up band is assumed to be parallel to an external magnetic field in this work.[10] The energy shift by an external magnetic field in Fig. 4.15 is $\pm\mu B$ where $-$ and $+$ should be taken for the spin-up and spin-down band respectively and μ is the Bohr magneton. Some electrons near the Fermi energy transfer from the spin-down band to the spin-up band such that the chemical potential (Fermi energy) of the

[10]The term, spin-up, in this work denotes spin-magnetic-moment-up since the magnetic moment is opposite in sign to the spin S for an electron.

spin-up band equals that of the spin-down band. The range of k corresponding to the range of the energy from the conduction band minimum to the Fermi energy adjusts as well.

$$\text{spin-up:} \quad 0 \leftrightarrow \sqrt{\epsilon_F + u}$$
$$\text{spin-down:} \quad 0 \leftrightarrow \sqrt{\epsilon_F - u} \ ,$$

where $u = \mu B$. The number of electrons is:

$$N_+ = \frac{V}{(2\pi)^3}\frac{4}{3}\pi(\epsilon_F + u)^{3/2} \quad \text{for spin-up} \tag{4.15}$$
$$N_- = \frac{V}{(2\pi)^3}\frac{4}{3}\pi(\epsilon_F - u)^{3/2} \quad \text{for spin-down.} \tag{4.16}$$

Now one can easily obtain the equation for the Fermi energy ϵ_F.

$$6\pi^2 n = (\epsilon_F + u)^{3/2} + (\epsilon_F - u)^{3/2} \ . \tag{4.17}$$

Note that the Bohr magneton μ in atomic Rydberg unit is $\sqrt{2}$ and one atomic Rydberg unit for the magnetic induction B corresponds to 3.324×10^5 T in SI.

Since the Fermi wave vector k_F of the spin-up band is different from that of the spin-down band with an external magnetic field, one can expect from the Friedel oscillations that the electronic density for each band behaves differently even at large distances. Now, since there are two different frequencies in the Friedel oscillations of the density, there should be patterns of beats[11] in the total electronic density induced by an impurity. The Coulomb potential calculated from the total

---

[11]The term, beat, is originally used to describe fluctuations in the amplitude variation caused by two sound waves of different frequency. In this work, beats are used to emphasize the alternating constructive and destructive interference of two electronic density oscillations of different frequency.

electronic density, hence, has also patterns of beats as well. In that case one can not use the method for the potential correction, which was introduced in Sec. 4.4.2 because the method takes advantage of the shape of the regular oscillations. However, one can avoid the beat patterns by calculating the Coulomb potential separately from the density of the spin-up and spin-down band and applying the method for each part of the Coulomb potential. After correcting each Coulomb potential, one can find the total Coulomb potential by adding both contributions to Coulomb potential and finally the effective potential for each band by adding the exchange-correlation potential of each band to the total Coulomb potential. The Coulomb potential separately calculated from the density of each band, however, still may have irregular patterns but not as strong as the total Coulomb potential. This is a second order effect since the calculations for the density are essentially based on an effective potential which has these beat patterns. Therefore it is important to use a very large maximum radius to reduce the numerical error in case that the irregular pattern causes a large numerical error. One often needs to examine the Coulomb potential and the effective potential during the iterative loops of numerical calculations and find the appropriate maximum radius. Note that the beat frequency k_{beat} is the difference of the two frequencies.

$$k_{beat} = 2k_F^+ - 2k_F^- \quad . \tag{4.18}$$

Thus one can estimate how many beats exist for a given range of r in the electronic density.

5. RESULTS AND DISCUSSION

Two important quantities for the model used in this work are the positive charge of an impurity and the electronic background density. The Coulomb potential is determined by the positive charge of an impurity and the induced electronic density while the exchange-correlation potential is determined by the induced electronic density and the electronic background density. If the induced electronic density remains the same for the same impurity,[1] the exchange-correlation interaction makes a difference between two different background densities, which, for a different background density, leads to a different self-consistent solution with different induced charge densities, potentials, bound states, phase shifts, densities of states, and dielectric functions. The system still obeys the Friedel sum rule and exhibits Friedel oscillations. The results in this chapter are categorized by spin polarization. For a spin-polarized system, the total spin-moment will also be an important physical quantity, which may distinguish between self-consistent solutions.

---

[1]This is not true. As the difference between background densities becomes larger, the response of an electron gas becomes more important due to the difference in Fermi energies and in Friedel oscillations. This effect is related to the amount of induced charge in the vicinity of an impurity as well as to the oscillations of the density at large distances.

5.1. Non-spin-polarized system

The non-spin-polarized system is tested mainly with a hydrogen impurity. The discussion in this section will proceed using a hydrogen impurity unless noted differently.

5.1.1. Behavior of a system during the numerical calculations

The number of electrons induced by a hydrogen impurity should always be equal to one in order to screen the hydrogen impurity in a self-consistent manner, as mentioned in Ch. 3. Fig. 5.1 shows one example how the system evolves to satisfy self-consistency. Since the input effective potential for the first iteration is calculated from the electronic density of a free hydrogen atom plus a background density of 0.06, the effective potential is sufficiently attractive at the beginning and thus there are two extra electrons in the bound states. The background density is, however, very high. Since the system with two electrons in the bound states of a hydrogen impurity can not be the self-consistent solutions for such a high background density, the system goes through a transition from having a bound state to not having a bound state and adds one extra electron in the conduction band. Notice in Fig. 5.1 that the Friedel sum during the transition responds to the change in the number of electrons in the bound states, while the conduction band continuously adds electrons to make one extra electron.

5.1.2. Charge densities and potentials

As already mentioned in Ch. 3, the Friedel oscillations are independent of the nature of an impurity. The induced electronic densities at large distances

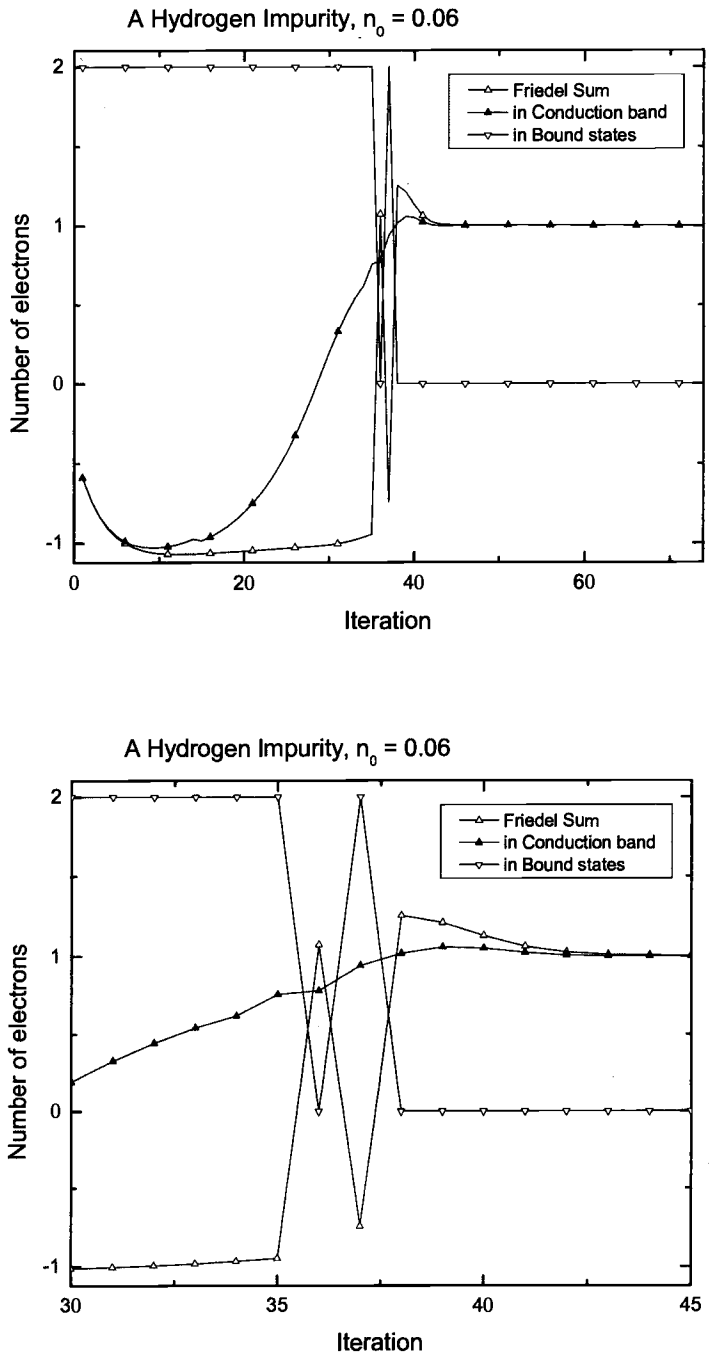

FIGURE 5.1. Variation of the number of extra electrons for a system with a hydrogen impurity during the iterative loops of the numerical calculations. The background electronic density is 0.06.

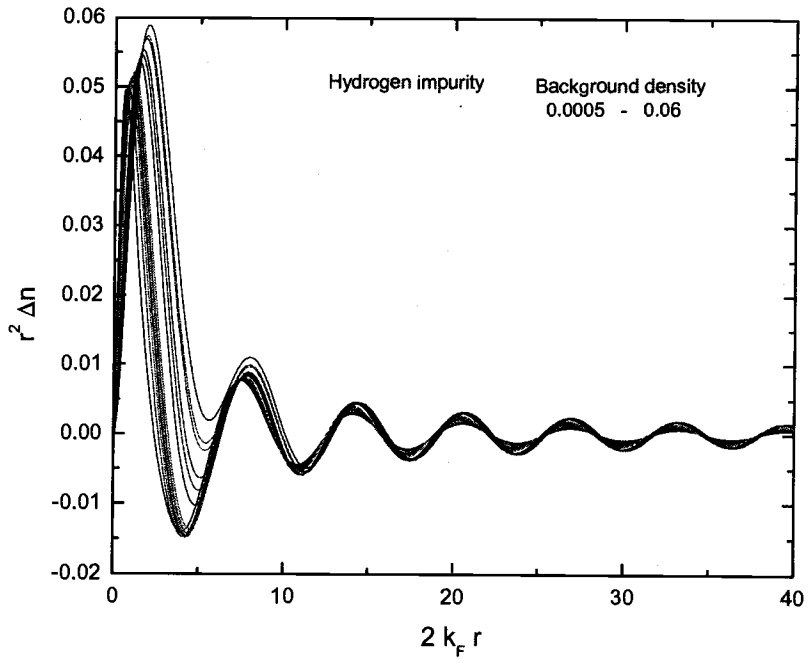

FIGURE 5.2. The electronic density induced by a hydrogen impurity. It is plotted as a function of $2k_F r$. Friedel oscillations are independent of the background density. The range of the background density is from 0.0005 to 0.06.

show Friedel oscillations and they all have the same frequency $2k_F$, as illustrated in Fig. 5.2. The induced electronic densities as a function of r are shown in Fig. 5.3. Note that although there is always one extra electron in the system of a hydrogen impurity, regardless of the background density, the amount of the electronic charge in the vicinity of the impurity ($r : 0 \sim 4$) is dependent upon the background density. There is relatively a large amount of electrons near the impurity for low background densities as a result of the effect of bound states and the Friedel oscillations in the conduction band. (Fig. 5.4 and Fig. 5.5) These phenomena are related to the behavior of the dielectric functions, different from

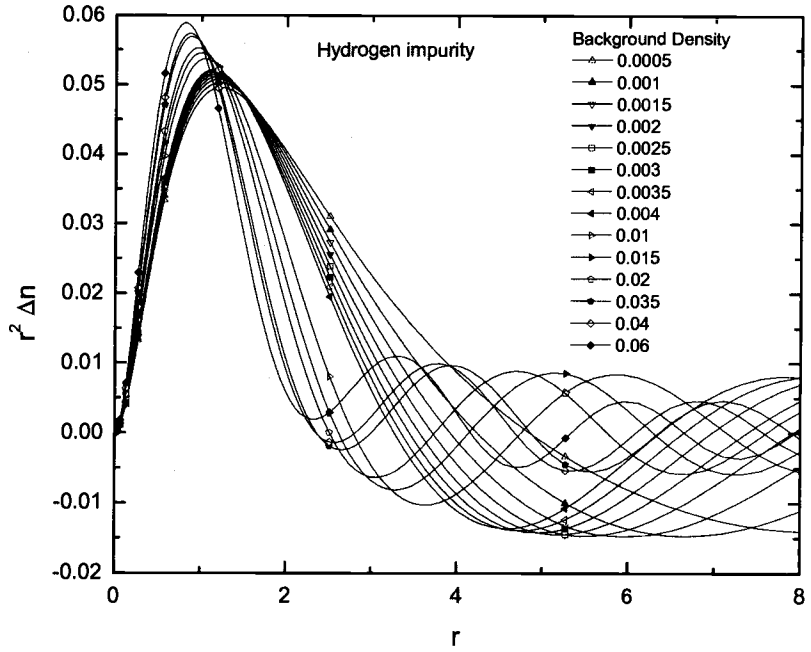

FIGURE 5.3. The electronic density induced by a hydrogen impurity.

the Thomas-Fermi dielectric functions, which will be discussed in Sec. 5.1.4. The electronic density in the bound states becomes more extended and the maximum value of the density decreases as the background density increases. (Fig. 5.4) The bound states disappear for the background density higher than about 0.03. The numerical calculations for the background density between 0.02 and 0.03 are very difficult due to the greatly extended bound states. These results are not included in Fig. 5.4 and Fig. 5.5 since the required convergence could not be obtained. As discussed in Sec. 3.5, however, the transition from bound states to resonance states should not result in any non-analytic behavior of the properties of the system such as the immersion energy. The maximum value of the induced electronic density in

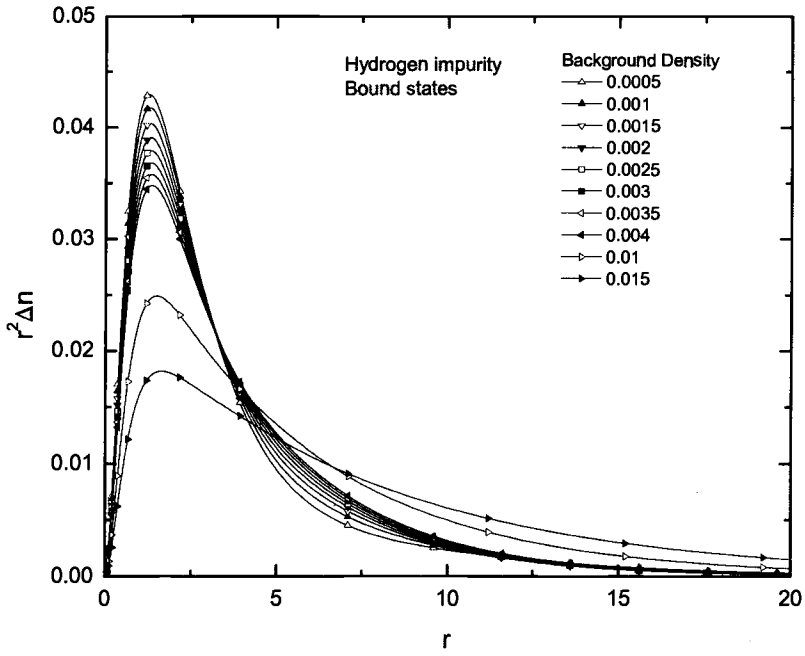

FIGURE 5.4. The electronic density induced by a hydrogen impurity in the bound states.

the conduction band increases in the vicinity of the impurity as the background density increases. (Fig. 5.5) As a result, the impurity is always screened sufficiently regardless of the existence of bound states.

5.1.3. Phase shift, Scattering length, and Density of induced states

Phase shifts for $l = 0$ at zero energy have the value of π for low background densities, due to the presence of a bound state of a hydrogen impurity. The result is shown in Fig. 5.6. Note that there are two electrons in the bound state due to the spin degeneracy. The variations of the phase shifts of p-waves in the case

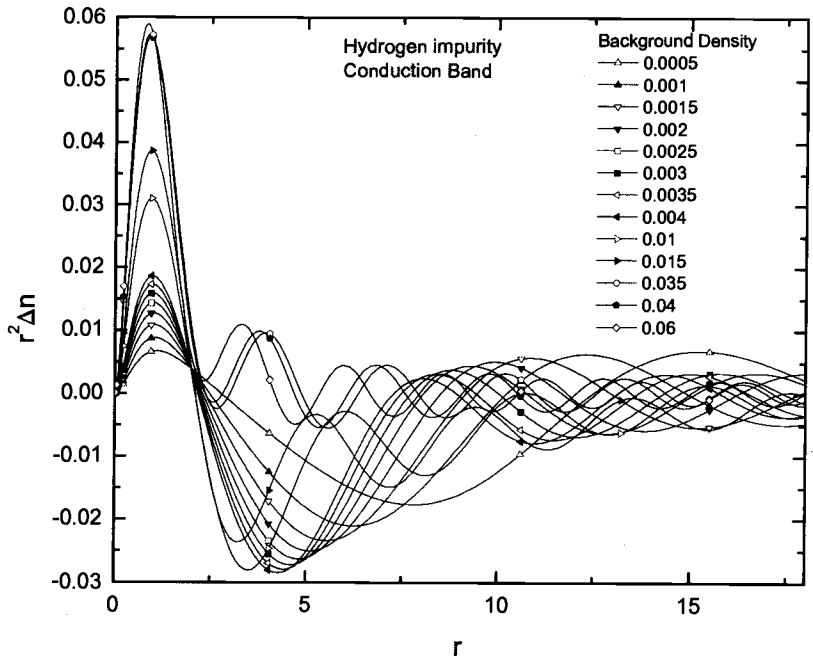

FIGURE 5.5. The electronic density induced by a hydrogen impurity in the conduction band.

of a hydrogen impurity are relatively very small compared to those of s-waves[2] and thus the leading contribution to the change in the density of states arises from the phase shifts for $l = 0$. The slope of the phase shift (or the scattering length) for low background densities is negative, from which one sees that the

---

[2]This is only true if there are two electrons in the bound states. If the number of electrons is smaller than two, phase shifts of p-waves also become important and contribute significantly to the change in the number of electrons in the conduction band. See Sec. 5.1.6.

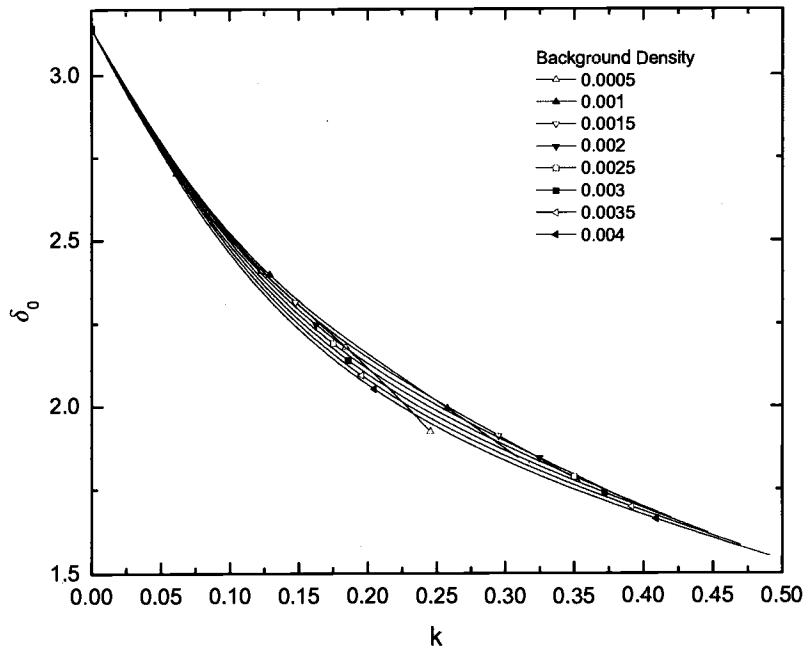

FIGURE 5.6. Phase shifts ($l = 0$) for a hydrogen impurity. Plotted for low background densities only.

potential is attractive enough to have a first bound state and, considering the density of states, the conduction band loses one electron to keep the number of total extra electrons one. The magnitude of the slope of the phase shifts in general becomes smaller in Fig. 5.6 as the background density decreases, which one can expect considering the relationship between the strength of the potential and the scattering length.[3] However, as the background density decreases more, the phase

---

[3]One may expect that the potentials become more attractive as the background density decreases, which means that the scattering length decreases in magnitude. [31]

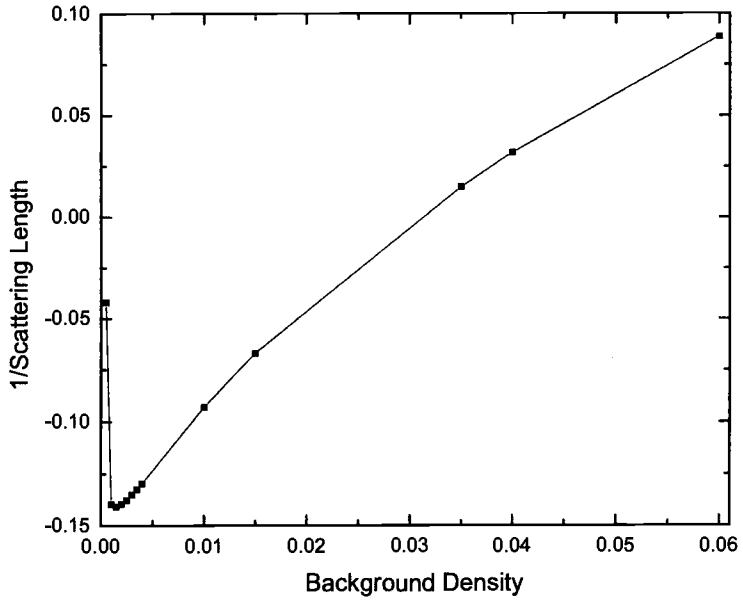

FIGURE 5.7. Inverse of scattering length versus background density for a hydrogen impurity.

shifts near the conduction band maximum tend to have a larger negative slope than those of the higher background densities. At extremely low background densities such as 0.0005, even the slope near the conduction band minimum becomes larger. (See Fig. 5.7.) The reason for this is that a smaller negative slope in the phase shifts can not yield a correct negative excess charge at such a low background density to satisfy the Friedel sum rule as *the conduction band becomes narrower.*[4]

---

[4]Moreover, as the background density decreases, the contribution of s-waves to the number of induced electrons becomes larger, and thus the phase shifts of s-waves at the Fermi energy should respond accordingly.

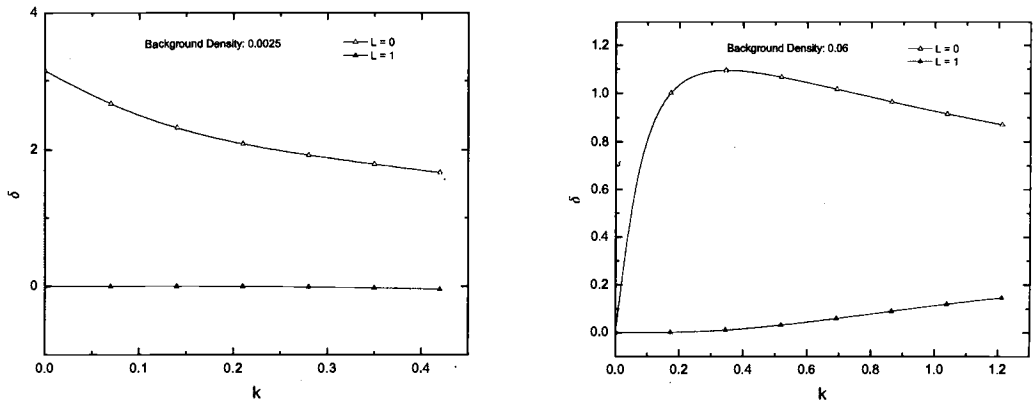

FIGURE 5.8. Phase shifts for a hydrogen impurity for two different background densities (0.0025 and 0.06).

As a result, the system behaves such that the potentials are less attractive at the extremely low background densities. For high background densities (≥ 0.03) for a hydrogen impurity, since there are no electrons in the bound states, there should be one extra electron in the conduction band, for which the contribution of s-waves to a virtual bound state resonance is significantly larger than the higher angular momentum states. (Fig. 5.8) The scattering lengths corresponding to the phase shifts in Fig. 5.9 are shown in Fig. 5.7. The transition from a bound state to a resonance state occurs at about 0.03 of the background density, close to when the sign of the scattering length changes. The inverse of the scattering length increases as the background density increases from 0.0015. The magnitude of the scattering length, however, rapidly increases as the background density decreases from 0.0015 and becomes large at extremely low background densities (≤ 0.001), which creates a minimum point at about 0.0015 in Fig. 5.7. This behavior is already discussed with the phase shifts above.

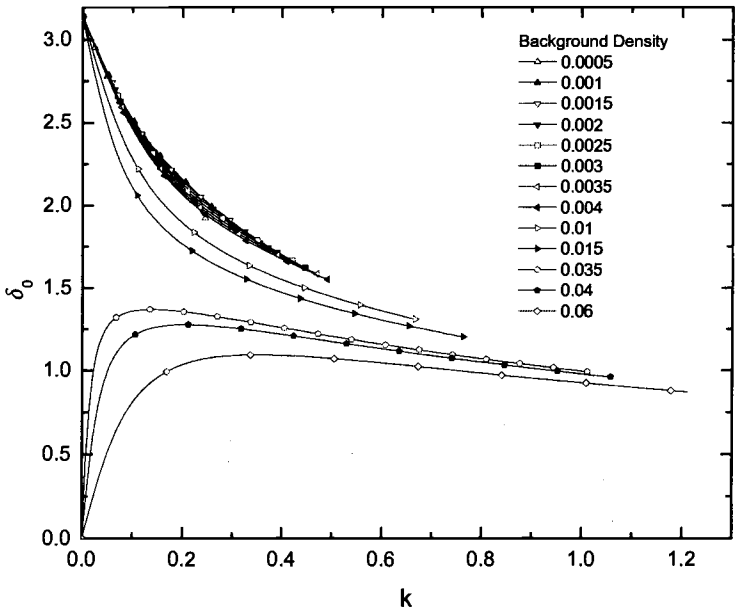

FIGURE 5.9. Phase shifts ($l = 0$) for a hydrogen impurity.

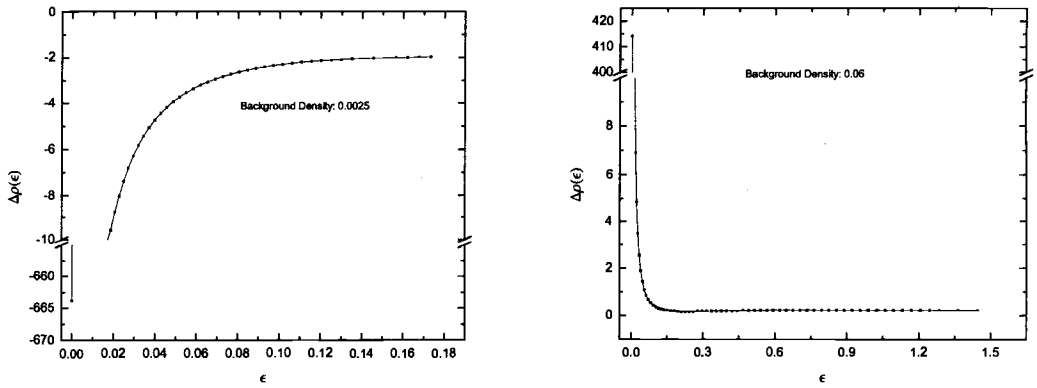

FIGURE 5.10. The density of states for a hydrogen impurity for two different background densities (0.0025 and 0.06).

Typical examples for the density of states are shown in Fig. 5.10. At the background density of 0.0025, there are two electrons in the bound state, and the leading contribution to the conduction density of states comes from s-states, which show a negative scattering length and a sharp negative peak at the conduction band minimum in the density of states. The conduction band loses one electron, which removes the excess charge of the bound state electrons. At the background density of 0.06, there are no electrons in the bound states. The effective potential is, however, attractive enough to induce an extra electron in the conduction band, which appears as a narrow peak in the conduction density of states due to the rapid increase of the phase shift of $l = 0$ in the region of the conduction band minimum. Therefore one sees that the Friedel sum rule is always satisfied and can be achieved at self-consistency during the numerical calculations. The phase shifts for a lithium impurity are shown in Fig. 5.11. At the background density of 0.0005, the electron configuration of a lithium impurity is $1s^2 2s^2$ and the phase shift of the zero energy must be 2π (third branch[5] of $\tan\delta_0$) by Levinson's theorem. The phase shift at 0.0005 shows a large negative slope, which gives rise to the negative density of states in the conduction band to remove the excess charge due to the bound states. As the background density increases, the effective potential becomes less attractive and the system loses a bound state (second branch of $tan\delta_0$) and the scattering length becomes positive. (phase shifts at 0.0025 in Fig. 5.11) If the background density further increases, the scattering length decreases (phase shifts at 0.03 in Fig. 5.11) and becomes negative. At the higher background density the

---

[5]See (3.26) and [31].

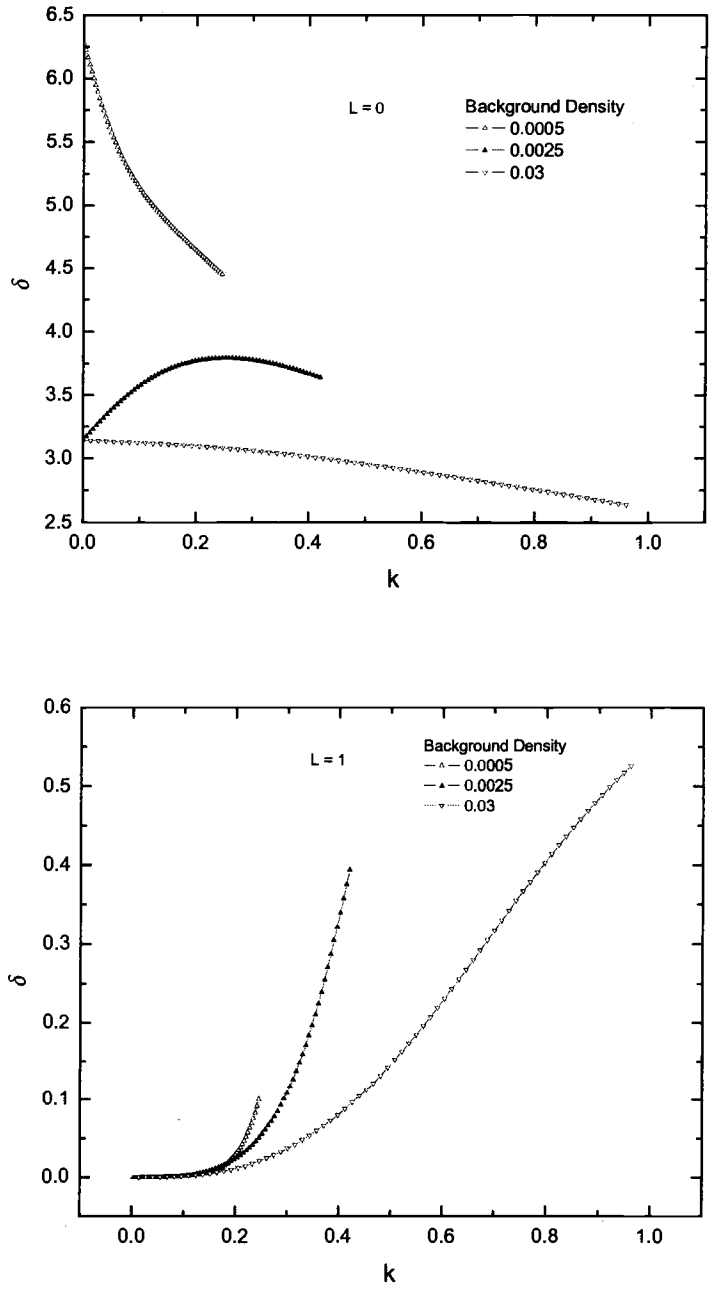

FIGURE 5.11. Phase shifts of $l = 0$ and $l = 1$ for a lithium impurity.

same cycle of the phase shifts repeats, after loosing one more bound state. (first branch of $tan\delta_0$)

5.1.4. Dielectric constant and compressibility

The dielectric constants can be easily calculated using the definition in (3.55) and the Fourier transform.

$$\epsilon(w, \boldsymbol{q}) = \frac{V_{\boldsymbol{q}}^{ext}}{V_{\boldsymbol{q}}^{eff}} \tag{5.1}$$

$$= \frac{\int d\boldsymbol{r}\ \exp(-iqr)\frac{-Ze^2}{r}}{\int d\boldsymbol{r}\ \exp(-iqr)V(r)} \tag{5.2}$$

$$= \frac{-e^2 Z}{q\int dr\, V(r) r \sin(qr)} \quad . \tag{5.3}$$

The Thomas-Fermi dielectric constant, already introduced in Sec. 3.4, is given by

$$\epsilon_{TF}(0, \boldsymbol{q}) = \frac{q^2 + q_{TF}^2}{q^2} \quad , \tag{5.4}$$

where $q_{TF}^2 = \frac{4e^2 m k_F}{\hbar^2 \pi}$. The Thomas-Fermi dielectric constants in Fig. 5.12 show a simple behavior which gives a screening length[6] proportional to $n^{-1/3}$. One can expect from the Thomas-Fermi dielectric constants that a higher background density has a shorter screening length. The numerical results of the dielectric constants for a hydrogen impurity and the Thomas-Fermi dielectric constants both approach the value of one as $q \to \infty$. The density functional calculations, however, show quite different results for the dielectric constants, especially at small q values. Note that the presence of electrons in the bound states and the long wave length of the

---

[6]The screening length for the Thomas-Fermi dielectric constants can be easily obtained from the Yukawa potential, $l = 1/q_{TF}$. See (3.67).

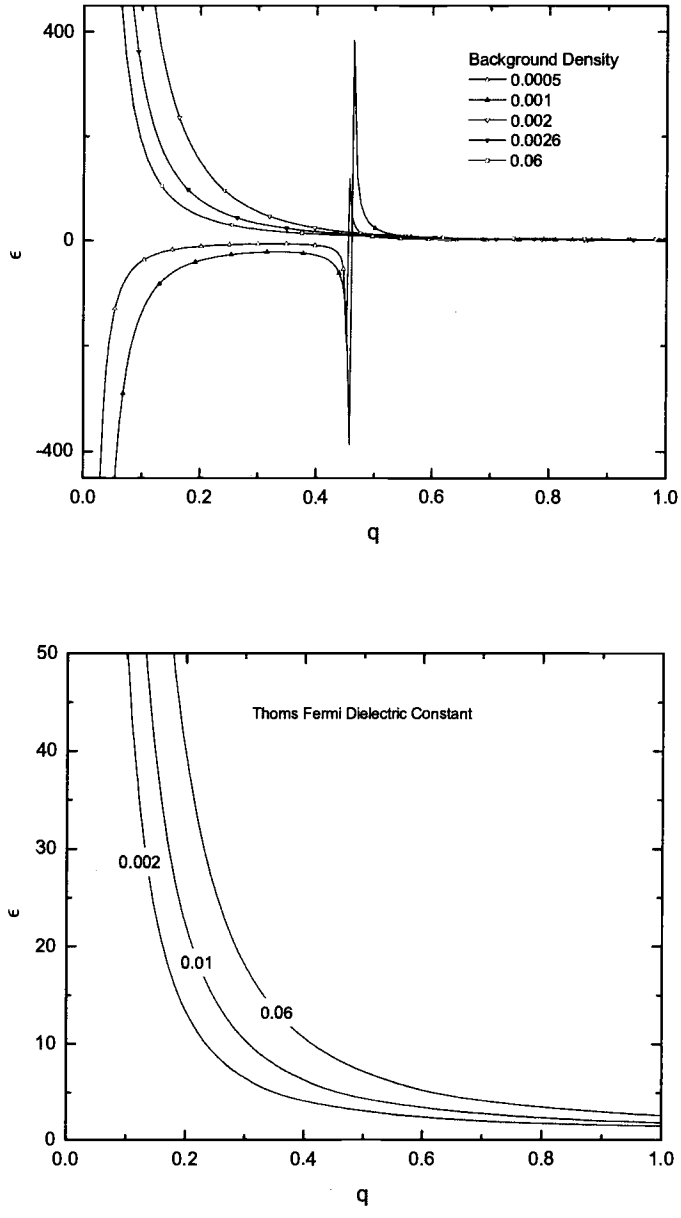

FIGURE 5.12. Dielectric constants which are numerically calculated for a hydrogen impurity. The Thomas-Fermi dielectric constants are also plotted for comparison.

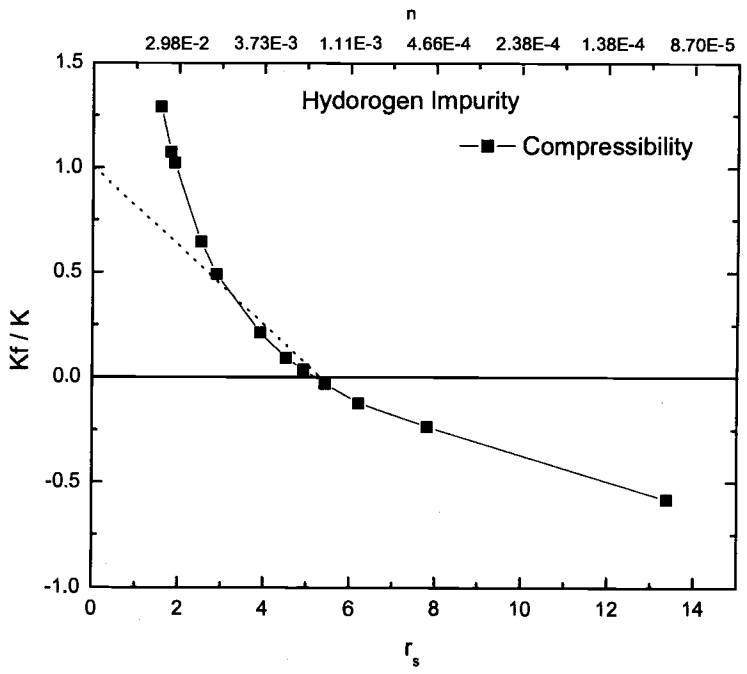

FIGURE 5.13. Compressibility calculated numerically for a hydrogen impurity. A dotted line which is taken from [6] is for the result predicted by theories such as Hubbard, VS, and SS. Both lines are going through zero around $r_s = 5.0$. The electronic density which corresponds to r_s of the bottom x-axis is given in the top x-axis.

Friedel oscillations result in a larger amount of screening charge near the impurity for low background densities than for high background densities, as already mentioned in Sec. 5.1.2. One sees that dielectric constants may have very large negative or positive values for a certain q while the integral term in (5.3) increases from negative to positive values near zero. Actually, it turns out that the integral term in (5.3) changes its sign from negative to positive as the low background density ($n \simeq 0.00191$ or $r_s \simeq 5.0$) decreases further. At extremely low background densities (≤ 0.0015), therefore, the dielectric constants for $q \to 0$ are negative, as

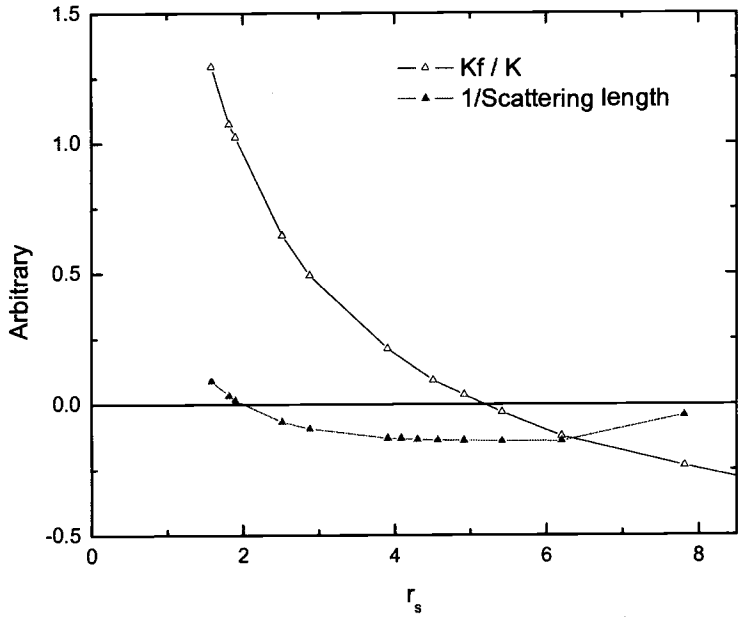

FIGURE 5.14. Comparison of the compressibility calculated numerically for a hydrogen impurity with scattering length.

illustrated by Fig. 5.12. This result can be verified by discussing compressibilities. The compressibility can be obtained in terms of the dielectric function by [13]

$$\lim_{q\to 0} \epsilon(q,0) = \frac{q^2+q_{TF}^2}{q^2}\frac{K}{K_f} \quad , \tag{5.5}$$

where $q_{TF} = 6\pi n e^2/\epsilon_F$ is the Thomas-Fermi wave number and the quantity $K_f = 3(3\pi^2)^{-2/3}n^{-5/3}[1/e^2a_0]$ is the isothermal compressibility of the non-interacting electron gas at zero temperature. The compressibility is already obtained by several theories.[7] The RPA gives the constant value 1.0 for K_f/K while many other

[7]Readers should refer to [18] for more details.

theories such as Hubbard, Singwi-Sjölander, and Vashishta-Singwi give results for K_f/K, which all go through 0 around $r_s = 5.0$. [18] The density functional calculations for the compressibility give rise to nearly the same result for K_f/K as those theories for low background densities but to much larger values for high background densities, which results in the curved line of a hyperbolic type in Fig. 5.13. One sees from (5.5) and Fig. 5.13 that the dielectric constant for the high background density as $q \to 0$ has a smaller value than expected by theories[8] while the dielectric constant for the low background density has a larger value.[9] In other words, if the screening length can be defined for any potential[10], it can be stated that the screening length for the high background density has a larger value than expected by analytical theories while the screening length for a low background density has a smaller value.

As shown in Fig. 5.14, one sees that the negative minimum (at $r_s \simeq 5.0$) of a value of the scattering length corresponds to infinity of the compressibility and infinity (at $r_s \simeq 2.0$) of a value of the scattering length corresponds to the compressibility close to K_f. Note that infinity of a scattering length indicates the transition from a bound state to a resonance state. One may think that the most attractive potential corresponds to the maximum of the compressibility, which

---

[8]See the dotted line in Fig. 5.13. As $r_s \to 0$, the expected dielectric constant is the Thomas-Fermi dielectric constant.

[9]Note that, in Fig. 5.13, the dielectric constants calculated by theories are always larger than or equal to the Thomas-Fermi dielectric constants.

[10]One can try to find the screening length for a particular potential by comparing with the Thomas-Fermi dielectric constant. $l = 1/q_{TF} = ((\epsilon(q) - 1)q^2)^{-1/2}$ as $q \to 0$

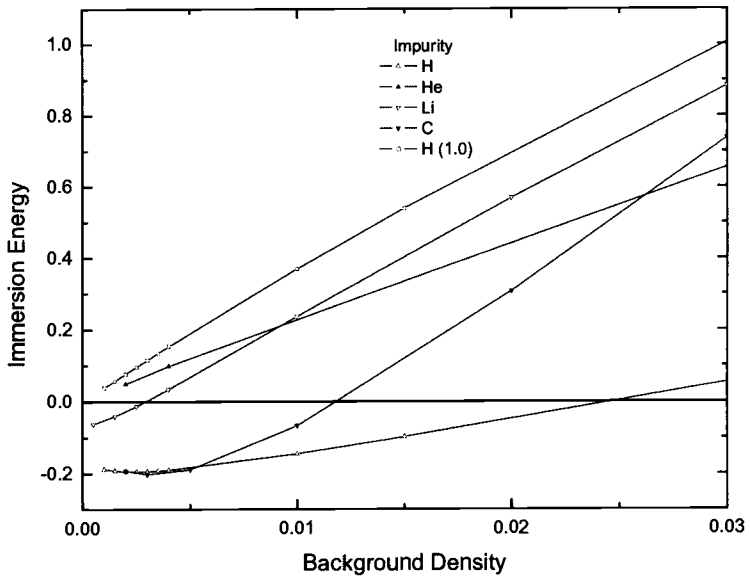

FIGURE 5.15. Immersion energies for several different impurities. 1.0 in the legend indicates that the number of electrons in the bound states is limited to 1.0. 465 points for the logarithmic r-space and 0.81205×10^{-5} for the first value of r-mesh are used in these calculations.

may be related to the localization of electrons [11]. The relationship between the scattering length and the compressibility, however, needs further investigation.

5.1.5. Immersion energy

Immersion energies for H, Li, and C are shown in Fig. 5.15. A minimum in the immersion energy exists for H and C, while calculations for Li can not verify

---

[11] Wigner lattice [18]

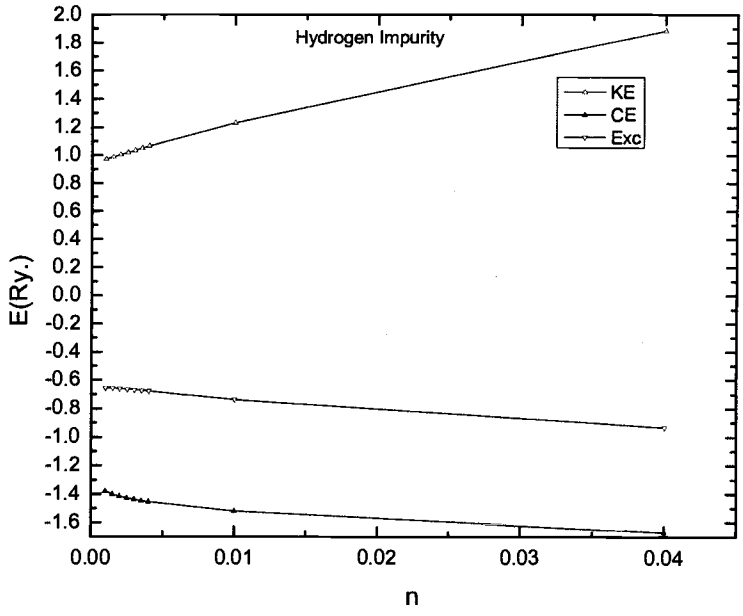

FIGURE 5.16. Variation in the kinetic, Coulomb, and exchange-correlation energies vs the background density for a hydrogen impurity. 465 points for the logarithmic r-space and 0.81205×10^{-5} for the first vale of r-mesh are used in these calculations.

the existence of a minimum immersion energy.[12] The background densities at which the minimum immersion energies exist are 0.0024 for H and 0.0033 for C. The immersion energy after the minimum value increases almost linearly as the background density increases, which is due to the repulsion related to the increase

---

[12]To verify the existence of the minimum immersion energy for Li, it is necessary to perform the calculations for very low background densities as shown in Fig. 5.15, which is, however, very difficult due to the long range wave length of the Friedel oscillations as mentioned in Ch. 4.

in the kinetic energy. [5] The Coulomb and exchange-correlation energies actually become lower as the background density increases. The rate of the increase in the kinetic energy is, however, large enough to compensate this decrease, as illustrated in Fig. 5.16.

The zero background density limit in this infinite system may be different from a free atom without an electron gas. Since the system, at constant chemical potential, is extended to infinity, the impurity will be screened, no matter how small the background density, (but not zero) and, for this non-spin-polarized infinite system, the impurity is not allowed to have partially occupied orbitals.[13] Calculations show that a hydrogen impurity has no electrons in the bound states for high background densities($\gtrsim 0.03$) and two electrons in the bound states for low background densities but no electrons again for extremely low background densities($\lesssim 0.0001$), which can be seen from the fact that a free hydrogen atom can not have two electrons in the bound states in LDA. The interesting result is that the immersion energy for a hydrogen impurity shows a linear behavior as illustrated in Fig. 5.15 when the hydrogen is forced to have only one electron in the bound states regardless of the background density. Immersion energy in this case approaches zero as the background density goes to zero, which one can easily expect from the fact that a free hydrogen atom has only one electron. A helium impurity which has two bound state electrons in a homogeneous electron gas shows the same linear behavior in Fig. 5.15.

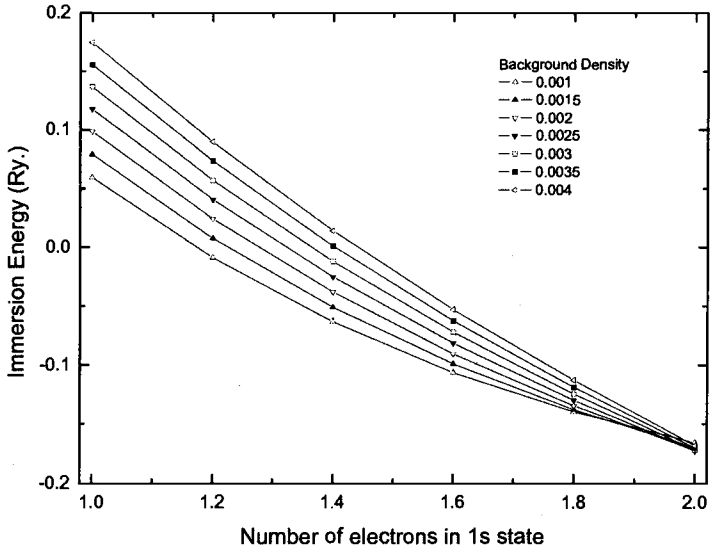

FIGURE 5.17. Immersion energies for the different number of electrons in the bound states. 465 points for the logarithmic r-space and 0.81205×10^{-5} for the first value of r-mesh are used in these calculations.

5.1.6. Excited system

One can easily calculate the immersion energies of excited systems and obtain the excitation energies by varying the number of electrons in the bound states as mentioned in Sec. 2.2.5. The bound state energy decreases as the number of electrons in an $1s$ state decreases while the immersion energy increases. (See Fig. 5.17.) This can be verified by Janak's theorem:

$$\frac{\partial E_{imm}}{\partial n_i} = \epsilon_i(n_i) \quad , \tag{5.6}$$

---

[13]For instance, only two or zero electrons are allowed in an $1s$ state.

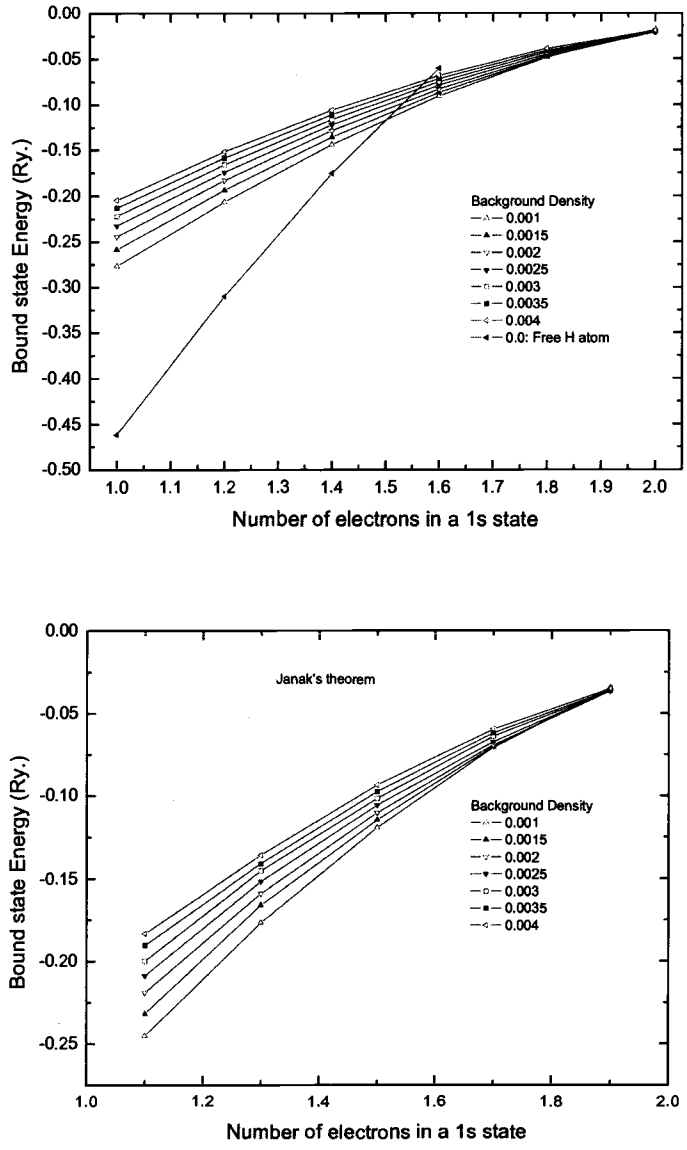

FIGURE 5.18. Variation in the bound state energy for the different number of electrons in the bound state. The second plot is obtained using (5.7) and slopes between two adjacent immersion energies in Fig. 5.17. 465 points for the logarithmic r-space and 0.81205×10^{-5} for the first value of r-mesh are used in these calculations.

where n_i denotes the occupation number of the level i. However, one needs to consider the change in the number of electrons at the Fermi energy as well as the bound states in order to compare the bound state energy with the variation of the immersion energy using Janak's theorem. Janak's theorem (5.6) should be modified as

$$\frac{\partial E_{imm}}{\partial n_i} = -\epsilon_F + \epsilon_i(n_i) \quad , \tag{5.7}$$

where ϵ_F is the Fermi energy. Fig. 5.18 shows the result of (5.7) with the bound state energy plot. Bound state energies obtained from (5.7) are in error with respect to actually calculated bound state energies by an energy difference smaller than 0.005 Rydbergs.[14] Bound state energies of a free hydrogen atom are included in Fig. 5.18. One should, however, recall that the zero background density limit may be different from a free atom as discussed in Sec. 5.1.5. One sees from the Friedel sum rule that the screening in the model used in this work will always occur as long as there is a background density. The extra electrons in the conduction band will respond to the excess core charge, which makes the zero background density limit different from a free atom. A hydrogen impurity which has only one electron in a homogeneous electronic gas is, however, expected to reach a free hydrogen atom as the background density goes to zero. Since the extra electron in the conduction band in this case must be zero, as the background density goes to zero, the only response of the conduction band will be that the wave length of the Friedel oscillation gets longer and it is found that the amplitude of the Friedel oscillation near an impurity gets smaller. This statement is, however, not

---

[14]These differences are mainly due to inaccurate numerical derivatives.

verified numerically for a background density lower than 0.001 due to the numerical problems discussed in Ch. 4.

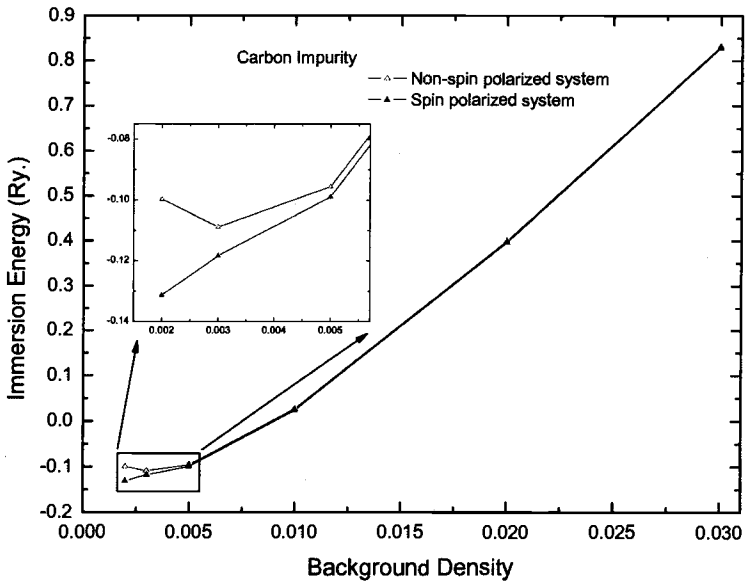

FIGURE 5.19. Comparison of immersion energies for a carbon impurity between a non-spin-polarized system and a spin-polarized system. The same reference energy for a free carbon atom is used for both calculations.

5.2. Spin polarized system

5.2.1. Zero external magnetic field

5.2.1.1. Carbon impurity at low background densities

A carbon impurity is mainly used for a spin-polarized system in this work and interesting results are obtained at low background densities. Fig. 5.19 shows immersion energies for a spin-polarized system and a non-spin-polarized system of a carbon impurity. Overall, immersion energies of a spin-polarized system are slightly lower than those of a non-spin-polarized system. Note that these calculations are based on the same energy of a free atom, that is, the same reference and thus only

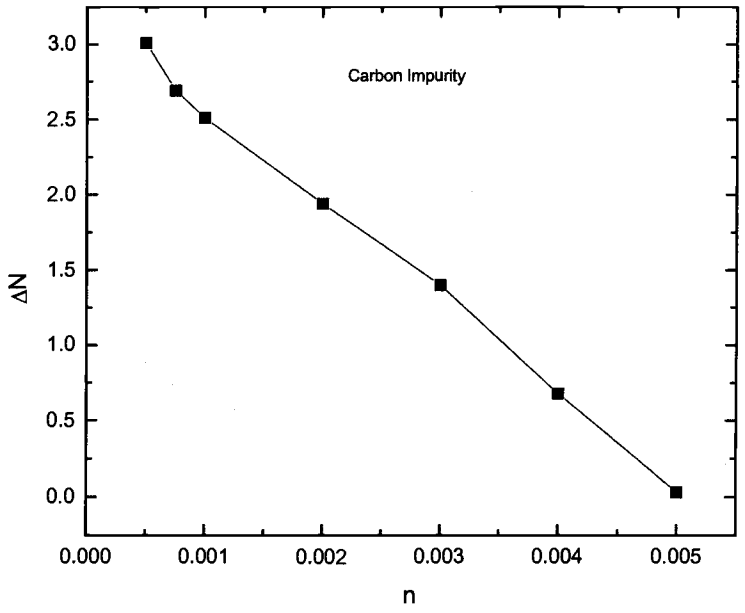

FIGURE 5.20. Plot of ΔN vs a background density where ΔN is the difference in the number of electrons between spin-up and spin-down electrons in a system.

relative energies between two systems are meaningful. One important difference between the two systems is the response of the conduction band to the number of extra electrons in the bound states at low background densities(≤ 0.005). For both systems, there are only four electrons in the bound states with the configuration $1s^2 2s^2$, for a background density higher than 0.002. Note that there should be two electrons in the conduction band due to the Friedel sum rule if there are four electrons in the bound states of a carbon impurity, which is true for both systems. However, a spin-polarized system shows a non-zero magnetization for a background density lower than 0.005, which makes a difference in the immersion energy compared to the non-spin-polarized system. One sees that, in Fig. 5.20,

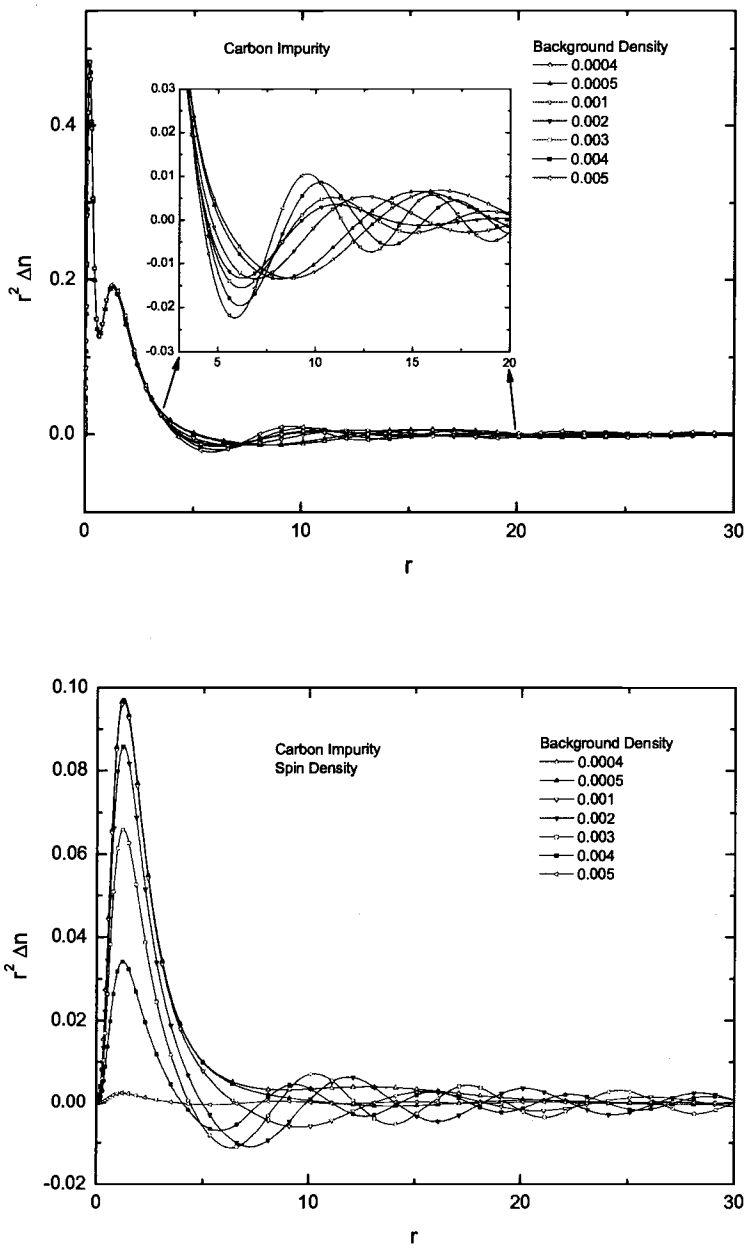

FIGURE 5.21. The electronic density and the spin density induced by a carbon impurity.

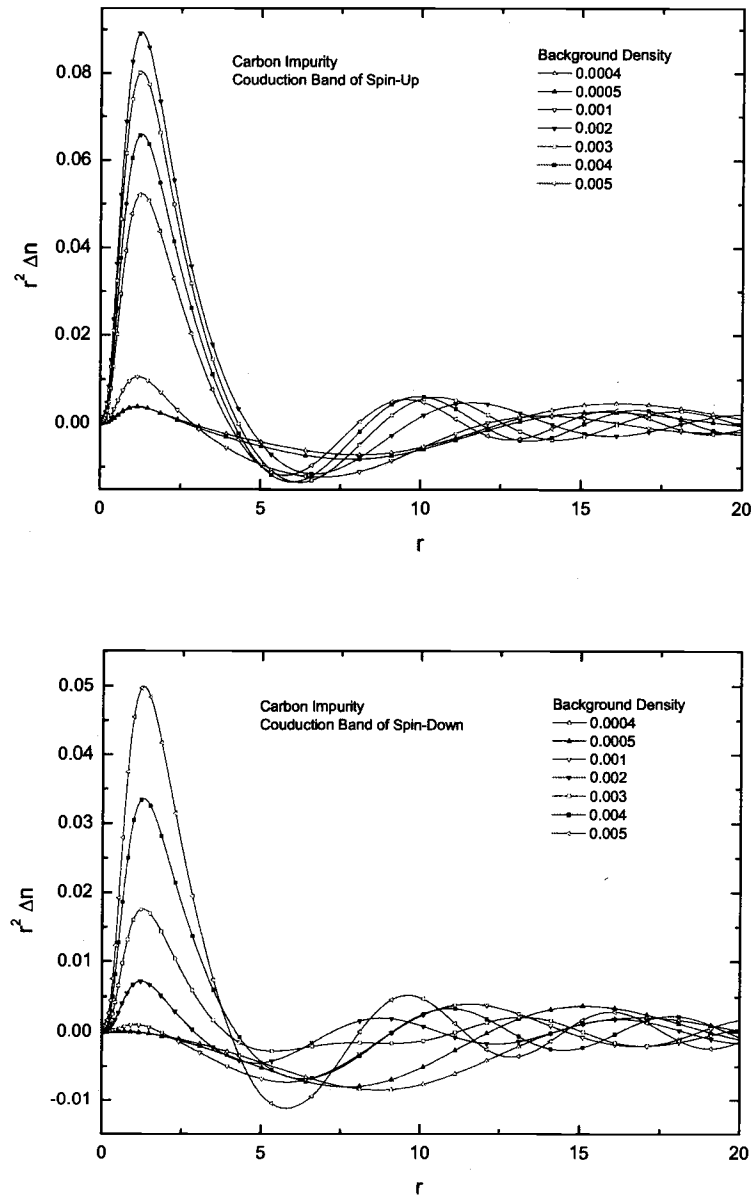

FIGURE 5.22. The electronic density (spin-up and spin-down) induced by a carbon impurity in the conduction band.

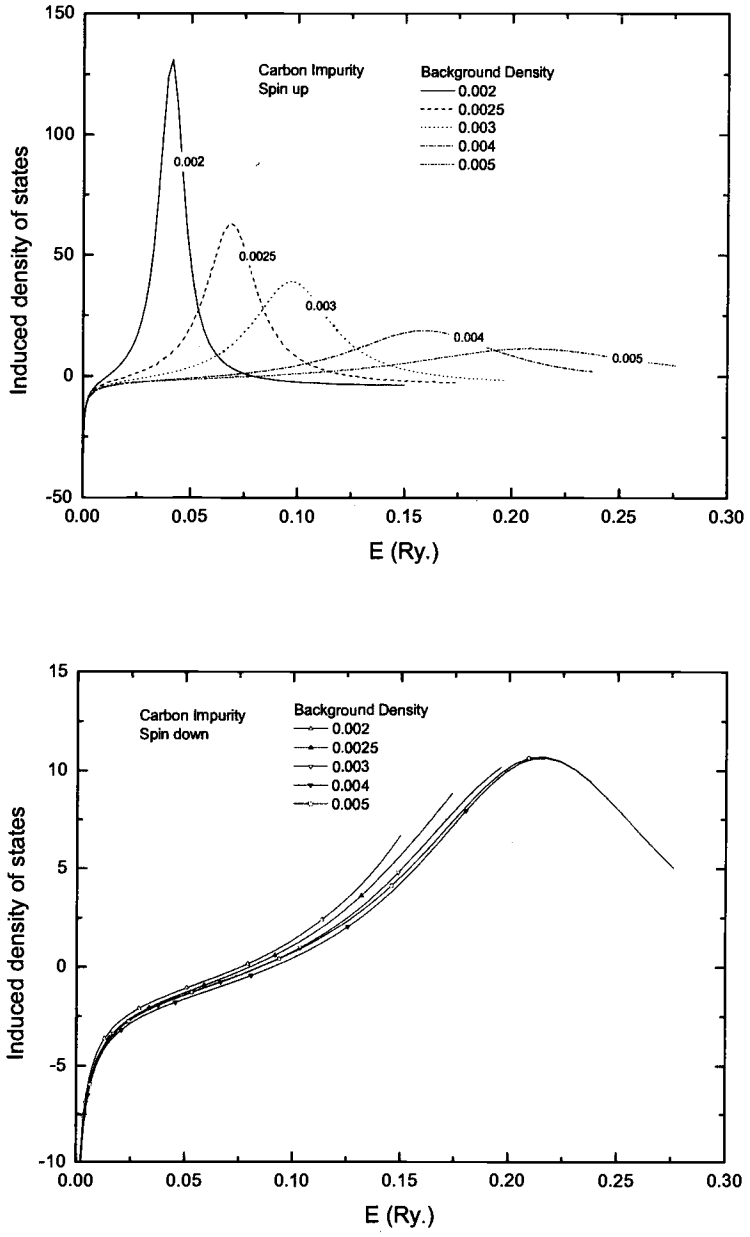

FIGURE 5.23. The density of states induced by a carbon impurity.

ΔN (which is the difference in the number of electrons between spin-up and spin-down electrons in a system) becomes larger as the background density decreases and thus a spin-polarized system favors a spin-polarized solution for a background density lower than 0.005. Fig. 5.21 shows that the spin density becomes larger in the vicinity of an impurity as the background density decreases while the total density induced by an impurity remains almost the same. This spin density also can be seen in Fig. 5.22. The maximum peak of the density induced by an impurity in the conduction band of spin-up electrons increases in the vicinity of an impurity between 0.002 and 0.005 background densities and decreases in the conduction band of spin-down electrons. The density of states in the conduction bands of spin-up and spin-down electrons in Fig. 5.23 clearly show that there is a resonance in the conduction band of spin-up electrons between 0.002 and 0.005 background densities while there is none in the conduction band of spin-down electrons. One other difference between a spin-polarized system and a non-spin-polarized system is that a spin-polarized system has a $2p$ bound state in the spin-up band for a background density smaller than 0.002 and hence there are seven bound state electrons in a system while a non-spin-polarized system can not have six electrons in a $2p$ bound state.[15] One sees now in Fig. 5.22 that, due to a $2p$ bound state, the induced density in the conduction band of spin-up electrons sharply drops in the vicinity of an impurity as the background density decreases from 0.002

---

[15]a non-spin-polarized system is not tested for a background density lower than 0.0005. It is, however, found by considering the rate of the variation of the bound state energy as a background density decreases that a non-spin-polarized system does not have a $2p$ bound state at any background density.

to 0.001. Note that the induced density in the conduction band of spin-down electrons at 0.0004 background density has a relatively large hole (radius around 10) compared to that at 0.0005 background density, while there is a small difference of the induced density in the conduction band of spin-up electrons between 0.0004 and 0.0005 background densities. One can expect that ΔN in Fig. 5.20 is even larger than 3.0 at 0.0004 background density.[16] One possible explanation for this is that, due to the strong effect of the exchange-correlation interaction, a system may get a lower immersion energy by making the magnetization larger at these extremely low background densities. (See Fig. 2.7, Fig. 2.8, and Fig. 2.9.)

5.2.1.2. Electrical Resistivity

The general idea is taken from [15] and [32].

Within the scheme of density functional theory, the single particle wave functions are used to calculate the ground state densities. The use of these wave functions for other purposes is not formally justified. However, the phase shifts (which are related to the wave functions) give reasonable agreement with experiment as discussed in [32].

The contribution of scattering centers to the electrical resistivity can be derived in terms of the phase shifts by

$$\Delta\rho = \frac{\hbar 4\pi n_i}{e^2 k_F Z_h} \sum_{l=0}^{\infty} (l+1) \sin^2[\delta_l(\epsilon_F) - \delta_{l+1}(\epsilon_F)] \quad , \tag{5.8}$$

---

[16] At 0.0004 background density, it is difficult to obtain a self-consistent solution with the required convergence due to the strong tendency toward a spin-polarized system.

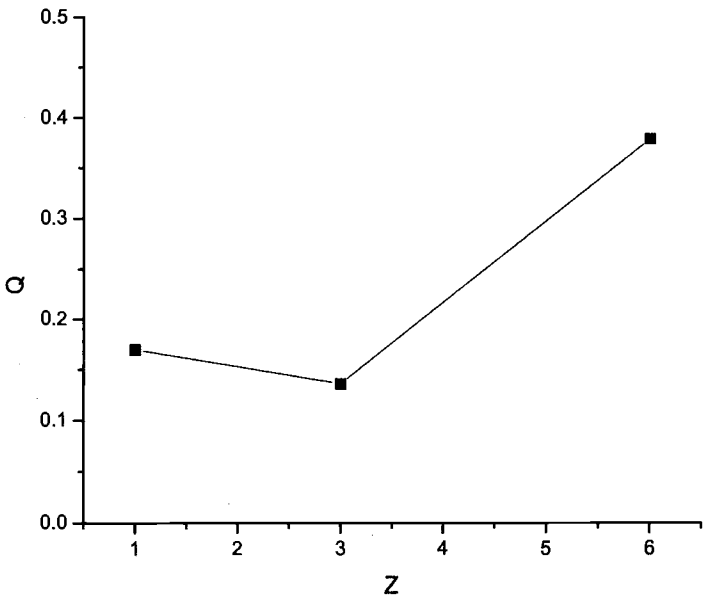

FIGURE 5.24. The values of Q versus Z for the background density of 0.01. The calculations are performed only for $Z = 1, 3, 6$. Note that, at this background density, there is no difference between spin-polarized and non-spin-polarized systems for these impurities.

where n_i is the impurity concentration and Z_h is the number of valence electrons per host ion.[17] (See [32] and [15].) A useful expression is

$$Q = \frac{3}{k_F r_s^3} \sum_{l=0}^{\infty} (l+1) \sin^2[\delta_l(\epsilon_F) - \delta_{l+1}(\epsilon_F)] \quad , \tag{5.9}$$

where r_s is the Wigner-Seitz radius. The electronic stopping power for an ion slowly moving through the electron gas can be obtained from this equation by multiplying Q by $\hbar v_I$, where v_I is the velocity of an ion. Fig. 5.24 shows the Q values for H, Li, and C. The result agrees with Ref. [32]. The one important feature

[17]CGS units are used in this section.

of such results is the oscillations of Q values as a function of Z.[18] These oscillations were observed experimentally in impurity residual resistivity measurements and in the stopping power data for well-channeled slow ions. [33] The reader should refer to [32] for more details.

5.2.1.3. Excited system

As discussed in Sec. 5.2.1.1, a spin-polarized system with a carbon impurity has a very strong tendency toward a large spin-moment solution(parallel to spin-up) at low background densities(< 0.005). (See Fig. 5.20.) However, a strong tendency toward an anti-spin-moment solution(parallel to spin-down) in the conduction band has been observed for excited systems as well. Fig. 5.25 shows the variation of immersion energies and ΔN as a function of the number of spin-up electrons in a $2p$ bound state.[19] The small variation in the slope of the immersion energies in Fig. 5.25 can be verified with the bound state energies (Fig. 5.26) of a $2p$ state using the Janak's theorem as in Sec. 5.1.6. Electrons in the conduction band behave in such a way that the difference in the total induced density due to the change in a $2p$ bound state is as small as possible as illustrated in Fig. 5.27 $\sim$ Fig. 5.38. However, one sees immediately in Fig. 5.25 that decreasing the number of spin-up electrons in a $2p$ bound state results in reducing the spin-moment, that is, in a large anti-spin-moment in the conduction band.

---

[18]In order to observe the oscillations of Q values, one needs to obtain the results for Z at least up to $Z = 20$. See [32].

[19]Note that there is no $2p$ bound state for spin-down electrons.

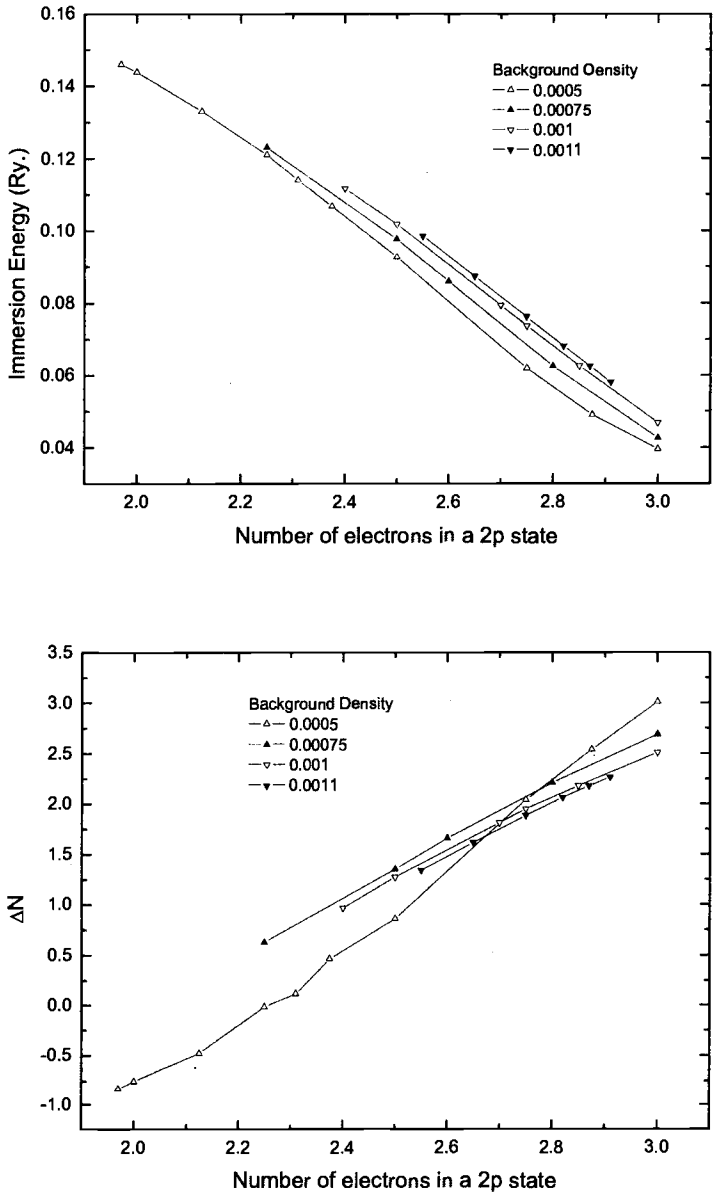

FIGURE 5.25. Immersion energies and ΔN for a carbon impurity vs the number of spin-up electrons in a $2p$ bound state. ΔN is the difference in the number of electrons between spin-up and spin-down electrons in a system.

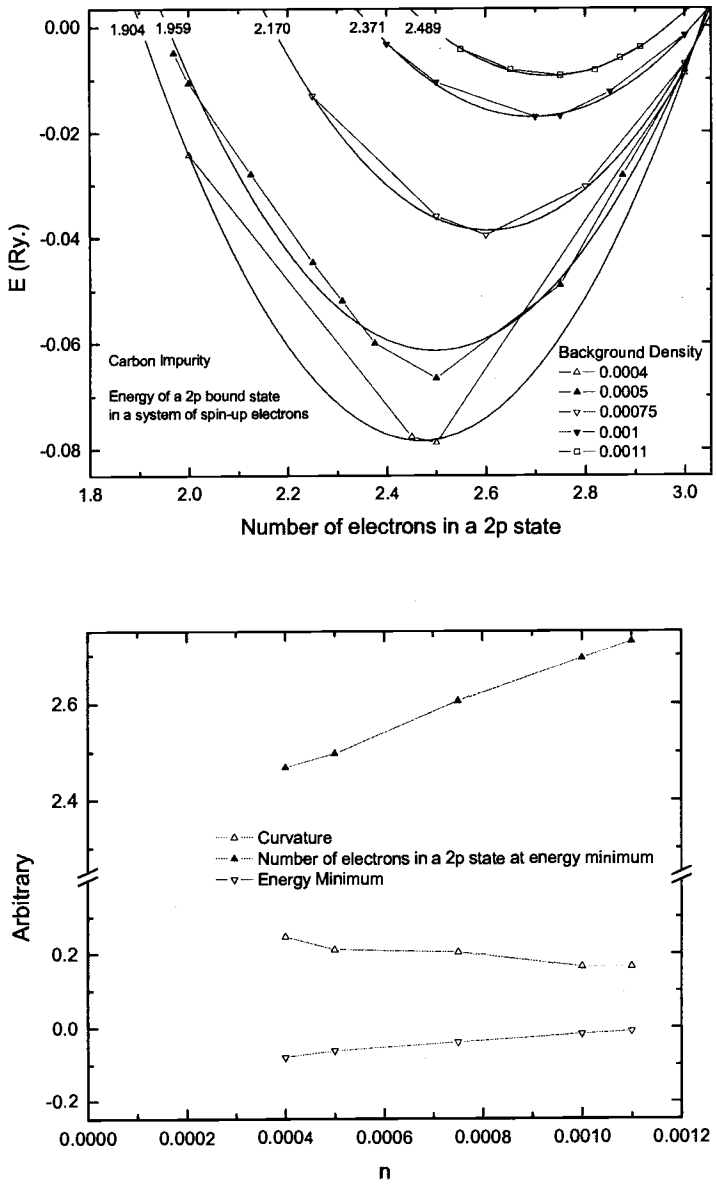

FIGURE 5.26. Bound state energies vs the number of spin-up electrons in a $2p$ bound state. The second plot shows the variation of the curvature, the energy minimum, and the number of electrons in a $2p$ bound state corresponding to the energy minimum in the first plot.

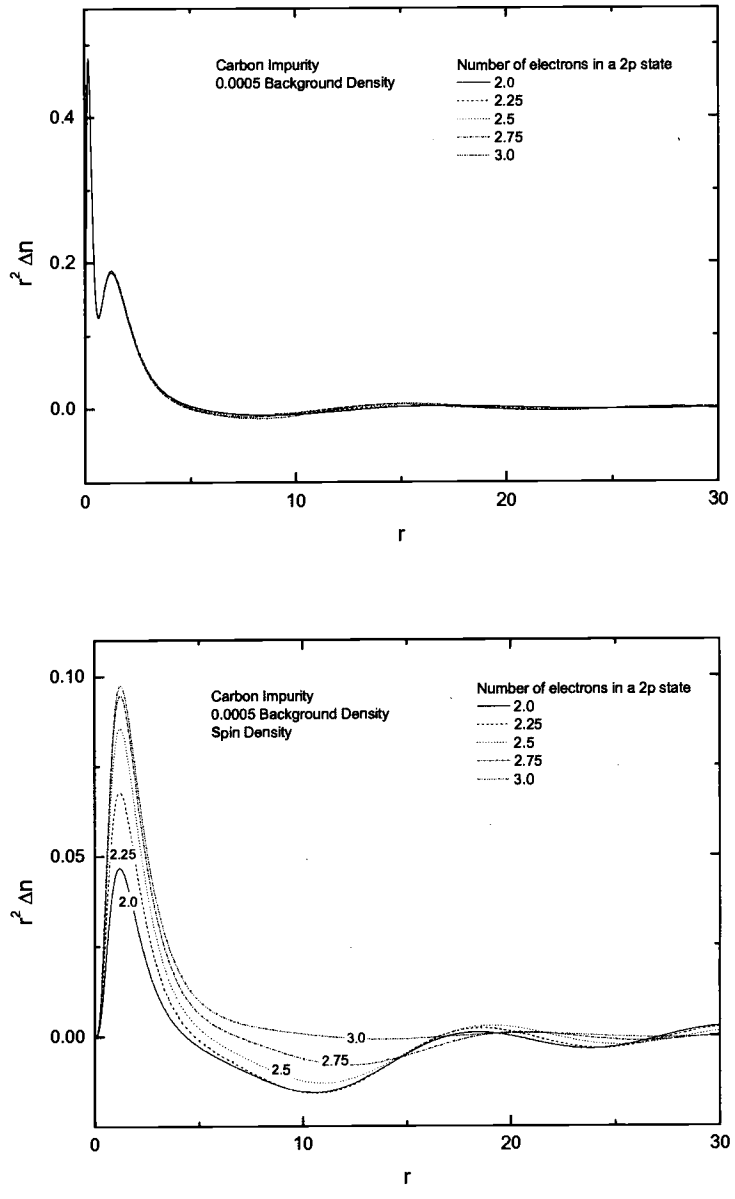

FIGURE 5.27. The density and the spin density induced by a carbon impurity at 0.0005 background density.

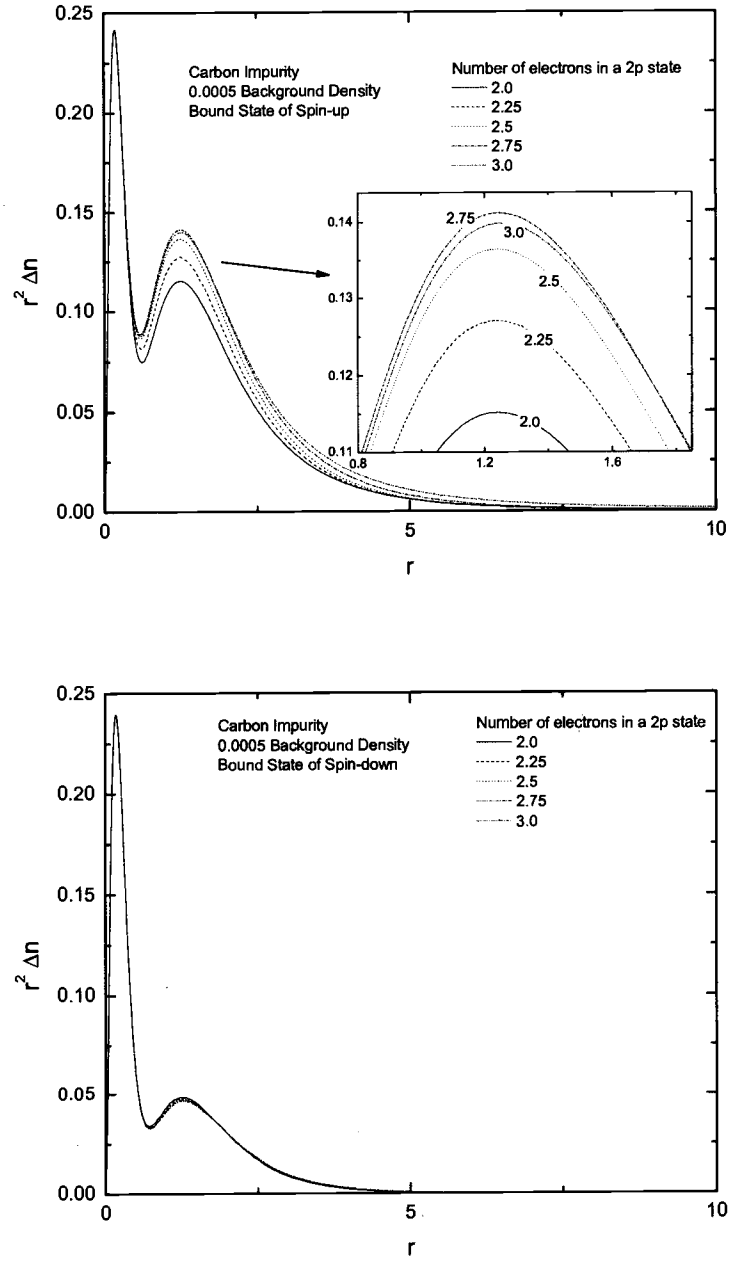

FIGURE 5.28. The density in the bound states of spin-up and spin-down electrons induced by a carbon impurity at 0.0005 background density.

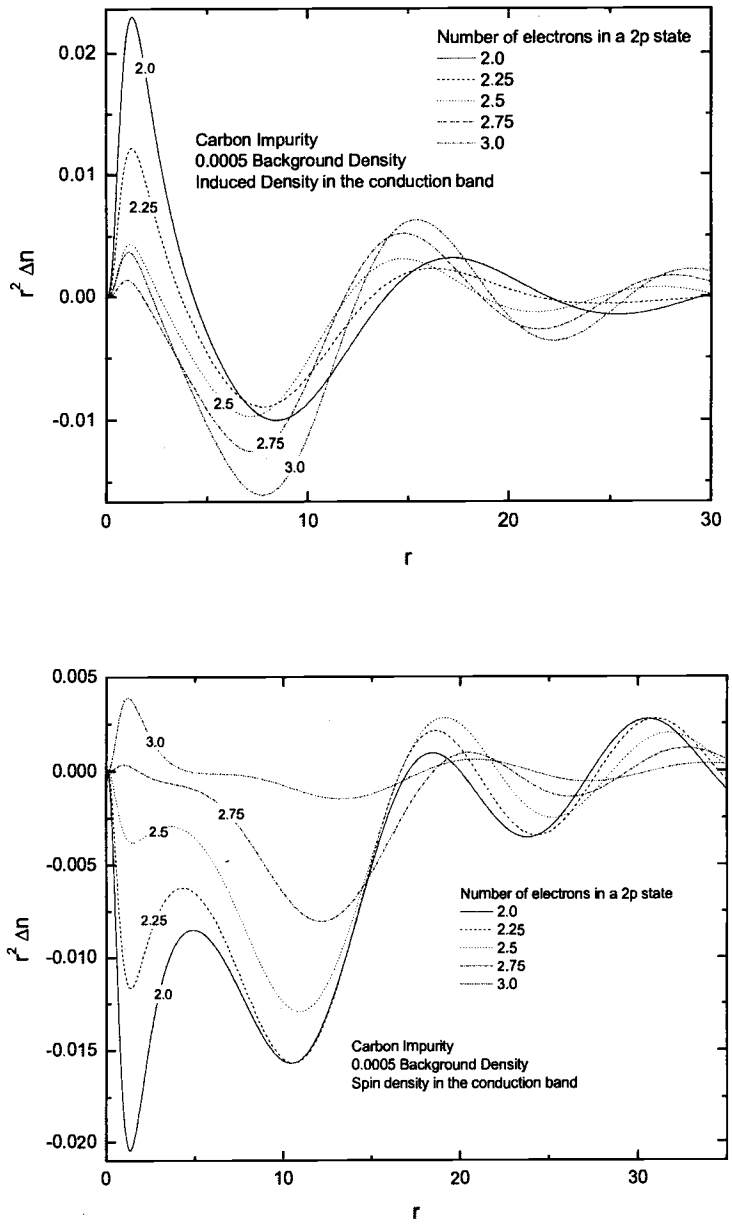

FIGURE 5.29. The density and the spin density in the conduction band induced by a carbon impurity at 0.0005 background density.

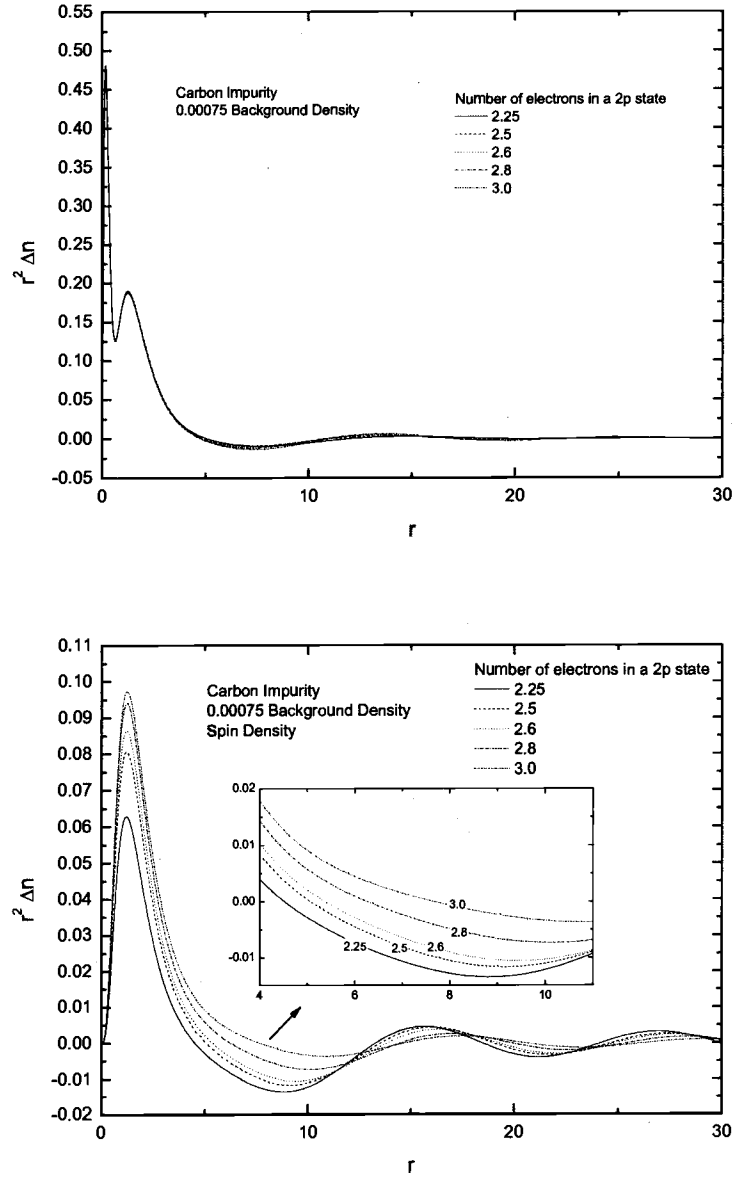

FIGURE 5.30. The density and the spin density induced by a carbon impurity at 0.00075 background density.

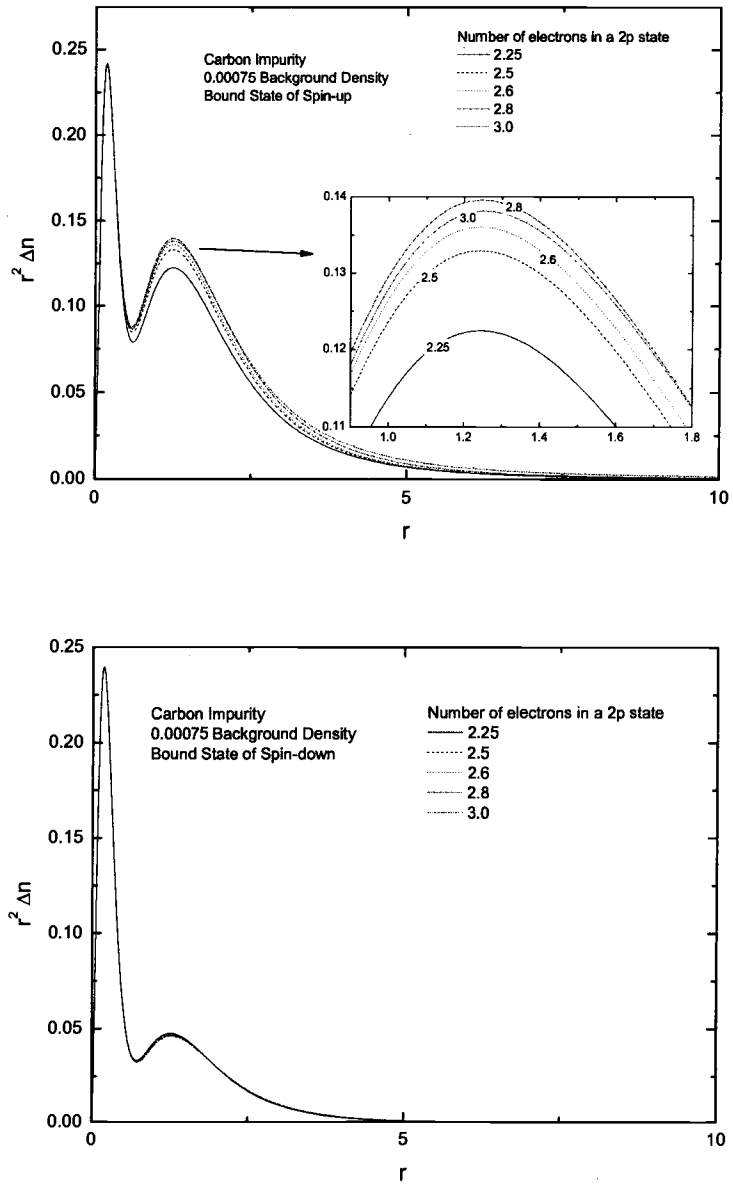

FIGURE 5.31. The density in the bound states of spin-up and spin-down electrons induced by a carbon impurity at 0.00075 background density.

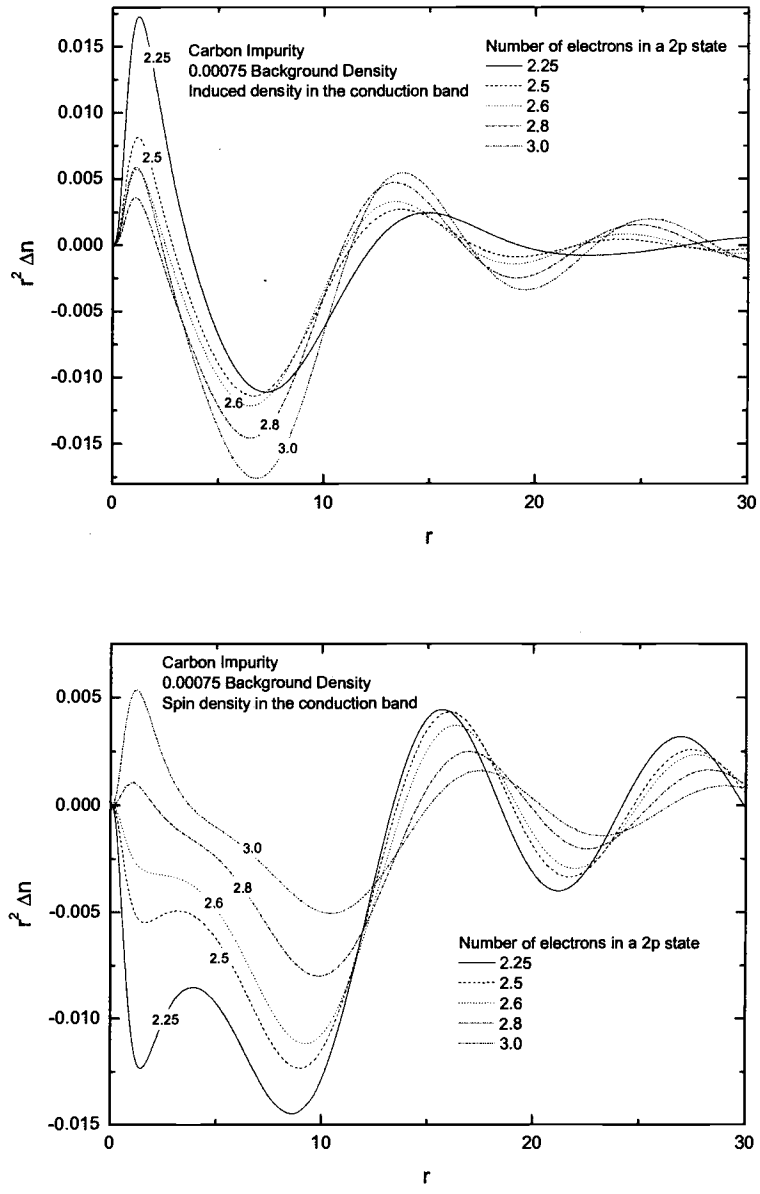

FIGURE 5.32. The density and the spin density in the conduction band induced by a carbon impurity at 0.00075 background density.

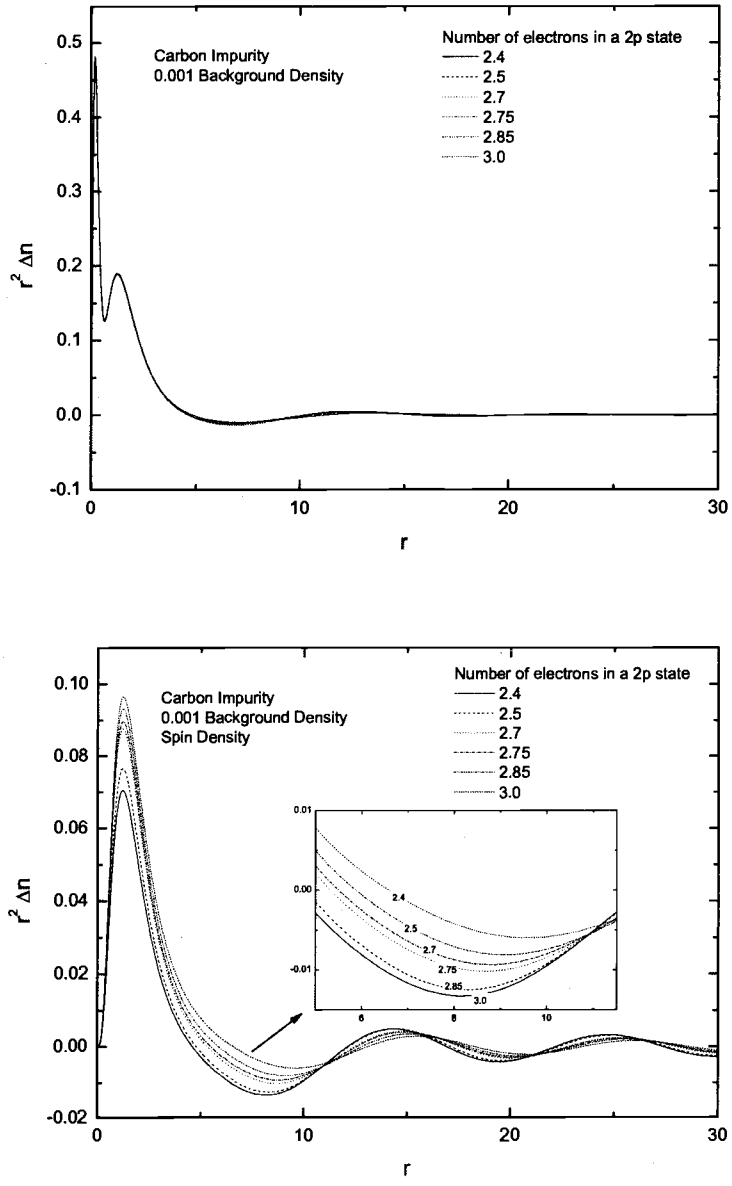

FIGURE 5.33. The density and the spin density induced by a carbon impurity at 0.001 background density.

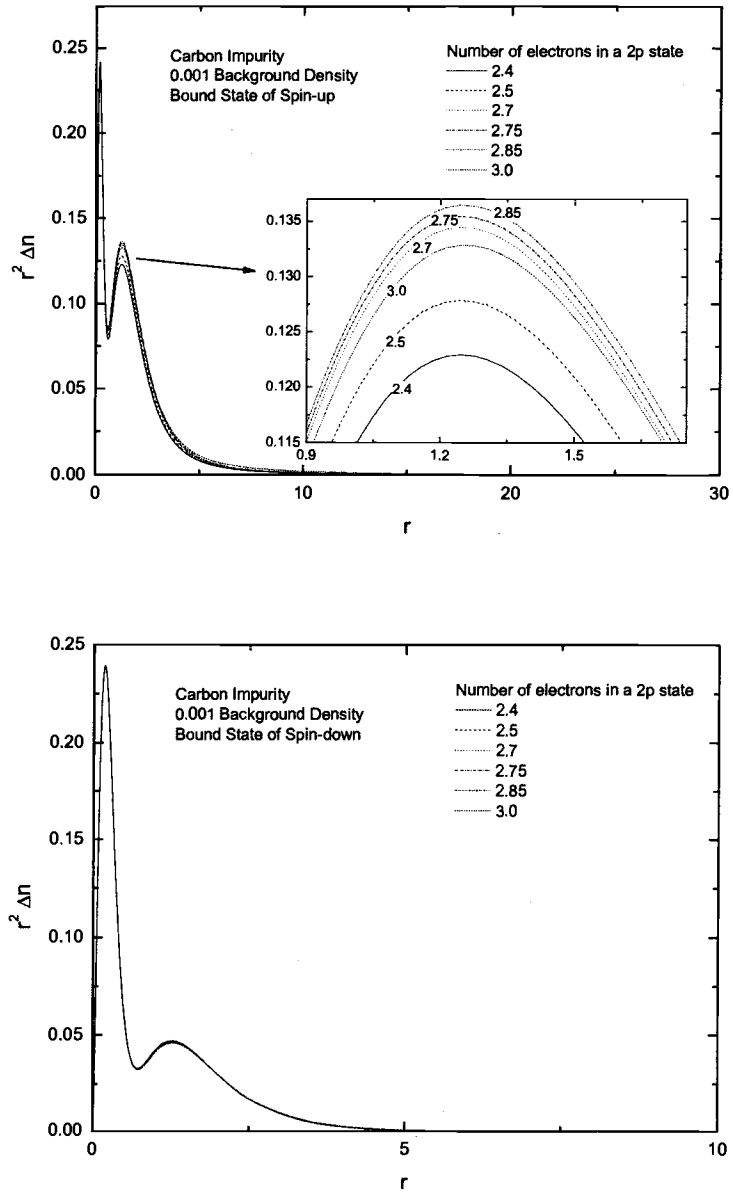

FIGURE 5.34. The density in the bound states of spin-up and spin-down electrons induced by a carbon impurity at 0.001 background density.

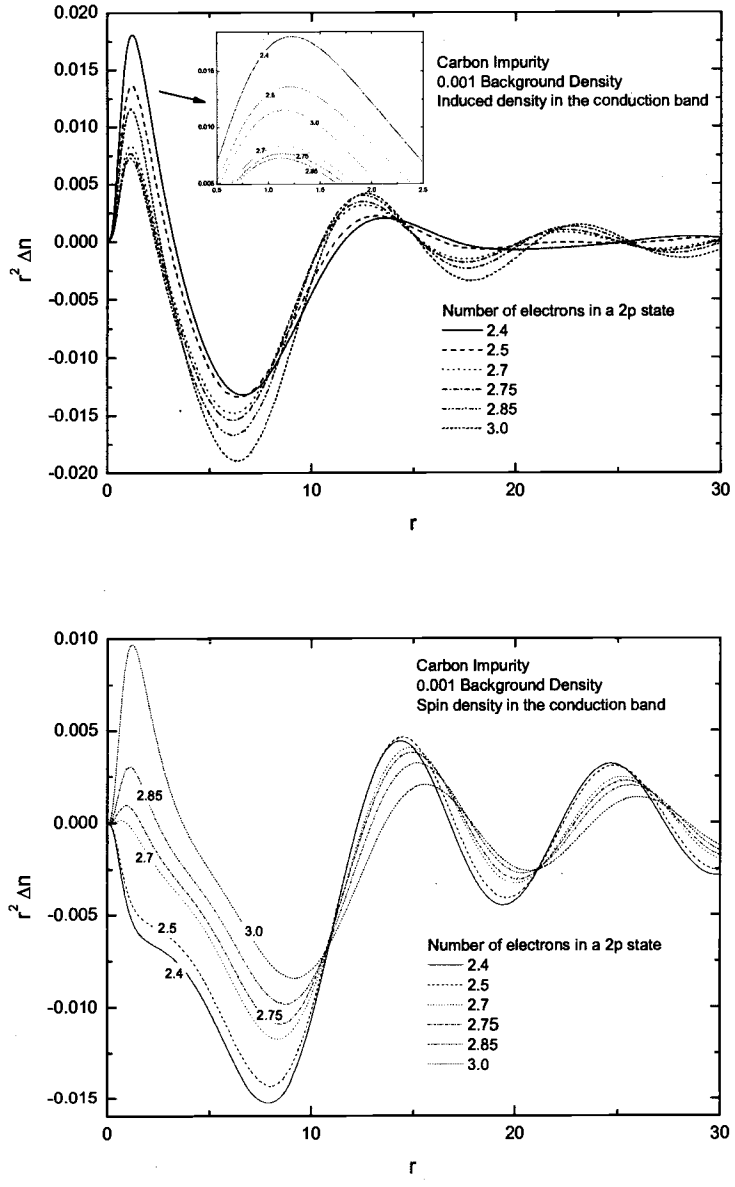

FIGURE 5.35. The density and the spin density in the conduction band induced by a carbon impurity at 0.001 background density.

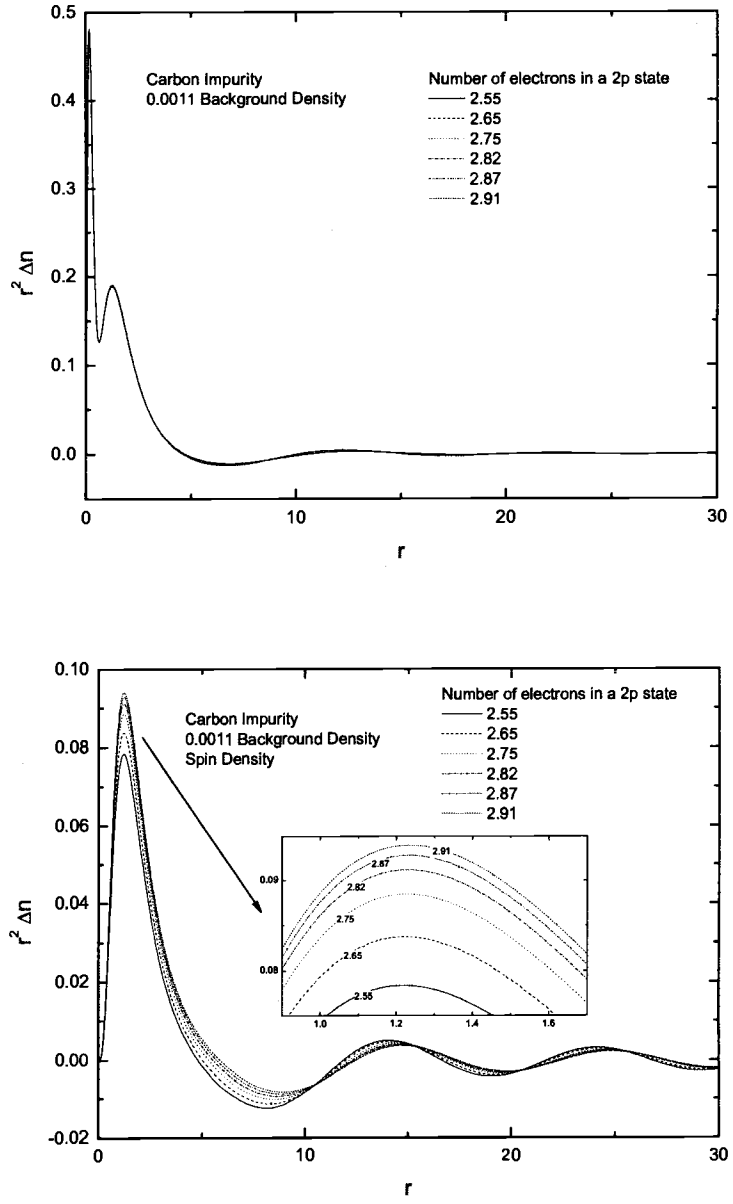

FIGURE 5.36. The density and the spin density induced by a carbon impurity at 0.0011 background density.

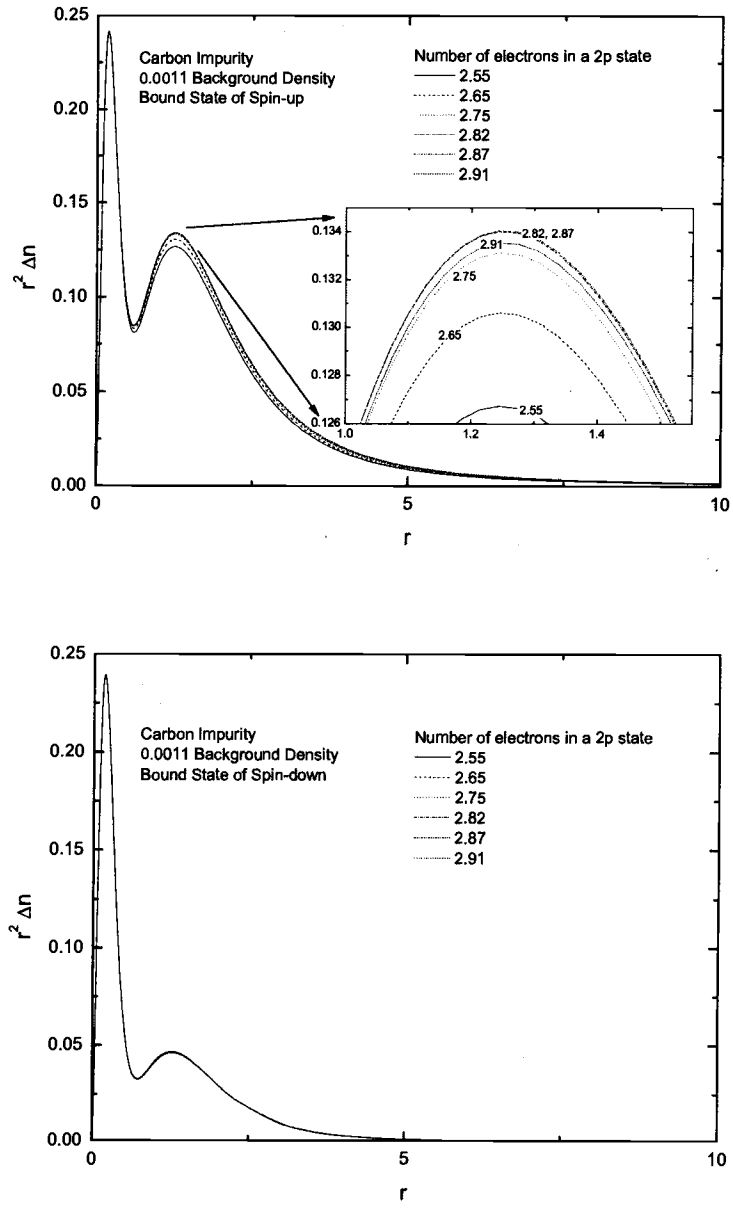

FIGURE 5.37. The density in the bound states of spin-up and spin-down electrons induced by a carbon impurity at 0.0011 background density.

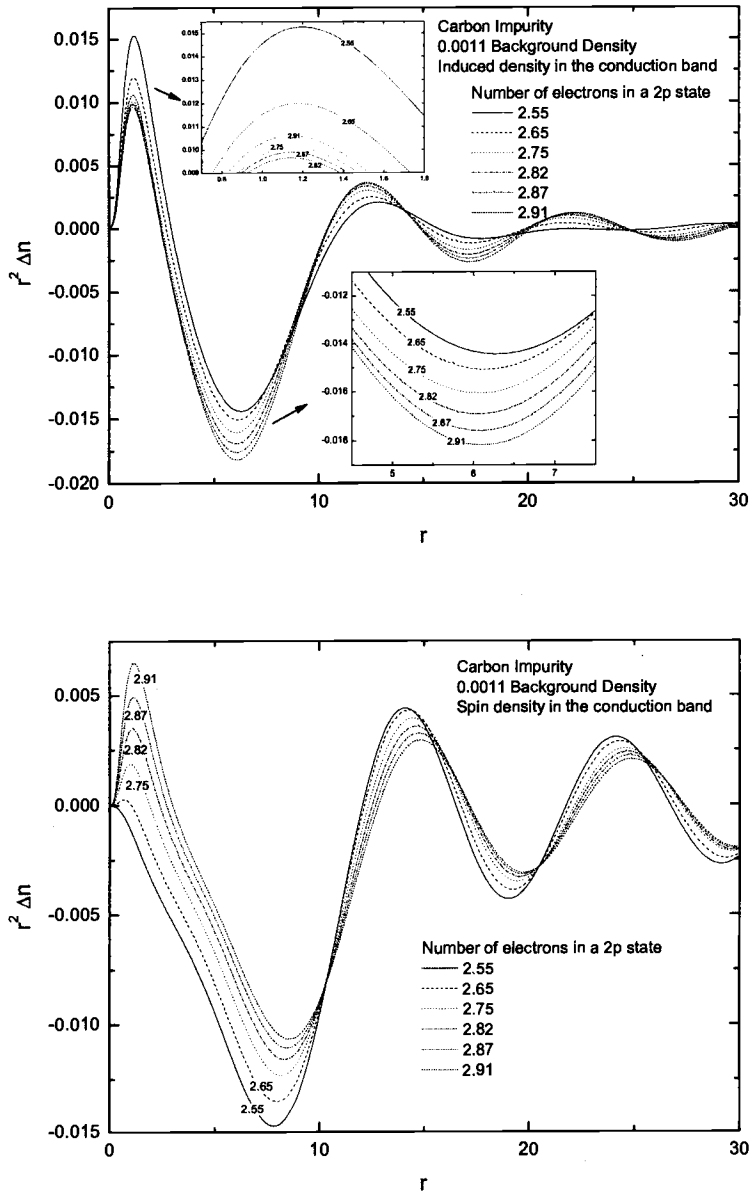

FIGURE 5.38. The density and the spin density in the conduction band induced by a carbon impurity at 0.0011 background density.

Fig. 5.26 shows in this system that the bound state energy as a function of the number of spin-up electrons in a $2p$ bound state behaves unusually as a quadratic function.[20] Important parameters of quadratic functions are also shown in Fig. 5.26. The bound state energy decreases as the number of spin-up electrons in a $2p$ bound state decreases from 3.0 electrons as expected. However, the bound state energy increases as the number of spin-up electrons in a $2p$ bound state decreases from the bound state energy minimum due to the largely induced spin-down electrons near an impurity in the conduction band.

This behavior is consistent with the potential.(Fig. 5.39) For instance, the induced spin up and down electrons results in a behavior of the Coulomb potential for each band for 0.0005 background density as illustrated in Fig. 5.40. The total Coulomb potential near an impurity ($r \leq 1$) in Fig. 5.41 decreases as the number of spin-up electrons in a $2p$ bound state decreases and increases as spin-up electrons in a $2p$ bound state decreases from 2.5. One sees also that the change in the total Coulomb potential ($r \leq 1$) between 2.0 and 2.5 spin-up electrons in a $2p$ bound state is not as large as that between 2.5 and 3.0 spin-up electrons in a $2p$ bound state. However, with the increase of spin-up exchange-correlation potential(Fig. 5.42), one sees that the total effective potential of spin-up electrons at 2.0 electrons in a $2p$ bound state is now close to that at 3.0 electrons. (See Fig. 5.39.) This potential behavior accounts for the variation of the bound state energy in Fig. 5.26 and the exchange-correlation interaction in Fig. 5.42 causes the decrease of

---

[20]Note that one can not use a simple first order of a Taylor series for this bound state energy as usual.

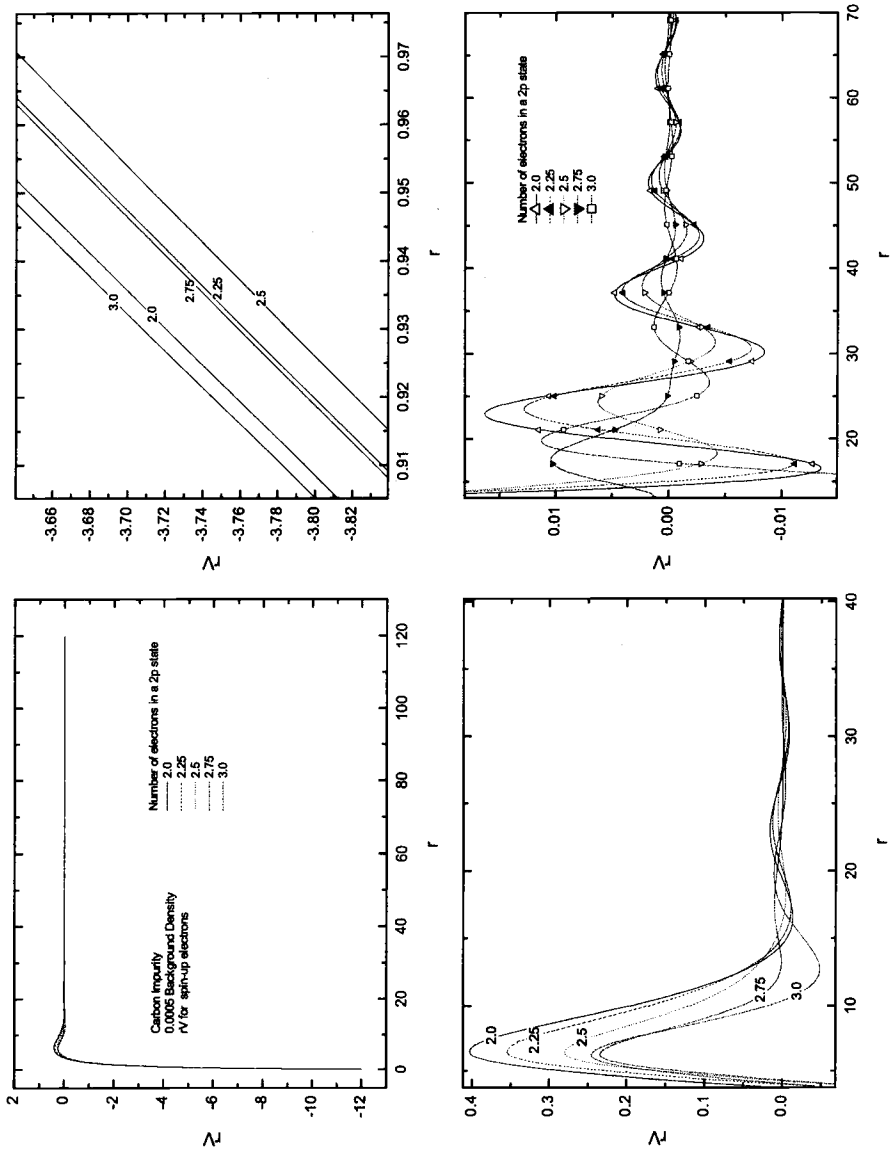

FIGURE 5.39. The effective potential of the spin-up band vs the number of spin-up electrons in a $2p$ bound state for 0.0005 background density.

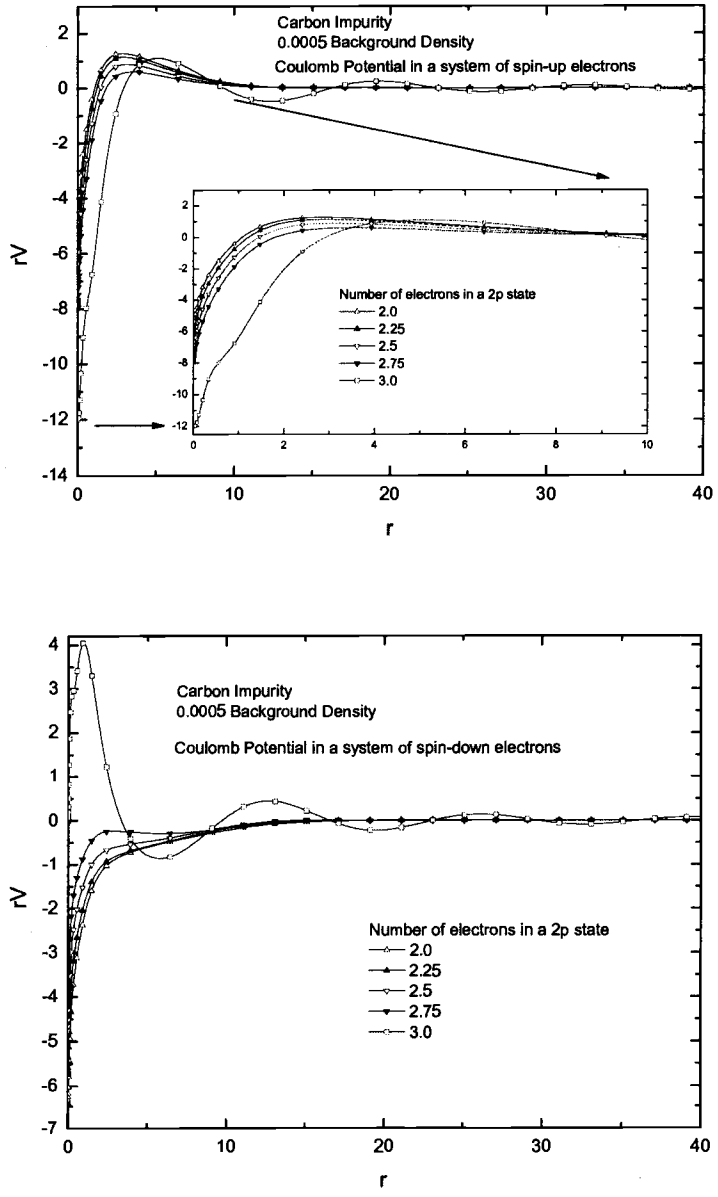

FIGURE 5.40. The Coulomb potentials calculated by induced spin-up and spin–down electrons vs the number of spin-up electrons in a $2p$ bound state for 0.0005 background density.

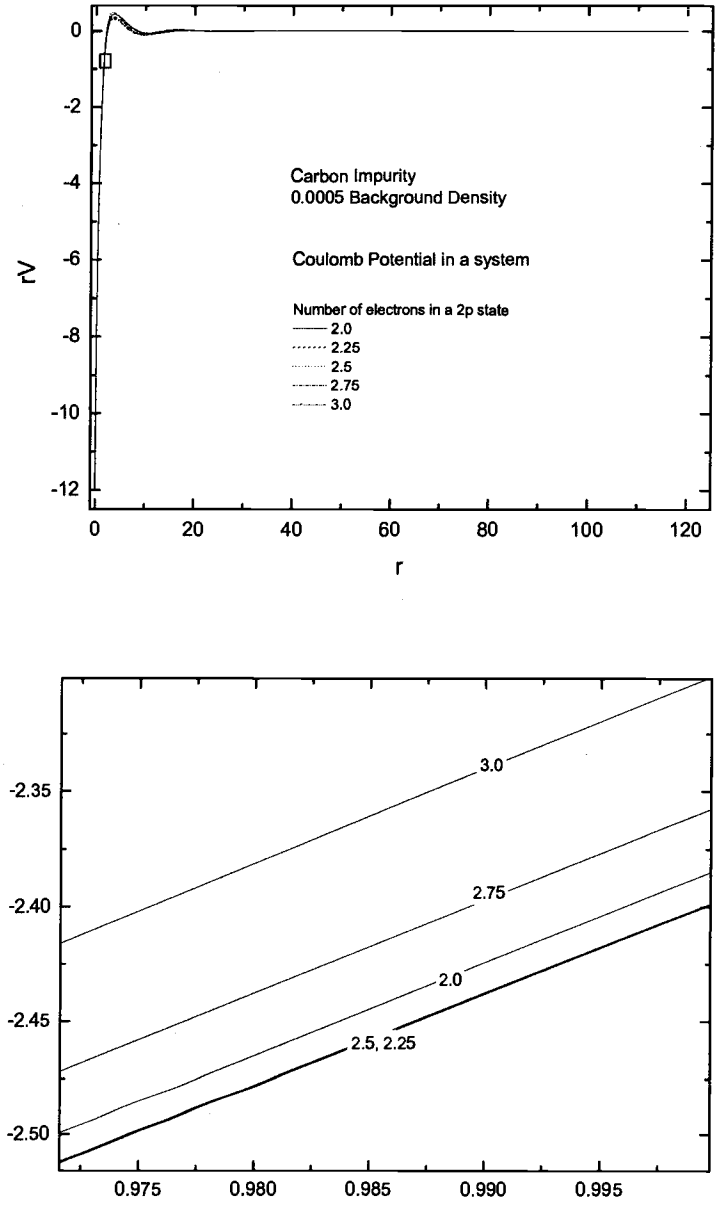

FIGURE 5.41. The Coulomb potentials vs the number of spin-up electrons in a $2p$ bound state for 0.0005 background density. The second plot shows the area which corresponds to the box in the first plot.

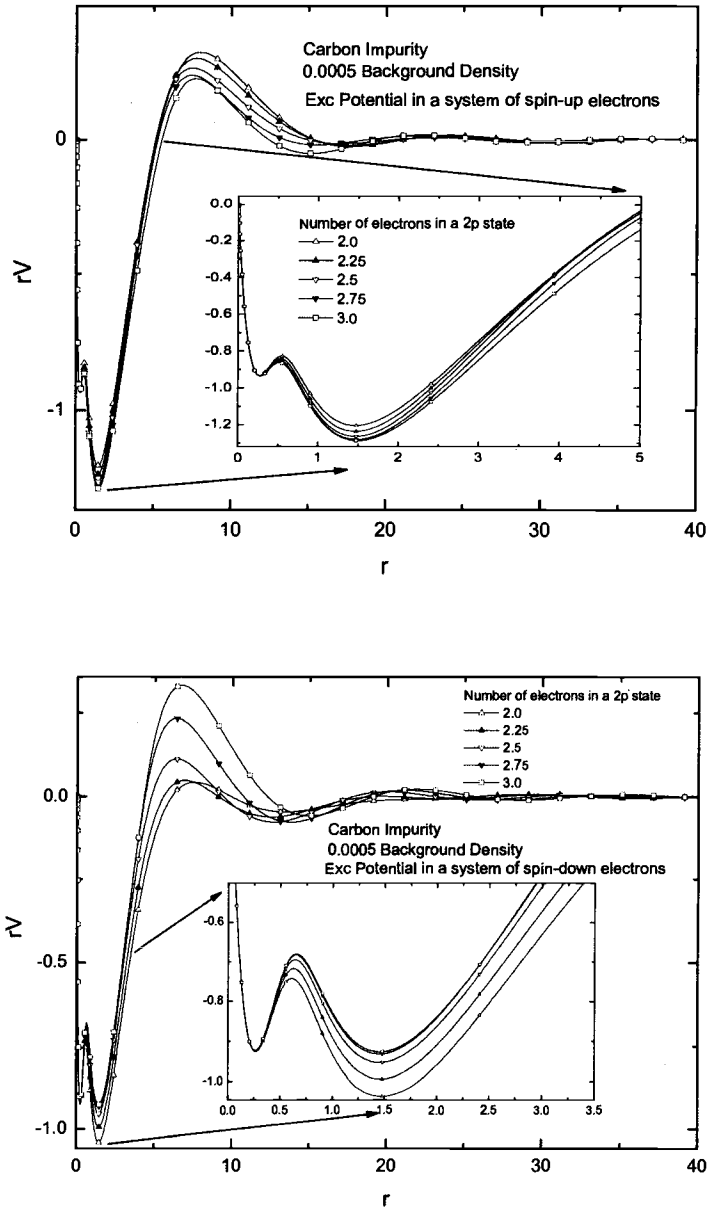

FIGURE 5.42. The exchange-correlation potentials of induced spin-up and spin–down electrons vs the number of spin-up electrons in a $2p$ bound state for 0.0005 background density.

the spin-moment(the increase of the anti-spin-moment in the conduction band) since spin-up and down electrons experience the same Coulomb potential.

The phase shift in Fig. 5.43 shows a consistent behavior. Note in the overall scattering length and volume a decrease for spin-up electrons and an increase for spin-down electrons. One knows that the Friedel sum rule forces the phase shift at the Fermi energy to adjust to screen the excess charge of the core correctly. The way this system behaves due to the Friedel sum rule is that the decrease in the number of spin-up electrons in a $2p$ bound state causes an increase in the phase shift of the spin-down electrons at the Fermi energy and the decrease in the phase shift of the spin-up electrons, which is consistent with the behavior of the spin-density in the conduction band. With 3.0 electrons in a $2p$ bound state, the phase shift in Fig. 5.43 shows that there is a scattering resonance in the high energy region ($\geq \epsilon_F$) of the phase shift of the spin-down electrons. The resonance moves closer to the Fermi energy as the number of electrons in a $2p$ bound state decreases. Accordingly, one sees large increases at the Fermi energy in the density of induced states of the spin-down band, as illustrated in Fig. 5.44 and Fig. 5.45.

These results can be explained by self-consistency and the exchange-correlation interaction.[21] If the induced density in the bound states is reduced artificially, electrons in the conduction band simply can not be induced more to maintain the same total induced density since the same total induced density yields the same Coulomb potentials and accordingly the same induced density in the con-

---

[21]These explanations need further investigation.

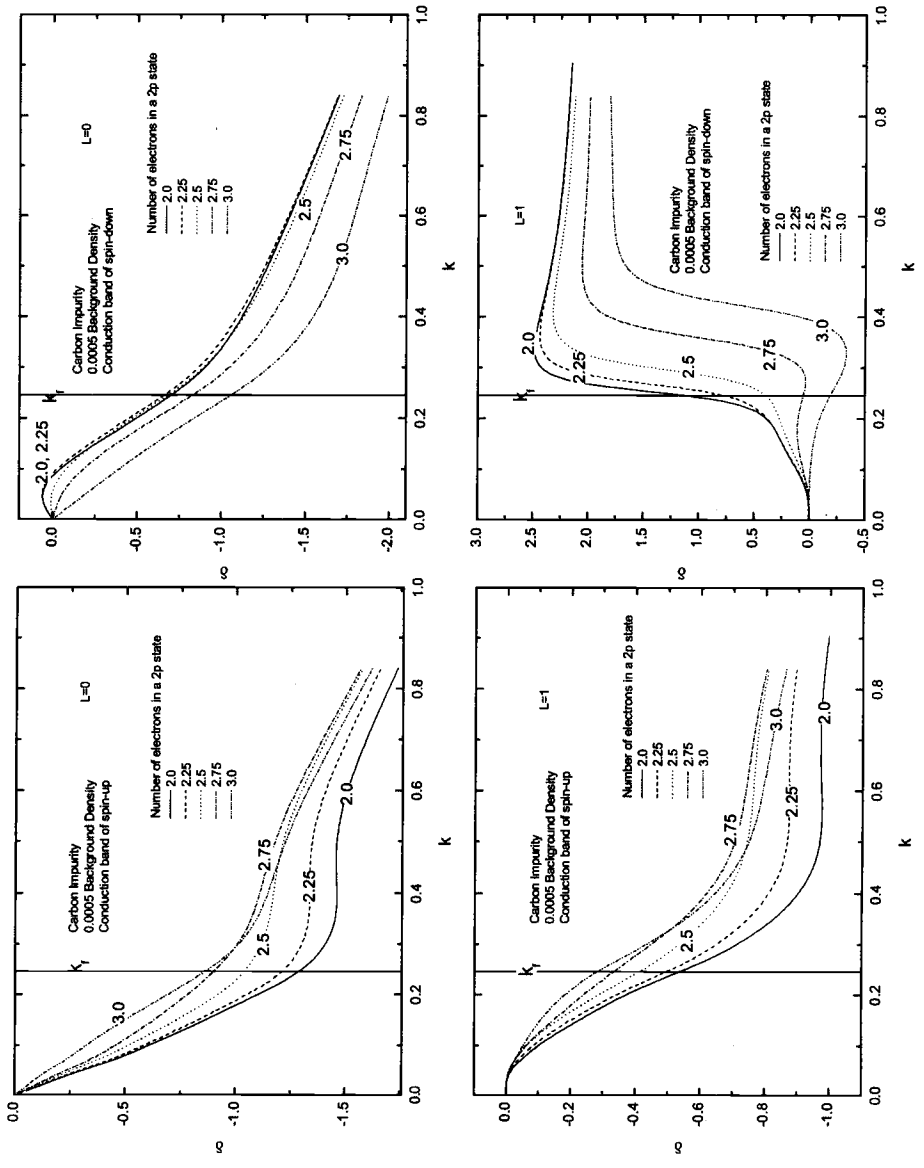

FIGURE 5.43. Phase shifts of $l = 0$ and $l = 1$ for spin-up and spin-down electrons.

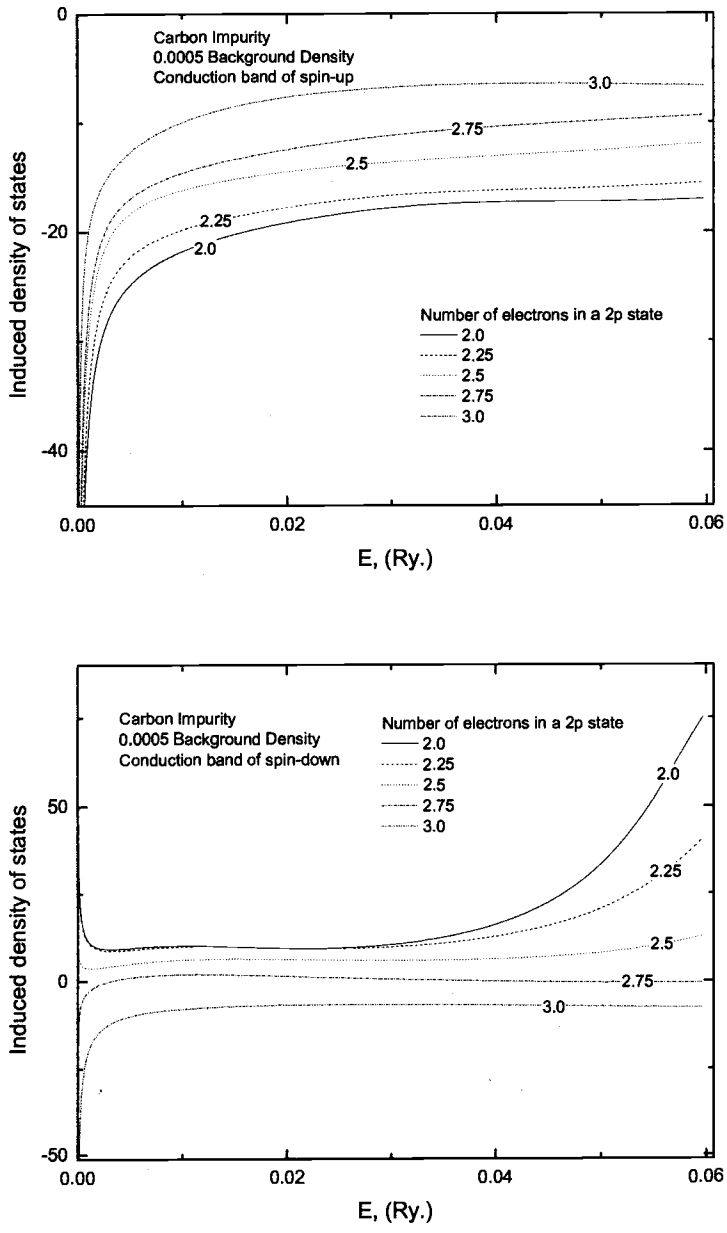

FIGURE 5.44. The density of induced states for spin-up and spin-down electrons at 0.0005 background density.

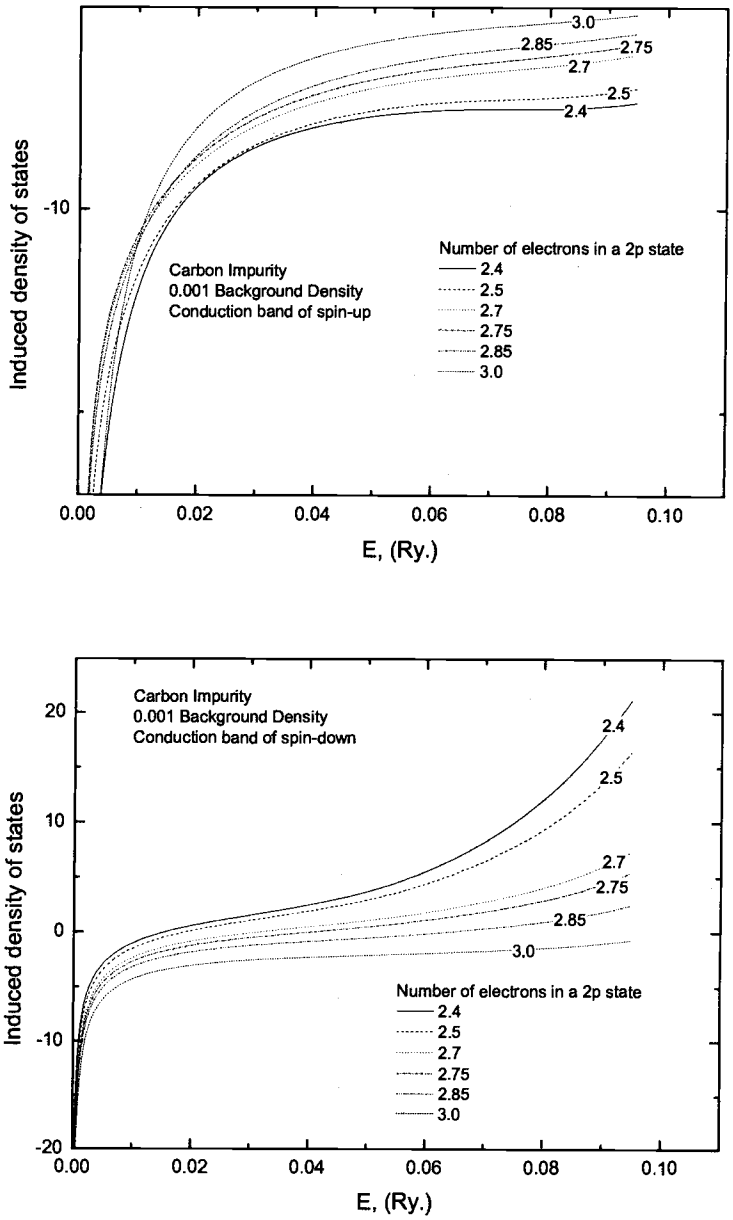

FIGURE 5.45. The density of induced states for spin-up and spin-down electrons at 0.001 background density.

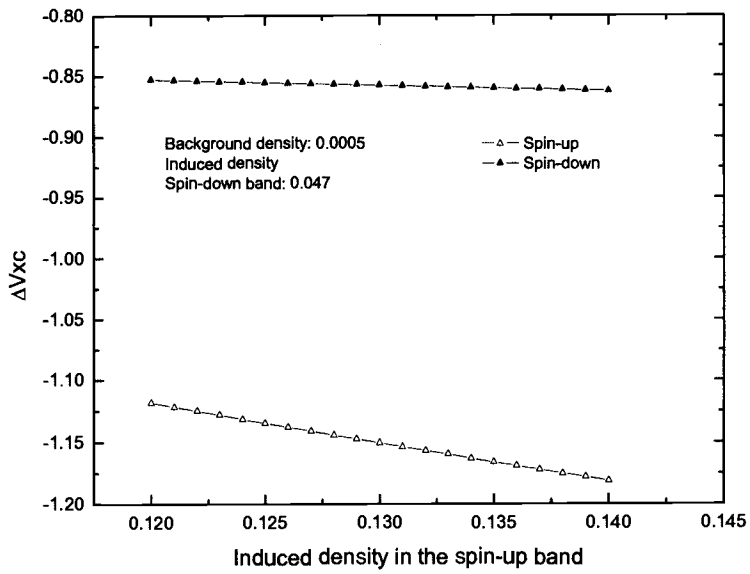

FIGURE 5.46. The exchange-correlation potential with different induced densities in the spin-up band. Background density is 0.0005. The induced density in the spin-down band is assumed to be 0.047.

duction band.[22] The reduced density in the bound states, thus, tends to cause a more extended induced density. Moreover, the potential due to the exchange-correlation interaction[23] also can vary corresponding to the change in the density. Fig. 5.46 shows one example of the exchange-correlation behavior in the case that the induced density in the spin-up band varies. The reduced density in the spin-

---

[22]Once the density in the bound states is changed, the old bound states and scattered states which are orthogonal to each other do not satisfy the self-consistency anymore.

[23]The exchange-correlation interaction used in this work only depends on the local density.

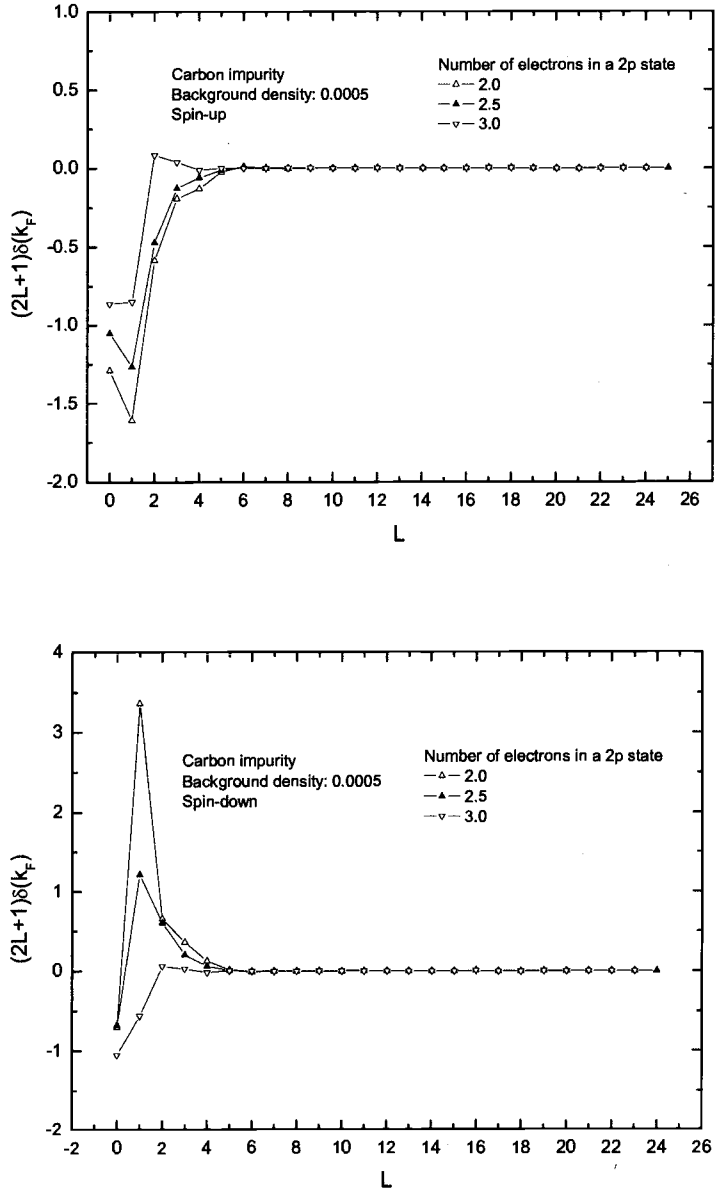

FIGURE 5.47. Partial wave decompositions of the Friedel sum rule. These plots show the change in the number of electrons induced by a carbon impurity for each band. 0.0005 is used for a background density. Bound states are not included.

up band gives rise to a more repulsive exchange-correlation potential and thus the spin-down band has relatively more induced electrons in the conduction band due to the Coulomb interaction as the number of electrons in a $2p$ bound state of the spin-up band decreases. Fig. 5.47 shows the response of the conduction bands in terms of the phase shifts at the Fermi energy. One sees that, as the the number of electrons in a $2p$ bound state of the spin-up band decreases, the spin-up conduction band loses more electrons in overall angular momentum states and the decrease of induced electrons in the p state of the spin-up band is compensated by mainly the same p state of the spin-down band.

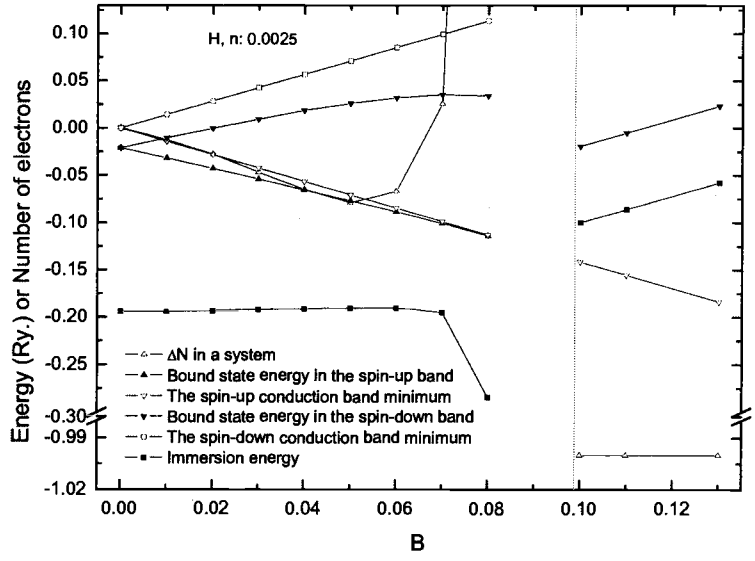

FIGURE 5.48. Bound state energies, the conduction band minimums, the spin–moment, and the immersion energies vs the magnetic field for a hydrogen impurity with 0.0025 background density.

5.2.2. Non-zero external magnetic field

A hydrogen impurity in a spin-polarized system has been tested by applying an external magnetic field. Detailed information for the implementation can be found in Sec. 4.6. Results for three different background densities are obtained. Fig. 5.48 shows the induced spin-moment in a system, bound state energies, the conduction band minimum, and the immersion energies for a background density of 0.0025. As the magnetic field increases, the background density (conduction band width) of spin-up (majority) electrons increases and the background density of spin-down (minority) electrons decreases. Therefore, ΔN in this case is the excess spin-moment, the deviation from the moment due to the background by

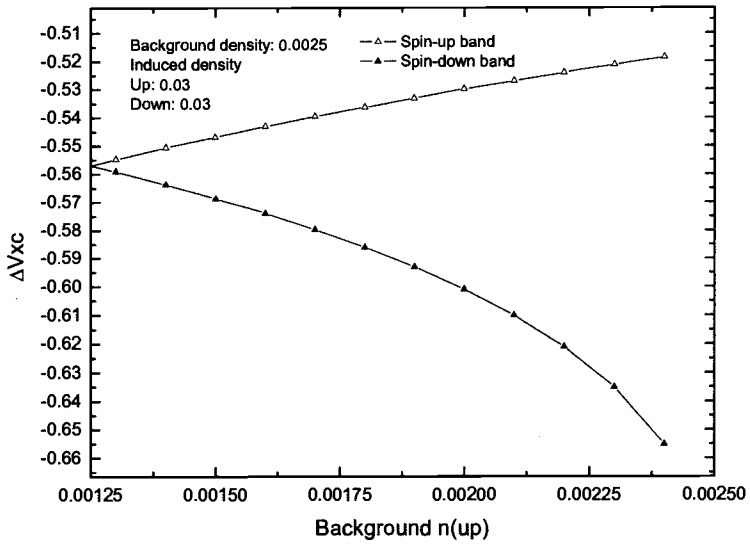

FIGURE 5.49. The exchange-correlation potential with different background densities of the spin-up band. The total background density is 0.0025 and the induced density is assumed to be 0.03 for each spin-up and spin-down band. This plot shows how the exchange-correlation potential for each band may vary with the increasing magnetic field.

itself. There are two electrons in a $1s$ state without an external magnetic field as in a non-spin polarized system. (See Sec. 5.1.) One sees that bound state energies behave as in non-spin polarized systems in Fig. 5.48. That is, the bound state energy in the spin-up band approaches the conduction band minimum as the background density of the spin-up band increases while the bound state energy in the spin-down band becomes lower compared to the band minimum. As the magnetic field in Fig. 5.48 approaches 0.09894,[24] where the spin-down conduction band com-

[24]The unit for the magnetic field in this work is $3.3241346 \cdot 10^5$ T, which will be omitted in this paper for convenience.

pletely disappears, the calculations are not performed correctly due to numerical problems (long wave length of Friedel oscillations) as mentioned in Ch. 4 and thus data are not available for a magnetic field between 0.08 and 0.10. One important phenomenon is the spin-moment which decreases with the increasing magnetic field and then rapidly increases after a magnetic field of 0.06, as illustrated in Fig. 5.48. Two important facts are, due to the difference between spin-up and spin-down electrons, the exchange-correlation interaction and the Coulomb interaction of the Friedel oscillations with two different Fermi wave vectors.

Fig. 5.49 shows that, if the total background density remains the same, the exchange-correlation potential of the spin-up band becomes more repulsive and the exchange-correlation potential of the spin-down band rapidly becomes more attractive due to the exchange-correlation interaction as the background density of the spin-down band approaches zero, which suggests that there may be a rapid variation in potentials of spin-up and spin-down electrons when the external magnetic field increases. The potential variation in Fig. 5.49 is actually very large compared to the potential difference at the atomic $2p$ location ($r \sim 4$) for a hydrogen impurity between the high and low background densities (such as 0.04 and 0.0025). As the external magnetic field increases, this behavior yields not only a more repulsive potential in the vicinity of an impurity but also a large peak in r times the potential near the $2p$ location for the background density of the spin-up band, as illustrated in Fig. 5.50, which is the opposite behavior compared to the potentials of systems without a magnetic field in Fig. 5.51.[25] The number of

---

[25]The lower background density has a larger fluctuation at large distances in the r times potential for a system without the external magnetic field as in Fig. 5.51.

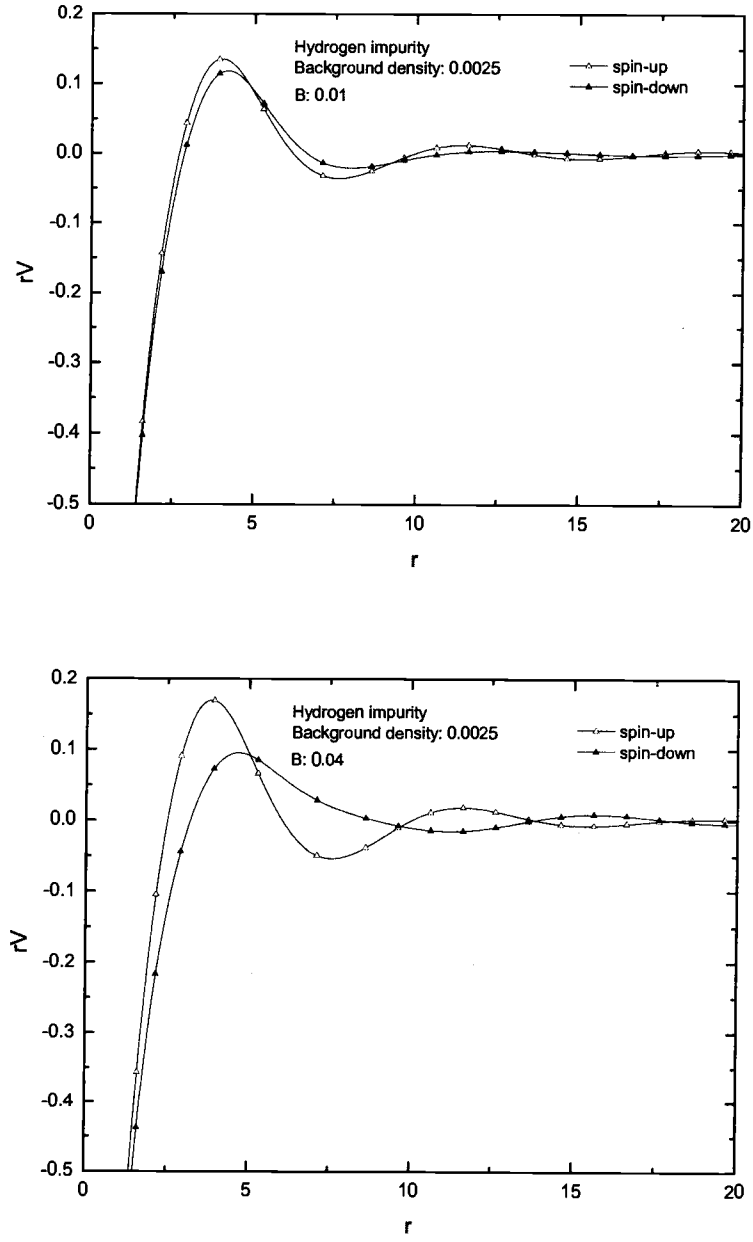

FIGURE 5.50. The effective potentials for the different magnetic field 0.01 and 0.04. A hydrogen impurity with 0.0025 background density is used.

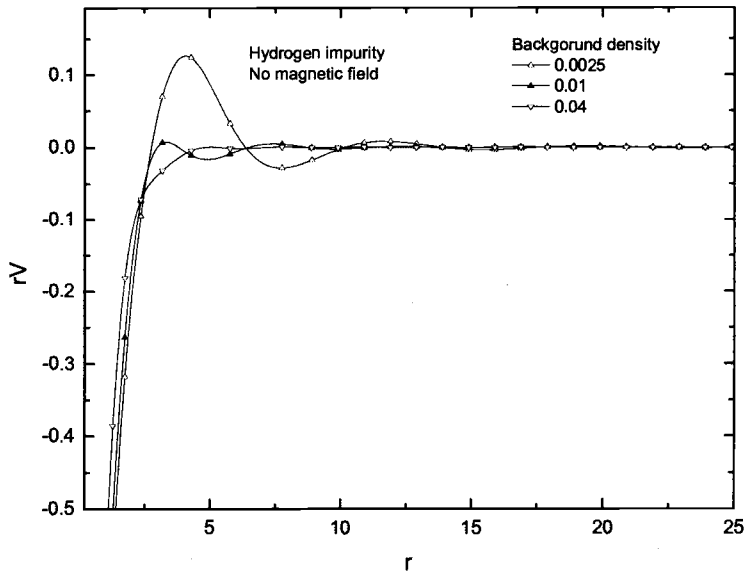

FIGURE 5.51. The effective potential for a hydrogen impurity. No external magnetic field is applied. The potential of the spin-up band is identical to that of the spin-down band.

induced electrons, therefore, decreases in the spin-up band due to the repulsive exchange-correlation interaction and increases in the spin-down band due to the attractive exchange-correlation interaction and, as a result, the spin-moment decreases up to 0.05 magnetic field as shown in Fig. 5.48. The phase shifts at the Fermi energy show a consistent behavior in Fig. 5.52. Without any external magnetic field, there is no difference between the spin-up and spin-down bands. This means that, if the number of induced electrons in the *s*-state of the conduction band is reduced by a higher background density, the higher angular momentum states must have a larger contribution to the number of induced electrons, due to the Friedel sum rule as shown in Fig. 5.53. The phase shifts at the Fermi energy

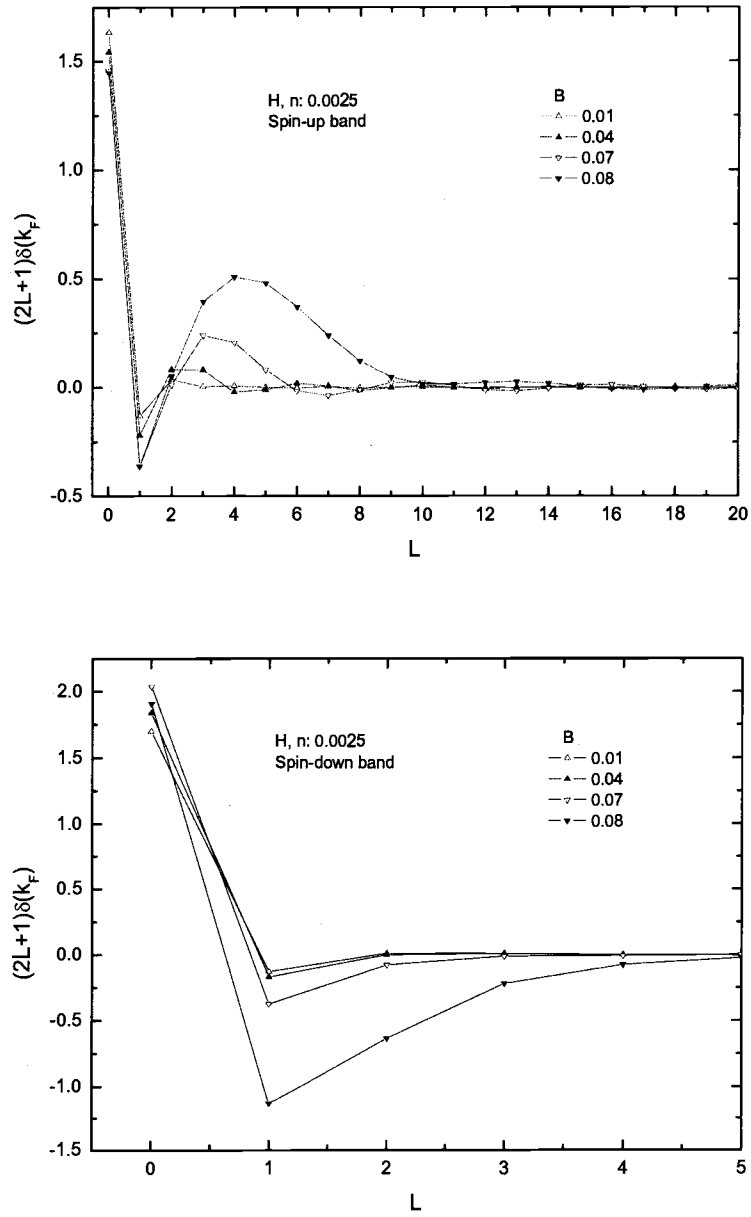

FIGURE 5.52. Partial wave decompositions of the Friedel sum rule. These plots show the change in the number of electrons induced by a hydrogen impurity for each band. 0.0025 is used for a background density.

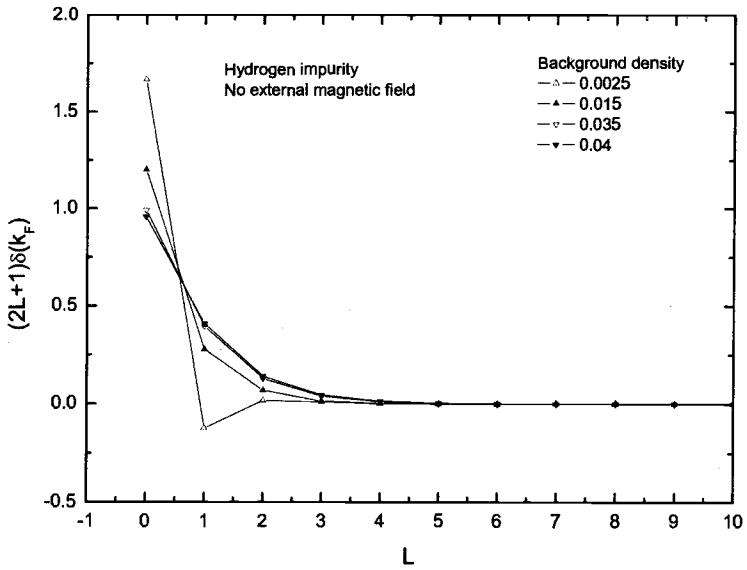

FIGURE 5.53. Partial wave decompositions of the Friedel sum rule. no external magnetic field is applied. This plot for the spin-up band is identical with that for the spin-down band.

with a non-zero magnetic field, however, in Fig. 5.52, show a different behavior for the higher angular momentum states. One sees in Fig. 5.52 that the variation in the number of induced electrons due to a different magnetic field for the high angular momentum states of the spin-down band ($\geq p$) is small up to 0.05 magnetic field compared to that for a system without a magnetic field(Fig. 5.53). One sees also that the phase shifts at the p-state in the spin-up band become lower as the magnetic field increases and thus lose more electrons in the p-state while the s-state lose electrons as well. This behavior is also opposite to a system without a magnetic field(Fig. 5.53). The strong exchange-correlation interaction due to the magnetic field for this background density is believed to cause these phenomena.

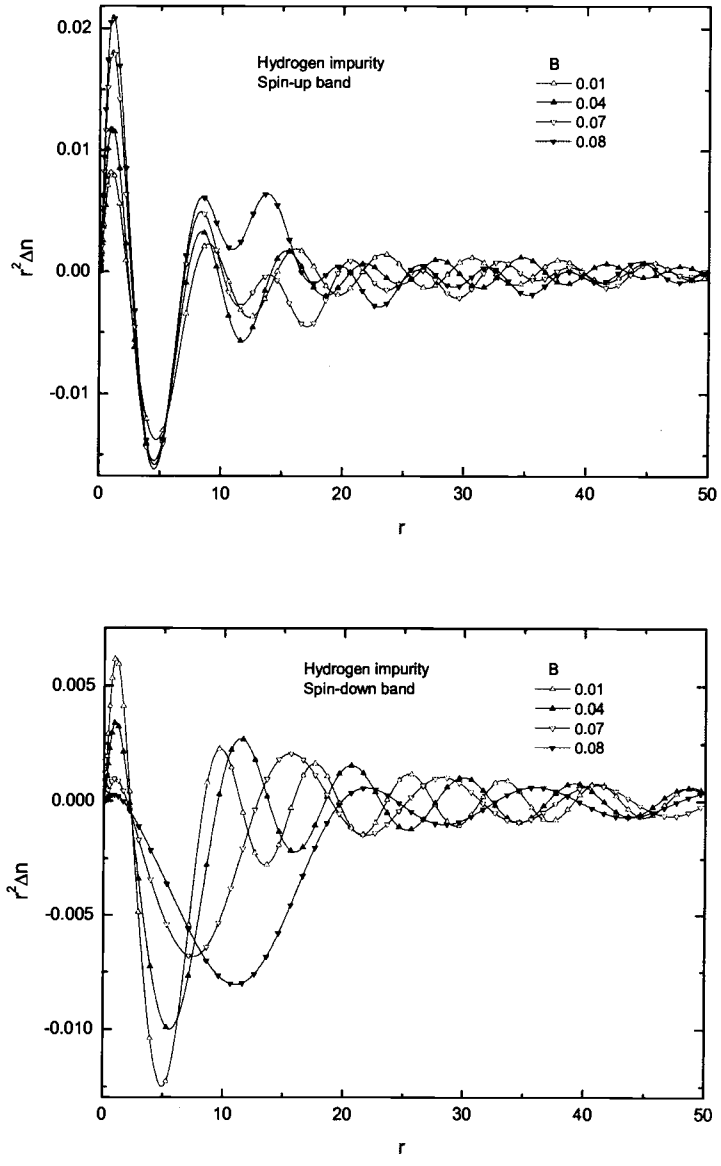

FIGURE 5.54. The induced electronic densities in the conduction band for different magnetic fields. A hydrogen impurity with 0.0025 background density is used.

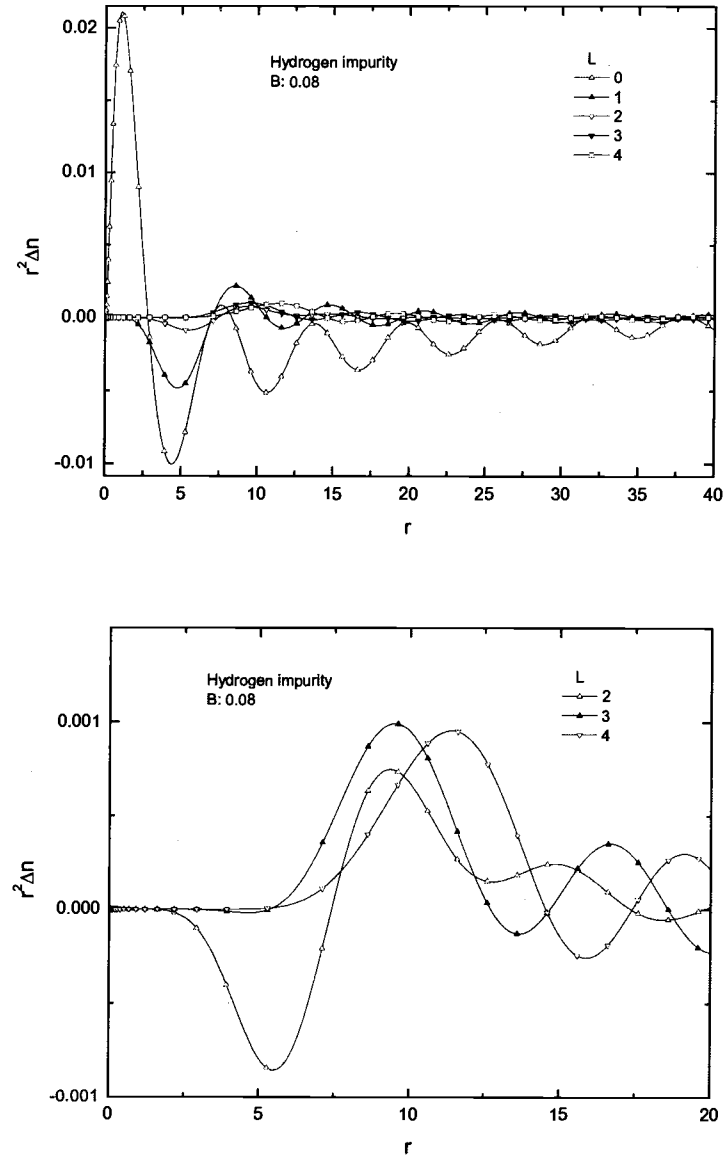

FIGURE 5.55. The induced electronic densities in the conduction band of spin-up electrons for each angular momentum state. These plots correspond to the magnetic field 0.08 in Fig. 5.48 and Fig. 5.54. A hydrogen impurity with 0.0025 background density is used.

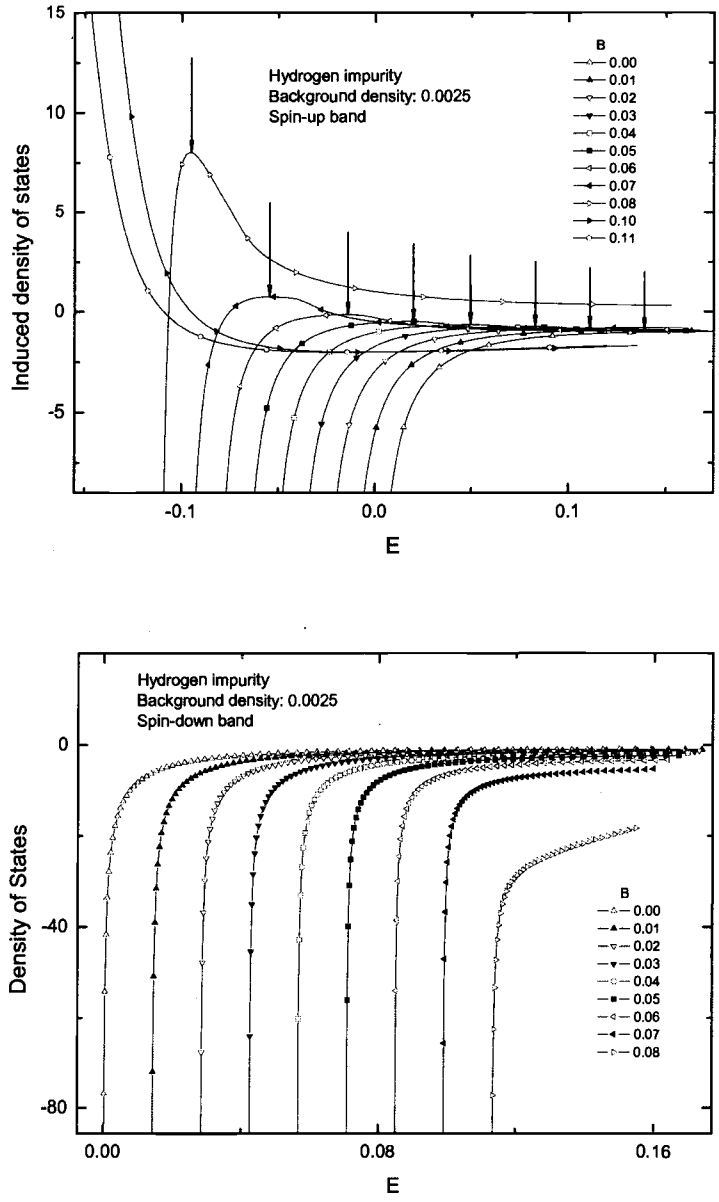

FIGURE 5.56. The density of states of the spin-up and spin-down bands for different magnetic fields. The arrows in the first plot indicate the locations of the scattering resonances. A hydrogen impurity with 0.0025 background density is used.

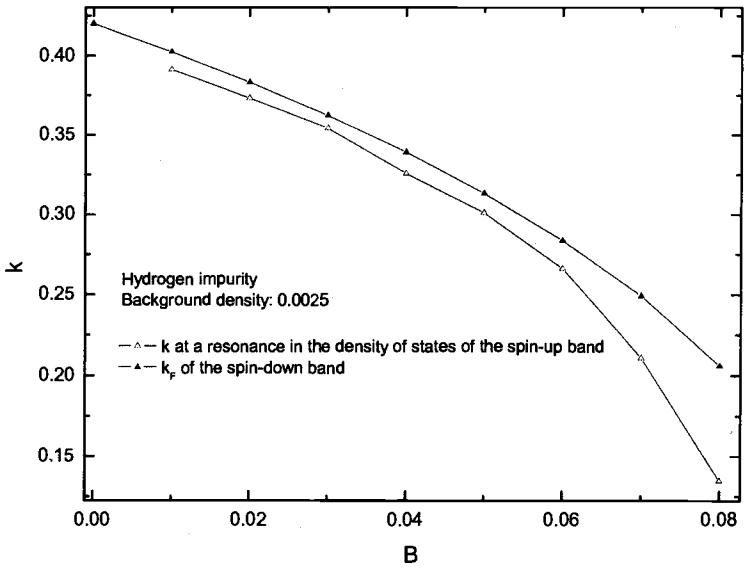

FIGURE 5.57. Comparison of k_F of the spin-down band with k values which correspond to the scattering resonances in Fig. 5.56.

There is another important interaction which causes the rapid increase in the spin-moment (Fig. 5.48) and the fluctuations in the high angular momentum states of the spin-up band as in Fig. 5.52. Since there is a difference in Fermi wave vector between the spin-up and spin-down bands, one may easily expect that there is a beat pattern in the induced density. The spin-down band has a larger range of Coulomb holes and peaks in the density than the spin-up band due to the smaller Fermi wave vector as shown in Fig. 5.54. The spin-up band tries to compensate a large range of these Coulomb fluctuations in the induced density of the spin-down band and results in the increased values of the phase shifts of high angular momentum states at the Fermi energies. On the other hand, the spin-down band also tries to keep the same Coulomb holes as usual by removing

spin-down electrons.[26] One sees that the increases for $l = 3$, 4, and 5 of the spin-up band in Fig. 5.52 and consistently the induced densities in the spin-up band for the high angular momentum states, which are at locations of the large Coulomb holes of the spin-down band, are unusually large as illustrated in Fig. 5.54 and Fig. 5.55. Also note that, for large magnetic fields, there are significant decreases in the $l = 1$, and 2 phase shifts of the spin-down band in Fig. 5.52. This interaction dominates the exchange-correlation interaction as the spin-down background density approaches zero and yields a large spin-moment as in Fig. 5.48. One can see this interaction in the density of states as well. (See Fig. 5.56.) There is a scattering resonance in the density of states for the spin-up band which becomes large as the background density of the spin-down band approaches zero. One sees also in Fig. 5.57 that the momentum value corresponding to the scattering resonance closely follows the Fermi wave vector of the spin-down band, which is related to the Coulomb compensation of the spin-up band. After the spin-down conduction band disappears, the spin-moment is simply -1 since only the spin-down band has a bound state. The immersion energy varies in Fig. 5.48 opposite to the spin-moment since the induced spin-up electrons have a lower energy when the energy is shifted by the magnetic field.

---

[26]This Coulomb interaction of the Friedel oscillations makes obtaining a numerical self-consistent solution much more difficult.

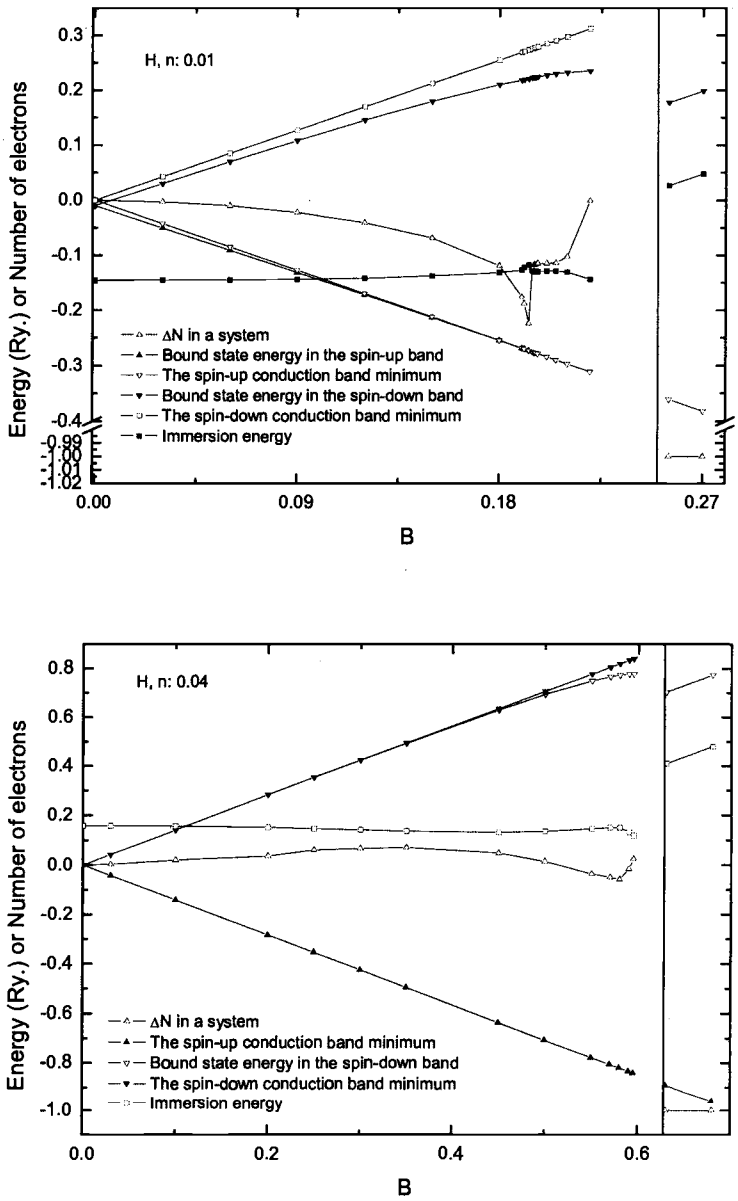

FIGURE 5.58. Bound state energies, the conduction band minimums, the spin–moment, and the immersion energies vs the magnetic field for a hydrogen impurity with two different background densities, 0.01 and 0.04.

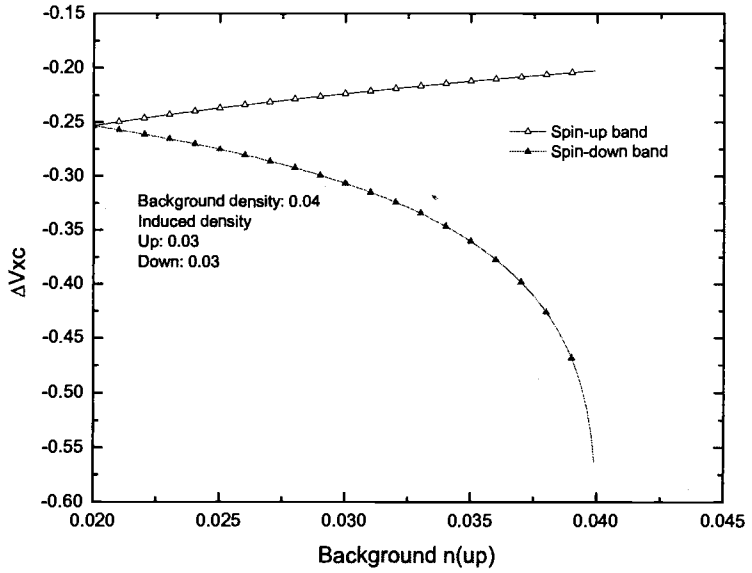

FIGURE 5.59. The exchange-correlation potential with different background densities of the spin-up band. The total background density is 0.04 and the induced density is assumed to be 0.03 for each spin-up and spin-down band. This plot shows how the exchange-correlation potential for each band may vary with the increasing magnetic field.

The calculations for a background density of 0.01 yield similar results as shown in Fig. 5.58.[27] The background density 0.04, however, gives different results as shown in Fig. 5.58. Note that, without an external magnetic field, there are no electrons in the bound states for a background density of 0.04 and a $1s$ bound state exists in the spin-down band for the magnetic field larger than 0.25. The main

---

[27]In the results for 0.01 background density, there is a discontinuity in the spin-moment near 0.19 magnetic field as shown in Fig. 5.58, which is believed to be a numerical problem due to the large spatial extension of the bound state in the spin-up band.

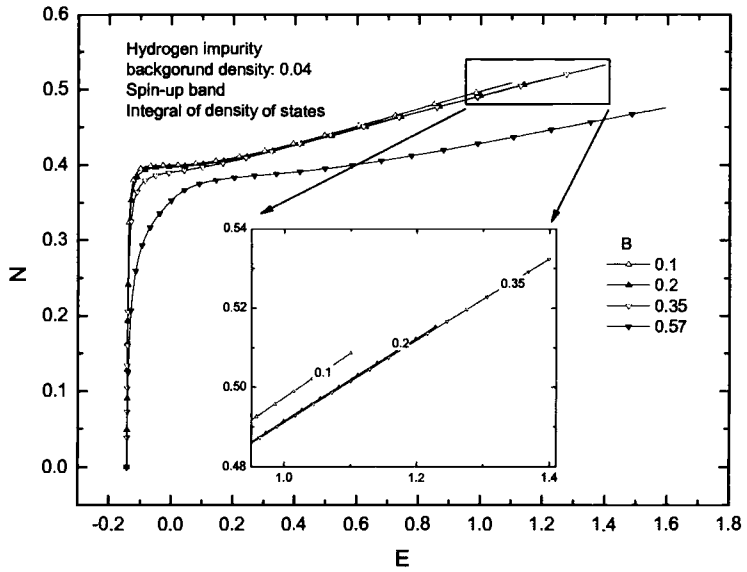

FIGURE 5.60. The integrated values of the density of states of the spin-up band for different magnetic fields to find the total induced number of electrons in the spin-up conduction band. A hydrogen impurity with 0.04 background density is used. The band minimums are shifted in such a way that they have the same minimum.

difference is that the spin-moment slightly increases as the magnetic field increases from zero but shows the same behavior as results for the background densities of 0.0025 and 0.01 after 0.035 magnetic field. This may be explained by the exchange-correlation interaction for this high background density and the difference in the band width(k_F) between spin-up and spin-down bands. Since this is such a high background density, the exchange-correlation potentials vary relatively slowly as the magnetic field increases from zero compared to Fig. 5.49 (See Fig. 5.59.) and the change in the band width due to the magnetic field becomes more important. In this case, the number of induced electrons increases as the Fermi wave vector

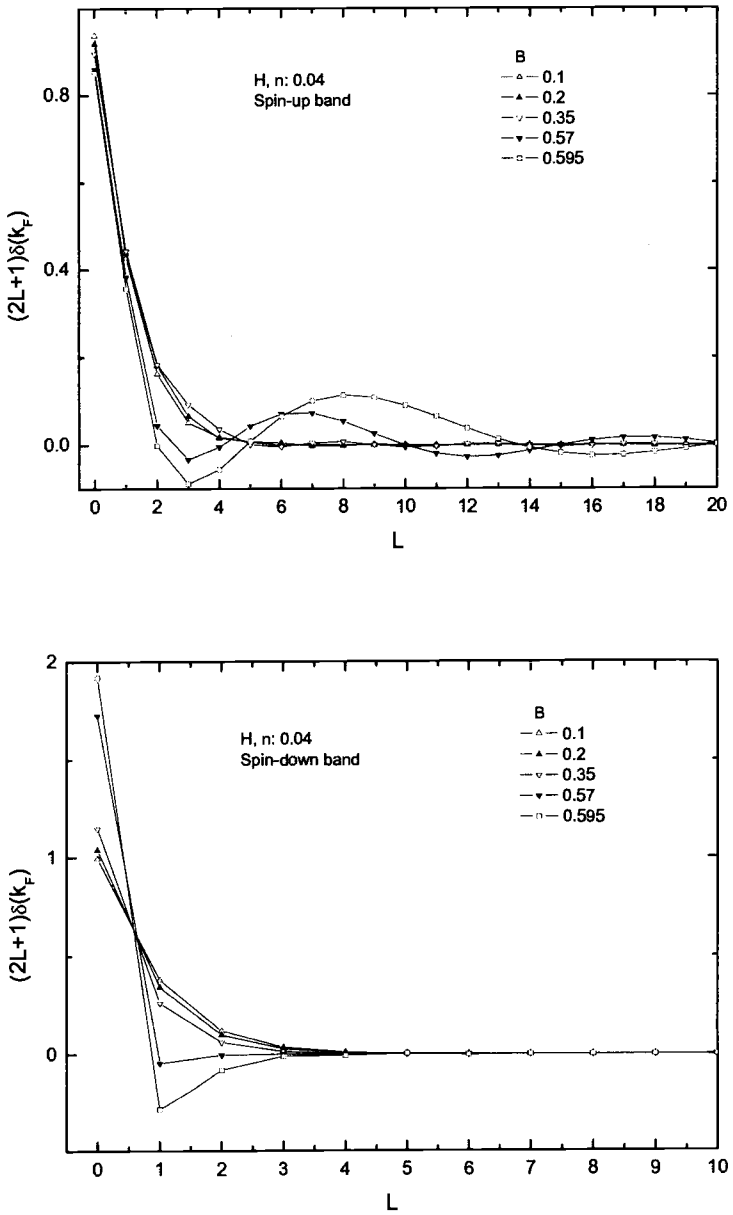

FIGURE 5.61. Partial wave decompositions of the Friedel sum rule. These plots show the change in the number of electrons induced by a hydrogen impurity for each band. 0.04 is used for a background density.

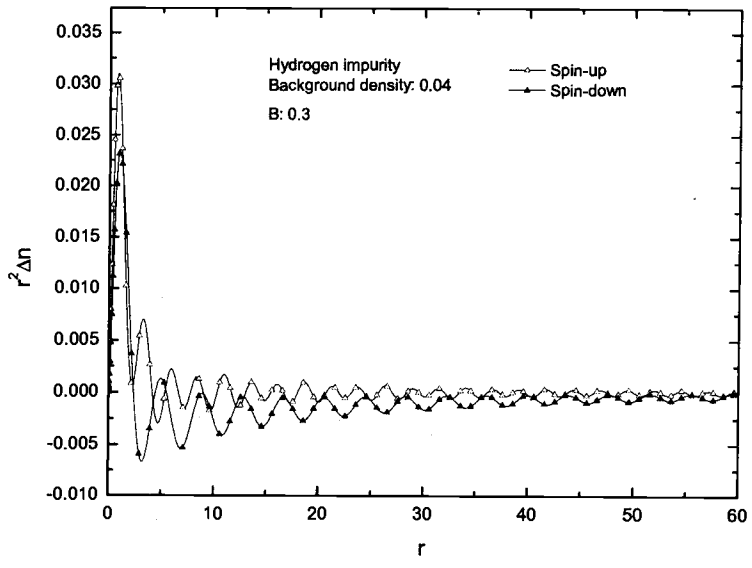

FIGURE 5.62. The density induced by a hydrogen impurity for each conduction band. The background density is 0.04 and the magnetic field is 0.3.

of the spin-up electrons increases, since there are more states available which can contribute to the induced electrons. One can integrate the density of states to find the number of induced electrons, which is shown in Fig. 5.60. The integrated number of induced electrons as a function of energy in the spin-up band is slightly different between a magnetic field of 0.1 and 0.35, but the higher Fermi wave vector results in a gain of more electrons as illustrated in Fig. 5.60. The phase shifts at the Fermi wave vector in Fig. 5.61 for values of the magnetic field between 0.1 and 0.35 show a significant change for high angular momentum states (such as $l = 1 \sim 4$) compared to the change in the s-state as the magnetic field increases. The induced density of the spin-up band is much larger than that of the spin-down band for a magnetic field greater than 0.35 as illustrated in Fig. 5.62. However, as

the magnetic field increases, the spin-moment in Fig. 5.58 decreases for a magnetic field larger than 0.035[28] where the exchange-correlation potential of the spin-down band may decrease very rapidly and thus the difference in the exchange-correlation potentials becomes very large as shown in Fig. 5.59. The same reasoning which is applied to analyze the results for a background density of 0.0025 can be applied to the results for a magnetic field larger than 0.035 for this high background density as well.

---

[28]0.035 magnetic field corresponds to 0.032796 background density of the spin-up band.

6. CONCLUSIONS

Immersion energies are calculated for H, Li, C, and excited systems of H and C using the Kohn-Sham equations in the LDA scheme. The self-consistent solutions are verified and compared with the Friedel sum rule, Friedel oscillations, phase shifts, the scattering length, bound state energies, potentials, Janak's theorem, and compressibilities.

In order to obtain the correct self-consistent solutions, numerical problems must be solved first. The numerical and theoretical errors in LDA due to the rapid density variation in the vicinity of an impurity are canceled out by subtracting the reference energy of a free atom. The Friedel sum rule and Friedel oscillations play a crucial role in solving numerical problems during the numerical iteration process. The long tail of the Friedel oscillations is strongly coupled to the induced density near an impurity by the Coulomb interaction. A mixing ratio as a function of r is used to accelerate the convergence by suppressing this coupled interaction in the mixing step in the self-consistent calculation. In the numerical calculation, infinity must be replaced with a cut-off large number and numerical results must be corrected using the behavior of the Friedel oscillations.

The background density at the immersion energy minimum is 0.0024 for a non-spin polarized system of H and 0.0033 for a non-spin polarized system of C. The behavior of immersion energies as a function of the background density depends on the number of bound states as well as on the impurity. For a neutral impurity, which is forced to have the same number of electrons as the impurity charge, the immersion energies show a simple linear behavior and approach zero as the background density becomes zero. The immersion energies for excited systems are verified with Janak's theorem.

The impurity is completely screened, which is consistent with the Friedel sum rule, regardless of the number of bound states or the background density. In the low energy scattering cases, one can predict the behavior of the phase shifts from the Friedel sum rule and the number of bound states. The phase shifts may, however, show a complicated behavior due to the narrow width of the conduction band at an extremely low background density. This behavior can be expressed in terms of scattering lengths and compressibilities, which is verified with analytical theories.

At low background densities, the calculations show that the immersion energy for the spin-polarized system of a carbon impurity continues to decrease as the background density decreases and does not have the immersion energy minimum near the background density where the non-spin-polarized system of a carbon impurity has a minimum. For these spin-polarized systems, the exchange-correlation interaction at low background densities becomes very important, causing a very strong tendency toward a spin-polarized solution. It induces a $2p$ bound state in the spin-up band only, and can yield a non-zero magnetization even without an external magnetic field. These phenomena lead to an unusual angular momentum state behavior in terms of the number of induced electrons for excited systems of a carbon impurity at low background densities.

With an external magnetic field, the strong Coulomb interaction appears due to two different wave lengths of Friedel oscillations, for spin-up and spin-down bands. With this Coulomb interaction, several interactions such as the exchange-correlation interaction and the change in the band width due to an external magnetic field give rise to a complicated behavior of the induced spin-moment. For instance, there is a rapid increase of the spin-moment as the band width of the spin-down band goes to zero. This magnetic behavior of a spin-polarized system

due to the exchange-correlation interaction at low background densities is driven by the response of an electron gas in the conduction band and, as a result, has a long range effect compared to usual lattice constants. These results, therefore, suggest that the separation distance between impurities is important, and the magnetic behavior of impurities may largely depend on the separation distance.

The model used in this work is spherically symmetric, the spin-orbit interaction is ignored, and the self-interaction correction is not implemented. A non-spherical model must be used for partially occupied angular momentum shells and, hence, may yield angular dependent results especially with an external magnetic field. The spin-orbit interaction also may lead to very different results since non-zero angular momentum states can show the complicated behavior as explained in Ch. 5. In the future, a non-spherical model should be studied with the spin-orbit interaction and the self-interaction correction. Further, a non-local density scheme for the exchange-correlation interaction should be used to investigate the important dependance of our results on the exchange-correlation potential.

BIBLIOGRAPHY

[1] P. Hohenberg and W. Kohn, Phys. Rev. **136**, B864 (1964)

[2] W. Kohn and L.J. Sham, Phys. Rev. **140**, A1133 (1965)

[3] H.J.F. Jansen and A.J. Freeman, *Phys. Rev.* B **30**, 561 (1984)

[4] David J. Singh, *Planewaves, Pseudopotentials and the LAPW Method.*, KAP (1994)

[5] M.J. Puska, R.M. Nieminen, M. Maninen, Phys. Rev. **B 24**, 3037 (1981)

[6] E. Zarembar, L.M. Sander, H.B. Shore, and J.H. Shore, J. Phys. F**7**, 1763 (1977)

[7] J.D. Kress and A.E. DePristo, J. Chem. Phys. **87**, 4700 (1987); **88**, 2596 (1988)

[8] A. Salin, A. Arnau, P.M. Echenique, and E. Zarembar, Phys. Rev. **B 59**, 2537 (1999)

[9] R. Díez Muiño and A. Salin, Phys. Rev. **B 60**, 2074-83 (1966)

[10] J. Friedel, *Philos. Mag.* **43**, 153-89 (1952)

[11] J. Friedel, Adv. Phys. **3**, 446-507 (1953)

[12] J. Friedel, *Nuovo cimento* **7**, 287-311 (1958)

[13] R.M. Dreizler and E.K.U. Gross, *Density Functional Theory*, Springer-Verlag (1990)

[14] S. Lundqvist and N.H. March, *Theory of the Inhomogeneous Electron Gas*, Plenum (1983)

[15] C. Kittel, *Quantum Theory of Solids*, Wiley (1987)

[16] John C. Inkson, *Many-body theory of solids*, Plenum (1984)

[17] L. Hedin and B. I. Lundqvist, J. Phys. C:Solid St. Phys. **4**, 2064-83 (1971)

[18] General D. Mahan, *Many-Particle Physics 3rd ed.*, KA/PP, (2000)

[19] U. von Barth and L. Hedin, J. Phys. C:Solid St. Phys. **5**, 1629-42 (1972)

[20] B. Y. Tong and L. J. Sham, Phys. Rev. **144**, 1-4 (1966)

[21] A. P. Albus, M.S. Thesis, Oregon State University (1999)

[22] Henri J. F. Jansen, unpublished, Oregon State University

[23] J. J. Sakurai, *Modern Quantum Mechanics.*, Addison-Wesley (1994)

[24] J. D. Jackson, *Classical Electrodynamics.*, Wiley (1975)

[25] Neil W. Ashcroft and N. David Mermin, *Solid State Physics.*, Saunders College Publishing (1976)

[26] A. C. Hewson, *The Kondo problem to heavy fermions.*, Cambridge (1992)

[27] W. Kohn and C. Majumdar, Phys. Rev. **138**, A1617-A1620 (1965)

[28] Stephen Gasiorowicz, *Quantum Physics.*, Wiley (1974)

[29] Amit Goswami, *Quantum Mechanics.*, Wm. C. Brown (1997)

[30] R. H. Landau, M. J. Paes, *Computational Physics.*, Wiley-Interscience (1997)

[31] R. H. Landau, *Quantum Mechanics II.*, Wiley-Interscience (1996)

[32] M.J. Puska and R.M. Nieminen, Phys. Rev. **B 27**, 6121 (1983)

[33] E. Babic, R. Krsnik, B. Leontic, M. Ocko, Z. Vucic, I. Zoric, and E. Girst, Solid State Commun. **10**, 691 (1972); G. Boato, M. Bugo, and C. Rizzuto, Nuovo Cimento **45**, 226 (1966); Y. Fukai, Phys Rev. **186**, 697 (1967)

[34] William H. Press, Saul A. Teukolsky, William T. Vetterling, Brian P. Flannery, *Numerical Recipes in C*, CAMBRIDGE UNIVERSITY PRESS (1997)

[35] A. Bechler and R. H. Pratt, Phys. Rev. **A 28**, 1190 (1983)

[36] A. Bechler and R. H. Pratt, J. Phys. A: Math. Gen. **20**, 133-141 (1987)

APPENDIX

APPENDIX A. Atomic Rydberg units

Atomic Rydberg units are defined by $\hbar = 2m_e = e^2/2 = 1$.

The unit for length is the Bohr radius:

$$a_0 = \frac{\hbar^2}{m_e e^2} = 1 \simeq 0.529 \cdot 10^{-8} \text{ cm} \quad .$$

The unit for time is the ratio of an angular momentum and the Rydberg energy:

$$t_0 = \frac{\hbar}{E_R} = \frac{2\hbar^3}{m_e e^4} = 1 \simeq 4.84 \cdot 10^{-17} \text{ s} \quad .$$

The unit for energy is the Rydberg energy:

$$E_R = \frac{e^2}{2a_0} = \frac{m_e e^4}{2\hbar^2} = 1 \text{ Rydberg } \simeq 13.6 \text{ eV} \quad .$$

The unit for charge is:

$$q_0 = 1 = \frac{e}{\sqrt{2}} \simeq 1.1329105 \cdot 10^{-19} \text{ C} \quad .$$

The unit for charge density is:

$$\rho_0 = 1 = 7.6452571 \cdot 10^{11} \text{ C/m}^3 \quad .$$

Other units for important physical quantities are as follows.

The unit for electric field:

$$E_0 = 1 \simeq 3.6360903 \cdot 10^{11} \text{ V/m} \quad .$$

The unit for current:

$$I_0 = 1 \simeq 2.3418037 \text{ mA} \quad .$$

The unit for conductivity:

$$\sigma_0 = 1 \simeq 2.2999241 \cdot 10^6 \text{ S/m} \quad .$$

The unit for resistance:

$$R_0 = 1 \simeq 8.2164712 \text{ k}\Omega \quad .$$

The unit for magnetic induction:

$$B_0 = 1 \simeq 3.3241346 \cdot 10^5 \text{ T} \quad .$$

The unit for magnetization:

$$M_0 = 1 \simeq 4.4253673 \cdot 10^7 \text{ A/m} \quad .$$

APPENDIX B. Comparison with published data

This section is dedicated to focus on the main difference between this thesis and Puska, Nieminen, and Maninen's work([5]).

B.1. Numerical aspects

In Puska, Nieminen, and Maninen's work, only 10 partial waves were used. The Pratt improvement scheme(Broyden's method) is used for the mixing ratio. They used a first order approximation of Taylor series to remove the dependence of the cut-off radius in the calculation of the exchange-correlation energy.

In this thesis, a cut-off value of 10^{-8} for the phase shifts is used to determine the number of partial waves for each k. Hence, the number of partial waves is variable. Exponential-like functions are used for the mixing ratio since discontinuities in the potential in r-space are found in Broyden's method. The information of the last two input potentials is utilized in the mixing scheme to consider the response of iteration process. The cut-off radius dependance of the calculations is removed by considering the oscillation of integrated values, which is believed to be accurate due to the regular behavior of the Friedel oscillations at large distances. The output potentials also must be corrected after each iteration of the numerical calculations. This is performed in such a way that the system satisfies the Friedel sum rule and correct Friedel oscillations. It is also pointed out that the systematic numerical error of core states of an impurity in an electronic gas can be canceled out by that of the reference of a free atom energy. In order to obtain this cancelation, one must use the same r-mesh for both calculations. Detailed information can be found in Ch. 4.

B.2. Results

The immersion energies obtained in this thesis are slightly lower than those in Puska, Nieminen, and Maninen's work. For instance, the background density is about 0.025 at zero immersion energy for H while it is 0.02 in Puska, Nieminen, and Maninen's work. However, the result for the background density at the immersion energy minimum is very close to that of Puska, Nieminen, and Maninen's work. They showed 0.0026 for H and 0.0035 for C while, in this work, 0.0024 for H and 0.0033 for C are obtained. While they focused on the partial-wave decompositions of the density of induced states, the results for the partial-wave decompositions of the Friedel sum rule[1] are obtained and used to analyze the behavior of the potentials especially for spin-polarized systems. The following new results are obtained. Dielectric functions and compressibilities for H are calculated and compared with the theory in this work. Immersion energies for excited systems are also calculated and verified with the Janak's theorem, and the results for spin-polarized systems and spin-coupling with an external magnetic field are also newly obtained in this work, which have not been performed in the older work.

---

[1]This kind of discussion also can be found in [32].

APPENDIX C. Boundary conditions for non-spherical potentials at small r

The general idea is taken from [8]. The equations to be solved are

$$\left[\frac{d^2}{dr^2} + \epsilon_n - \frac{l(l+1)}{r^2}\right] u_{nlm}(r) = \sum_{l'} V^m_{ll'}(r) u_{nl'm}(r) \quad , \tag{C1}$$

where

$$V^m_{ll'}(r) = \int \mathrm{d}\mathbf{\Omega}\, Y^*_{lm}(\Omega_r) V_{eff}(r,\theta) Y_{l'm}(\Omega_r) \quad . \tag{C2}$$

The coupling terms must be examined in order to find the boundary conditions of a set of linearly independent solutions of the coupled equations at small r. The potential can be expanded due to its cylindrical symmetry as

$$V(\boldsymbol{r}) = \sum_i V_i(r) P_i(\cos\theta) \quad , \tag{C3}$$

where $P_i(\cos\theta)$ is a Legendre polynomial. The behavior of the components $V_i(r)$ of the potential at small r can be shown, which is

$$\lim_{r\to 0} V_i(r) \sim \begin{cases} r^i & \text{if } i > 0 \quad , \\ -\frac{Z}{r} & \text{if } i = 0 \quad . \end{cases} \tag{C4}$$

Using the expansion for $V(\boldsymbol{r})$,

$$\begin{aligned} V^m_{ll'}(r) = \int \mathrm{d}\mathbf{\Omega}\, [&Y^*_{lm}(\Omega_r) V_0(r) P_0(\cos\theta) Y_{l'm}(\Omega_r) + Y^*_{lm}(\Omega_r) V_1(r) P_1(\cos\theta) Y_{l'm}(\Omega_r) \\ &+ Y^*_{lm}(\Omega_r) V_2(r) P_2(\cos\theta) Y_{l'm}(\Omega_r) + \cdots] \quad . \end{aligned} \tag{C5}$$

Note that

$$\int \mathrm{d}\mathbf{\Omega}\, Y^*_{lm}(\Omega_r) P_v(\cos\theta) Y_{l'm}(\Omega_r) = \beta \delta_{(l-v)+2i,l'} \quad , \tag{C6}$$

where $i = 0, 1, 2, \cdots$ until $l' \leq (l+v)$.

Now, using the form of $V_i(r)$ at small r in (C4), each term in (C5) contributes to $V_{ll'}^m(r)$ at small r as

$$\lim_{r\to 0} V_{ll'}^m(r) = \alpha_0 \frac{1}{r}\delta_{l,l'} + \alpha_1 r \int Y_{lm}^*(\Omega_r) P_1(\cos\theta) Y_{l'm}(\Omega_r) + \alpha_2 r^2 \int Y_{lm}^*(\Omega_r) P_2(\cos\theta) Y_{l'm}(\Omega_r) + \cdots \quad \text{(C7)}$$

$$= \beta_0 \frac{1}{r}\delta_{l,l'} + \beta_1 \delta_{l\pm 1,l'} r + \beta_2 \delta_{l\pm 2,l'} r^2 + \cdots \ , \quad \text{(C8)}$$

where only the lowest order terms of r are kept for each coupling term l' and β_i simply represents constants produced in integrals and coefficients in $V_i(r)$. For spherically symmetric potential, the form of u_{lm} at small r is

$$\lim_{r\to 0} u_{lm}(r) = A r^{l+1} \quad \text{(C9)}$$

Using this form, the coupling terms become at small r

$$\lim_{r\to 0} \sum_{l'} V_{ll'}^m(r) u_{l'm}^{l'}(r) = \beta_0 \frac{1}{r} r^{l+1} + \beta_1 r^{l+3} + \beta_1 r^{l+1} + \beta_2 r^{l+5} + \beta_2 r^{l+1} + \beta_3 r^{l+7} + \beta_3 r^{l+1} + \cdots \ . \quad \text{(C10)}$$

One can see that the coupling terms follow the form of

$$\begin{aligned} r^{l+1} \quad & \text{if } j < l \ , \\ r^{2j+l+1} \quad & \text{if } j \geq l \ , \end{aligned} \quad \text{(C11)}$$

where $j = 0, 1, 2, \cdots, l_{max}$.[2] Since there exist solutions following these form of coupling terms, one can finally write power series form for linearly independent solutions of coupled equations.

---

[2] l_{max} is the maximum l value used in the numerical calculation to truncate the partial wave expansion in (3.3).

$$u^j_{lm}(r) = r^{j+|l-j|+1} \sum_{i=1}^{\infty} b^l_i r^{i-1} \quad . \tag{C12}$$

The lowest order terms r^{l+1} satisfy automatically the boundary conditions at small r. For the higher order terms than r^{l+1}, there are lower order terms to be coupled in (C1).

APPENDIX D. Singular value decomposition(SVD)

The singular value decomposition(or SVD) is very popular, used for many different areas such as image compression but essentially a technique to deal with matrices which are singular or very close to singular and thus for which Gaussian elimination or other decomposition methods may fail.

Any real $m \times n$ matrix A can be decomposed uniquely with a $m \times m$ orthogonal matrix U and an $n \times n$ orthogonal matrix V such that

$$A = U \cdot D \cdot V^T \quad , \tag{D1}$$

where $D = \text{diag}(\sigma_1, \sigma_2, \cdots, \sigma_n)$ and follows order of $\sigma_1 \geq \sigma_2 \geq \cdots \geq \sigma_n$. The scalars $\sigma_1, \sigma_2, \cdots, \sigma_n$ are called the singular values of A and columns of U and V are eigenvectors of AA^T and A^TA, respectively.

Let's consider a system of linear equations.

$$A \cdot x = b \quad . \tag{D2}$$

The nullspace is defined as a subspace of x such that $A \cdot x = 0$ if A is a singular. The range is defined as a subspace of b which can be obtained by mapping x with A. The dimension of the range is actually the rank of A. The dimension of the range is also can be obtained by subtracting the dimension of the nullspace from m. If A is nonsingular, its range is all of the vector space b. If A is singular, the rank r is less than m and $\sigma_{r+1} = \sigma_{r+2} = \cdots = \sigma_n = 0$. Suppose that A is singular. If $b = 0$, any column of V which corresponds to zero σ_j becomes a solution of $Ax = 0$. A solution is in this case $x = a_1 v_r + a_2 v_{r+1} + \cdots + a_{n-r} v_n$ where v_j is a j column of V and $a_1^2 + a_2^2 + \cdots + a_{n-r}^2 = 1$. If the vector b is not zero and lies in the range of A, solutions can be found by

$$x = V \cdot [\text{diag}(1/\sigma_j)] \cdot U^T \cdot b \tag{D3}$$

with a condition of the smallest length $|x|^2$ which removes any redundant solutions since any column of V with a zero σ_j(solutions correspond to the nullspace) can be added to x in any linear combination. One important trick in (D3) is to equate $1/\sigma_j$ to zero if $\sigma_j = 0$. The readers should refer to [34] for more details.

- An example for $A \cdot x = 0$ (calculated in Mathematica):

The matrix A is given by

$$A = \begin{pmatrix} 1 & 3 & 6 & 10 \\ 2 & 4 & 5 & 3 \\ 2 & 6 & 12 & 20 \\ 4 & 8 & 10 & 6 \end{pmatrix} . \tag{D4}$$

Since the last two rows of A are just twice the first two rows, the rank of A is 2. The matrix A can be decomposed using SVD as mentioned before. U, D, and V are

$$U = \begin{pmatrix} -0.390888 & 0.217271 & -0.729017 & 0.518202 \\ -0.217271 & -0.390888 & 0.518202 & 0.729017 \\ -0.781776 & 0.434542 & 0.364509 & -0.259101 \\ -0.434542 & -0.781776 & -0.259101 & -0.364509 \end{pmatrix} , \tag{D5}$$

$$D = \begin{pmatrix} 30.5886 & 0 & 0 & 0 \\ 0 & 8.0212 & 0 & 0 \\ 0 & 0 & 0 & 0 \\ 0 & 0 & 0 & 0 \end{pmatrix} , \text{ and} \tag{D6}$$

$$V = \begin{pmatrix} -0.134925 & -0.351883 & 0.695905 & -0.611301 \\ -0.333743 & -0.568331 & 0.265892 & 0.703503 \\ -0.560942 & -0.405685 & -0.627282 & -0.356765 \\ -0.74549 & 0.623376 & 0.227011 & 0.064138 \end{pmatrix} , \tag{D7}$$

Since the rank of A is 2, $\sigma_3 = \sigma_4 = 0$ which correspond to the nullspace. The calculation can be confirmed as

$$U \cdot D \cdot V^T = \begin{pmatrix} 1 & 3 & 6 & 10 \\ 2 & 4 & 5 & 3 \\ 2 & 6 & 12 & 20 \\ 4 & 8 & 10 & 6 \end{pmatrix} = A \quad . \tag{D8}$$

Last two columns of V give solutions of $A \cdot x = 0$, which can be confirmed as

$$A \cdot \begin{pmatrix} 0.695905 \\ 0.265892 \\ -0.627282 \\ 0.227011 \end{pmatrix} = \begin{pmatrix} -1. \times 10^{-6} \\ 1. \times 10^{-6} \\ -2. \times 10^{-6} \\ 2. \times 10^{-6} \end{pmatrix} \quad . \tag{D9}$$

$$A \cdot \begin{pmatrix} -0.611301 \\ 0.703503 \\ -0.356765 \\ 0.064138 \end{pmatrix} = \begin{pmatrix} -2. \times 10^{-6} \\ -1. \times 10^{-6} \\ -4. \times 10^{-6} \\ -2. \times 10^{-6} \end{pmatrix} \quad . \tag{D10}$$

The right hand sides in the above equations show very small values which are actually zero within the numerical tolerance. Note that for any column v_j of V, $v_j^T \cdot v_j = 1$.

APPENDIX E. Behavior of phase shifts for $E \to \infty$

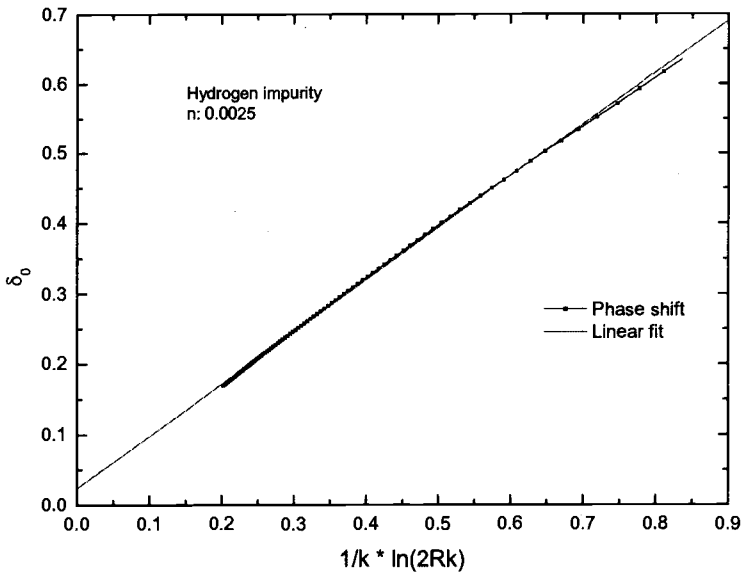

FIGURE 6.1. Behavior of phase shifts for $k \to \infty$.

The high energy behavior of phase shifts is tested numerically with a hydrogen impurity and a background density of 0.0025. A discussion of phase shifts in Coulomb-like potentials can be found in several places. [31] [35] [36]

For a potential of the type [36]

$$V(r) = -\frac{ag(\lambda r)}{r} \quad , \tag{E1}$$

approximate expressions for high energy phase shifts are, up to a first order,

$$\delta_l(k) \simeq \delta_{cl} + \frac{a}{k}\left[\ln(2k/\lambda)\right] \quad , \tag{E2}$$

where δ_{cl} is the point-Coulomb phase shift, which is, as k is increasing, vanishing much faster than the second term in (E2). The results in Fig. 6.1 are obtained with the assumption, $\lambda = 1/R_m$, which is correct for $g(\lambda r) = 1 - r/R_m$.[3]

One can see in Fig. 6.1 that numerically obtained results well agree with the analytic form.

---

[3]The potential is zero for $r \geq R_m$.

APPENDIX F. Scattering length and bound state energy

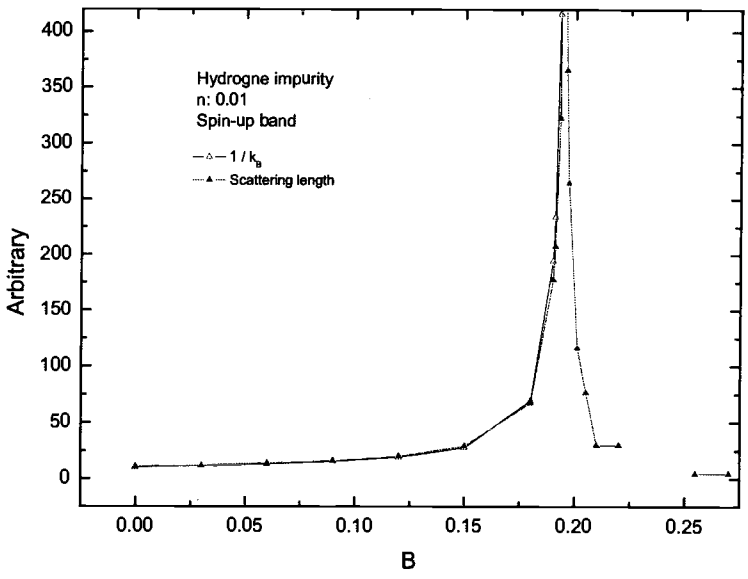

FIGURE 6.2. Scattering length versus $1/\sqrt{|E_B|}$, where E_B is the bound state energy relative to the conduction band minimum.

It is shown in 3.6 that the scattering length a can be related to the bound state energy as in

$$a = r_0 + \frac{1}{k_B} \quad . \tag{F1}$$

If the effective potential range r_0 is sufficiently small, as in the screened cases, the scattering length can be estimated from the bound state energies using (F1).

Fig. 6.2 shows that the numerical results calculated in this work are consistent with (F1).